TIME-FREQUENCY METHODS IN OPTICAL SIGNAL PROCESSING

THE UNIVERSITY *of* LIVERPOOL

Thesis submitted in accordance with the requirements of the University of Liverpool for the Degree of Doctor in Philosophy by

Lampros K. Stergioulas

April, 1997

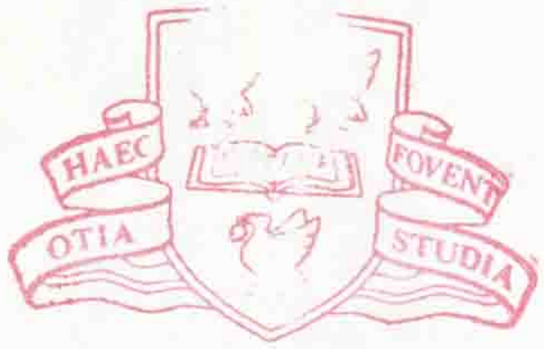

For my parents

Prolegomena

The work described in this thesis was carried out in the Department of Electrical Engineering and Electronics at the University of Liverpool between October 1993 and March 1997. Some of the results of this work have been presented at conferences (*14th International Maximum Entropy Workshop*, Cambridge, England (1994); *Quantum Dynamics of Simple Systems*, 44th Scottish Universities Summer School in Physics, Stirling, Scotland (1994); *Information Theory in Classical and Quantum Optics*, Adriatico Research Conference, Trieste, Italy (1995)).

There is a considerable list of people to whom I would like to express my gratitude for kindnesses received during this period.

My first thanks must go to Dr. Apostolos Vourdas who suggested and supervised the work. His encouragement, advice, and help have been invaluable, to say the least. I stand in his debt.

Particular thanks are due to Professor Gordon R. Jones for his helpful advice and energetic contribution throughout this project.

I would also like to express my thanks to my colleagues David Messent, Joe Cosgrave, Dimitris Tomtsis, and all the others at the Fibre Optics Laboratory for their help and for providing too many interesting signals!

Support and assistance generously offered by the staff at the Department of Electrical Engineering and Electronics, the University of Liverpool, are gratefully acknowledged. Special thanks to Brenda Lussey, Gary Tagoe and David Turner for making my life as a graduate student a lot easier.

My thanks and gratitude also go to Professor Michael T.C. Fang, Department of Electrical Engineering and Electronics, the University of Liverpool, and

Professor Paolo Lisboa, School of Computing and Mathematical Sciences, Liverpool John Moores University, for their valuable advice and guidance; Professor Konstantinos Karoumbalos, Department of Informatics, National University of Athens, for his constructive suggestions and comments; Professor A. Mohammad-Djafari, Ecole Supérieure d'Electricité, France, for many inspiring suggestions; Dr. David Cebon of Cambridge University Engineering Department, for his continuous support during the last year; and Dr. Giannis Giakas, Division of Sport, Health and Exercise, Staffordshire University, for his help and for providing useful biomechanical data.

This Ph.D. project was fully funded by the State Scholarships Foundation (S.S.F. or I.K.Y.), Greece, to whom I am very much indebted.

Last, but obviously not least, I would like to thank my sister Stella and all my friends for the generous moral support throughout my time in Liverpool.

To them all, many thanks

Lampros K. Stergioulas

Liverpool

England

April 1997

Synopsis

Traditional signal representations are defined on one-dimensional axes (time or frequency representations). Alternative two-dimensional time-frequency representations are considered and their properties explored. The significant advantage of this approach is the detailed description of the 'instantaneous' frequency content of a signal as a function of time. Signal analysis using time-frequency representations is mathematically analogous to the coherent state theory of quantum mechanics. The uncertainty principle in signal processing and its consequences are studied in the context of time-frequency analysis.

Three different representations on the time-frequency plane are used: the Wigner function, the Gabor transform and the Bargmann analytic representation. The properties of these methods are studied and transforms between them are investigated. Implementation of these ideas on realistic signals (at optical frequencies) are considered in the context of areas like signal compression, signal synthesis, chromatic analysis, and optical sensing. The same mathematical techniques are also applied in the context of quantum optics and quantum optical communication, where the construction of non-classical states as a superposition of a few coherent states is presented. The Maximum Entropy method is also used for noise suppression. Applications of these methods for solving current problems in the practical areas of optical sensing and signal detection and processing are also studied.

Contents

List of Tables

List of Figures

Chapter 1

Introduction

1.1 The Scope of This Thesis

During the last two decades, there has been an increasing interest in joint *time-frequency* representations of signals. The need for such alternative representations has been recognised not only by the community of signal processing theorists, but also by practical signal processing researchers. Although the pioneering papers of D. Gabor [63] (1946) and J. Ville [173] (1948) had suggested joint signal representations a long time ago, time-frequency representations obtained considerable attention quite recently, partly because of the increase in the available computation power.

These methods aim to offer a satisfactory representation of signals which is complementary to the traditional Fourier analysis. Speech processing was one of the first areas to use this kind of representation (sound spectrogram), due to the difficulties arising from the non-stationary nature of speech signals. Recently, time-frequency analysis is an important issue in vision research.

In many cases of practical importance, traditional Fourier techniques are insufficient. Time-frequency representations can be used in such cases to overcome the drawbacks of Fourier analysis. As they can sufficiently describe the randomness and nonstationarities of noisy and time-varying signals, they are powerful tools for signal analysis and synthesis as well as for the design of systems with

time-varying characteristics.

In this thesis, various time-frequency signal representations are considered, their useful properties are studied, new ideas and methods for applying these representations are introduced. In a general context, the various representations (of both time-frequency and traditional approaches) are compared, their suitability for specific applications is examined and their potential for signal processing is explored.

More specifically, the aim of this work is to use time-frequency representations in the context of *optical* signal processing. Applications for various types of optical signals are suggested and practically implemented. So far the processing of optical signals has been performed mainly using Fourier transform techniques. In this work, various alternative time-frequency representations are applied and their potential for analysis and synthesis of optical signals is explored.

Although the examples presented in this thesis are limited to applications in optical signal processing, the suggested methods are rather general and can be easily applied to other areas related to signal processing and communication.

One of the objectives of this thesis is to provide a more complete and critical view of the various methods and to introduce new techniques and applications in the context of time-frequency analysis. Inter-relations between the different representations are also investigated.

An attempt has been made to interpret the results in a consistent way. Practical implementation and potential applications are discussed and a comparison with traditional Fourier analysis is made. Quantitative analysis of the results is carried out and several methods of measuring the efficiency of the numerical approximations are considered.

In this work, concepts from the mathematical theory of communication, signal theory and information theory are used. The mathematical framework is taken from probability theory, the theory of analytic functions, and theoretical physics. As it will be pointed out, there exists a mathematical analogy between signal theory and quantum mechanics.

In this respect, applications of the developed techniques in the context of

quantum optics are also considered. A convenient method for constructing non-classical states of light is implemented, promising important practical applications in the fields of quantum state engineering and quantum optical communications.

One method of current interest for processing noisy signals and images is the *Maximum Entropy method*. This method uses probabilistic criteria to estimate the 'most likely' original (undistorted) signal. The Maximum Entropy principle plays an important role in information theory and its rigorous formulation is due to E.T. Jaynes [87, 88], who introduced a new formalism of probabilistic inference based on concepts of statistical mechanics. Here, this technique is used in the context of speckle noise analysis. The method is powerful and could be also used in other areas.

1.2 A Brief Overview

The main body of this thesis is organised in two parts. The first part (Chapters 2-6) deals with time-frequency representations of signals; the Wigner distribution function, the Gaussian expansion and the Bargmann representation are examined in detail. The second part contains one chapter (Chapter 7) and explores maximum entropy techniques in optical signal processing. An effort has been made to follow a natural development of the ideas from the early chapters to the later ones and to maintain a uniform logical structure throughout the thesis. Different chapters have been dedicated to the different subjects addressed in this work.

The second and the third chapters of this thesis are more or less introductory. Chapter 2 provides a general background in signal theory and traditional Fourier analysis, which will be necessary for the chapters to follow. In this chapter, the fundamental concepts of signal theory are described and basic definitions are given. The concepts of orthogonality and completeness of representations are introduced. A brief discussion on traditional methods (Fourier transform representation) is included; the properties of the Fourier transform are mentioned, its discrete version is considered, and the advantages and disadvantages of Fourier analysis are presented. The very important uncertainty principle is discussed in the context of communication theory. This chapter also offers an introduction

to the ideas of modern signal processing, which further analysis in later chapters will be based on.

Chapter 3 serves as an introduction to time-frequency analysis. A brief review of the various time-frequency representations is given. The implications of the well-known analogy between signal processing and quantum mechanics are pointed out. The notion of the analytic signal is introduced and relevant examples with optical signals are presented.

Chapters 4-7 are the central chapters of this thesis. The theme in Chapter 4 is the Wigner distribution function representation. The properties of the Wigner function and its relation to the well-known ambiguity function are presented. Interpretation of the Wigner representation and its potential for signal processing are discussed in considerable detail. Implementation of the method for optical signal processing applications is described and further developments are discussed.

Chapter 5 develops a practical method to represent a signal using Gabor's Gaussian expansion. The Gabor expansion is introduced and its analogy with the coherent state representation in quantum optics is discussed. A convenient basis of a 'truncated' von-Neumann lattice is proposed and numerical implementation for the case of optical signals is demonstrated with various examples. Emphasis is given to the robustness property of the calculated representation. The potential of the method for practical applications in optical and acoustical frequencies is explored and the idea of 'Gabor devices' is suggested. At the end of Chapter 4, the Bargmann analytic representation, which is another time-frequency representation, is considered and the relationship between the Bargmann transform and other representations is investigated. Potential applications of the Bargmann transform in optical signal processing are also discussed.

Chapter 6 applies the same techniques in the context of quantum optics and quantum optical communication. More specifically, it describes an application of the 'truncated' Gaussian expansion (described in Chapter 4) in the context of quantum state engineering. Here, construction of quantum states is considered, by means of linear combinations of coherent states on a 'truncated' von-Neumann lattice. Numerical examples are given, followed by potential applications in quan-

tum optical communications.

Chapter 7 introduces the Maximum Entropy method, which is a probabilistic approach suitable for the processing of noisy or incomplete data. An analytic solution for the problem of two moments is given, and the technique is then applied to speckle pattern images for noise suppression. Applications in optical fibre sensing and communications are considered.

Finally, in Chapter 8, the main conclusions and recommendations for further work are given.

Most chapters contain worked examples. The corresponding figures are also included at the end of each chapter.

Part I

TIME-FREQUENCY ANALYSIS OF OPTICAL SIGNALS

Chapter 2

Elements of Signal Theory and Fourier Analysis

2.1 Introduction

In this chapter, a brief introduction to the fundamental theoretical aspects of signal analysis is made. The concepts of stationarity and causality are presented and basic definitions necessary for the chapters to follow are given. Signal representations using orthogonal bases are introduced. The Fourier transform receives special attention, to be followed by an additional section on the uncertainty principle in signal theory. Finally, the differences between deterministic and the stochastic(random) signals are pointed out and the implications of non-stationarity are discussed.

2.2 Orthogonal Bases for Signal Analysis

A signal defined on the whole time axis is called a *continuous-time* signal or an *analogue* signal. All physically-realizable signals (defined in a time domain) are causal. A *causal* signal is one which is zero-valued on the negative time half-axis; that is, an arbitrary signal $s(t)$ is causal if

$$s(t) = 0, \quad \forall t < 0.$$

Real-life signals that are used in processing applications or observed and measured in nature are of finite energy. For this reason, natural signals belong to the class of *square* (or *absolutely*) *integrable* or *square-modulus measurable* or simply *energy signals*. They can be described as elements $s(t)$ of the Hilbert space $L^2_{\mathbf{C}}$ of square-integrable functions:

$$s \in \mathbf{C}: \quad \int_{-\infty}^{+\infty} |s(t)|^2 dt = E_s < \infty, \tag{2.1}$$

where $|s(t)|$ stands for the absolute value (or modulus) of the signal $s(t)$. Such natural signals are always real-valued. In the following sections, the general case of complex signals is considered. A generalisation from real-valued to complex-valued signals is described in Chapter 3 in detail.

Sometimes, in certain applications, it is convenient to express the signal $s(t)$ as a set of numbers $u_s(f)$ (*coefficient space*) which, when combined with a properly chosen set of elementary signals $r(t; f)$ (the *coordinate space* or the *basis*), will uniquely specify the signal $s(t)$. These special signals $r(t; f)$ are called the *basis signals* and are characterised by the variable f, which here is considered to be real just for the sake of simplicity. It is desirable that the basis signals satisfy two requirements:

Orthogonality. A basis is defined to be *orthogonal* if for any signals $r(t; f_1)$ and $r(t; f_2)$ of the basis:

$$\int_{-\infty}^{+\infty} r(t; f_1) r^*(t; f_2) dt = \delta(f_1 - f_2). \tag{2.2}$$

where the asterisk indicates the complex conjugate. This means that the members of the basis are linearly independent on each other. $r(t; f_1)r^*(t; f_2)$ is called the *inner product* of the signals $r(t; f_1)$ and $r(t; f_2)$.

The set of the basis signals $r(t; f)$ is *normalised* if

$$\int_{-\infty}^{+\infty} |r(t; f)|^2 dt = 1 \tag{2.3}$$

for all f; that is, the energy of the basis signals is equal to unity. An orthogonal basis which is normalised according to Eq. (2.3) is called *orthonormal* and the integral on left-hand side of Eq. (2.3) is called the *norm*.

Completeness. A basis is *complete* if any signal $s(t)$ can be uniquely expressed in terms of the basis signals $r(t; f)$ as:

$$s(t) = \int_{-\infty}^{+\infty} u_s(f) r^*(t; f) df; \tag{2.4}$$

The completeness implies that there is no such signal which is orthogonal to every member of an orthogonal basis.

In the case of representations of square-integrable signals using a complete orthogonal basis, it is known that

$$\int_{-\infty}^{+\infty} |s(t)|^2 dt = \int_{\infty}^{+\infty} |u_s(f)|^2 df. \tag{2.5}$$

This relation offers an expression of the energy of the signal in terms of the given representation and is known as the *Parseval's theorem for energy signals.*

In the general case, the set of coefficients and the basis are infinite continuous sets. In applications, however, discrete (and sometimes finite) sets have been considered, which can provide exact representations or good approximations of signals. A representation using an infinite discrete orthonormal basis is sometimes called a "generalised (non-harmonic) Fourier series representation".

2.3 The Fourier Transform Representation

Fourier analysis is a well known mathematical tool with a vast range of applications in sciences and engineering. It is named after the great physicist Jean Baptiste Fourier (1768-1830), who proved that periodic functions can be expressed as a sum of harmonic functions.

The *Fourier transform* is an orthogonal-basis signal representation which plays a fundamental role in signal processing. In this section, an introduction to the basic aspects of the Fourier transform will be made.

2.3.1 The Continuous-Time Fourier transform

The Fourier transform $\tilde{s}(f)$ of a square-integrable signal $s(t)$ is an integral transformation defined by:

$$\tilde{s}(f) = \int_{-\infty}^{+\infty} s(t)e^{-j2\pi ft}dt, \tag{2.6}$$

where the tilde denotes the Fourier transform and f is the characteristic variable of the representation; in the context of signal processing, f is the variable in the frequency domain. The *inverse Fourier transform* is given by

$$s(t) = \int_{-\infty}^{+\infty} \tilde{s}(f)e^{j2\pi ft}df. \tag{2.7}$$

The Fourier basis is both orthogonal and complete and its members are complex exponential functions. In signal theory, the Fourier transform $\tilde{s}(f)$ (or its absolute value $|\tilde{s}(f)|$) of a signal $s(t)$ of finite energy is sometimes referred to as the *(frequency) spectrum* and it is used for frequency domain analysis. The squared modulus of the Fourier transform ($|\tilde{s}(f)|^2$) gives the so-called *energy spectral density function* or shortly *spectral density* of the signal, which represents its energy per unit of frequency. In applications, the energy spectral density related to a continuous Fourier transform can be measured directly by specially designed analogue systems called *spectrum analysers*.

2.3.2 Properties of the Fourier transform

In this section, we summarise the most important properties of the Fourier transform. For clarity, the symbol $\mathcal{F}$ is used as an alternative notation for the Fourier transform operation.

I *Linearity/Superposition.* For any signals $s_1(t)$ and $s_2(t)$ and any arbitrary numbers α_1 and α_2, we have

$$\mathcal{F}\{\alpha_1 s_1(t) + \alpha_2 s_2(t)\} = \alpha_1\mathcal{F}\{s_1(t)\} + \alpha_2\mathcal{F}\{s_2(t)\}. \tag{2.8}$$

II *Complex Conjugate.* For complex-valued signals, we have

$$\mathcal{F}\{s^*(t)\} = \tilde{s}^*(f). \tag{2.9}$$

III *Symmetry.* The Fourier transform of a signal which is an even function of time is real, and the Fourier transform of a signal which is an odd function is imaginary.

IV *Duality.* A duality exists between the time domain and the frequency domain as expressed by the perfect symmetry of Eqs. (2.6) and (2.7). This can be expressed by

$$\mathcal{F}\{\tilde{s}(f)\} = s(-t). \tag{2.10}$$

V *Coordinate scaling theorem.* For any real-valued scaling constant α (in some fields referred to as the "magnification factor"),

$$\mathcal{F}\{s(\alpha t)\} = \frac{1}{|\alpha|}\tilde{s}(\frac{f}{\alpha}). \tag{2.11}$$

If we compress the function in the time domain, its frequency spectrum will be expanded, and vice versa. This phenomenon is called *reciprocal spreading* and is directly associated with the uncertainty relation discussed in Section 2.4.

VI *Time shifting* (delay/advance). The effect of the translation of the time origin by t_0 is described by

$$\mathcal{F}\{s(t-t_0)\} = \tilde{s}(f)e^{-j2\pi f t_0}. \tag{2.12}$$

VII *Frequency shifting* (modulation). This is the dual of the time shifting. For frequency-translation by f_0, we have

$$\mathcal{F}\{s(t)e^{-j2\pi f_0 t}\} = \tilde{s}(f-f_0). \tag{2.13}$$

VIII *Differentiation/Integration.* If ds/dt is square-integrable,

$$\mathcal{F}\left\{\frac{ds(t)}{dt}\right\} = j2\pi f\tilde{s}(f). \tag{2.14}$$

The derivative in the frequency domain is

$$\frac{d\tilde{s}(f)}{df} = \mathcal{F}\{-j2\pi t s(t)\}. \tag{2.15}$$

Differentiation in time enhances the frequency components of a signal, whilst integration in time suppresses them. Relations for the integration operation over time or frequency can be easily derived from Eq. (2.14) and (2.15).

IX *Convolution.* An important property of the Fourier transform is that it reduces the integral operation of convolution in time between two signals $s_1(t)$ and $s_2(t)$

$$s_1(t) * s_2(t) \equiv \int_{-\infty}^{+\infty} s_1(\tau) s_2(t-\tau) d\tau = \int_{-\infty}^{+\infty} s_1(t-\tau) s_2(\tau) d\tau \qquad (2.16)$$

to an algebraic product:

$$\mathcal{F}\{s_1(t) * s_2(t)\} = \tilde{s}_1(f)\tilde{s}_2(f). \qquad (2.17)$$

This is a very important theorem in the theory of linear systems. The dual property (frequency-convolution) is the following:

$$\mathcal{F}\{s_1(t)s_2(t)\} = \tilde{s}_1(f) * \tilde{s}_2(f). \qquad (2.18)$$

The spectra of modulated signals are easily obtained through frequency-convolution of the carrier and modulating signals, i.e. through multiplication of the two signals in the time domain.

X *Parseval's formula.* In the Fourier representation, Eq. (2.5) becomes

$$\int_{-\infty}^{+\infty} |s(t)|^2 dt = \int_{-\infty}^{+\infty} |\tilde{s}(f)|^2 df = E \qquad (2.19)$$

and provides the total energy of the signal. This is also known as the *energy theorem.*

2.3.3 Digital Signal Processing and the Discrete Fourier Transform

A signal which is defined on a discrete set of points in time is called a *discrete-time* signal or a *digital* signal; that is, a discrete-time signal can be described

by a sequence of complex or real numbers. In many cases, practical application involves digital data, even if the original signal is analogue. Manipulation of digital data is very popular nowadays due to the availability of fast analogue-to-digital (A/D) converters and powerful digital computers. The topic dealing with the theory of digital signals is known as Digital Signal Processing (DSP).

A discrete-time signal $s[n]$ can be obtained from a continuous-time signal $s(t)$ by means of sampling (usually uniform), provided that $s(t)$ is *band-limited*; i.e. it contains no frequency components above a certain frequency. The process of sampling can be considered as multiplication of the given continuous-time signal with a periodic train of unit impulses (i.e. δ-functions). It always produces a periodic spectrum.

The sufficient condition that there is no loss of information in the sampling process is given by *Shannon's (uniform) sampling theorem* [142] which states that "a band-limited real signal having no spectral components above f_b is completely described by uniformly spaced samples if the sampling frequency is greater than twice f_b". The critical frequency $f_s = 2f_b$ is called the *Nyquist rate* or the *folding frequency*. Sampling below the Nyquist rate results in overlapping of the individual spectra due to periodicity in the frequency domain (a phenomenon often referred to as *aliasing* or *interference*). In this case, complete reconstruction of the original continuous-time signal is impossible.

In practical situations, there are always limitations. Ideal samplers corresponding to delta-functions do not exist and natural signals are not strictly band-limited. However, it is generally acceptable that the energy content of a signal is negligible beyond a certain frequency.

For digital applications, a discrete version of the Fourier transform is necessary. The *Discrete Fourier Transform* (DFT) can be applied in the case of time-limited signals and assumes periodicity. The DFT of a finite discrete-time signal $s[n]$, $(n = 0, 1, ..., N-1)$ is defined by

$$\tilde{s}[k] = \sum_{n=0}^{N-1} s[n] e^{-j2\pi kn/N}, \quad k = 0, 1, .., N-1 \,, \tag{2.20}$$

where k is the variable in the frequency domain. The *Inverse Discrete Fourier*

Transform (IDFT) is given by

$$s[n] = \frac{1}{N} \sum_{k=0}^{N-1} \tilde{s}[k] e^{j2\pi kn/N}, \quad n = 0, 1, .., N-1. \tag{2.21}$$

It can be seen that the DFT produces a discrete frequency spectrum. Numerically, the DFT is equivalent to the well-known Fourier series for periodic discrete-time signals. Many of its properties correspond to properties of the continuous Fourier transform, but generally the discrete case can not be derived directly from the continuous case.

The DFT method is the basic tool of modern digital signal analysis. Only for ill-posed problems, the aliasing effect may present a considerable limitation in its practical use. For the analysis of an N-point digital signal, the ordinary DFT algorithm requires N^2 complex multiplications. A more efficient algorithm for DFT computation, known as the *Fast Fourier Transform* (FFT), was developed by Cooley and Tukey in 1965 [40]. The FFT reduces dramatically the amount of required calculations (only $N \log_2 N$ multiplications are required for an N-point transform). It offers not only enormous savings in computer processing time, but also better accuracy. The FFT algorithm has been used with overwhelming success for a wide range of digital processing problems.

2.3.4 Limitations of the Fourier transform representation

The Fourier transform is an integral transformation which provides a representation of the frequency content of a signal. It offers a powerful theoretical framework and possesses many important properties that have been widely used in applications of telecommunications and signal processing. Additionally, in the discrete case, its calculation is very fast and efficient.

Its ability to provide meaningful interpretation, however, is limited, based on an assumption of periodicity or stationarity. In the case of signals which are time-varying in nature or possess some random non-stationary features, ordinary Fourier analysis fails to describe the dynamics of change of the frequency components.

The basic limitation of the traditional Fourier transform techniques is that

the frequency information arises from averaging over the complete duration of the signal. Indeed, the Fourier integral of Eq. (2.6) extends over all time from $-\infty$ to $+\infty$. This means that, if at some point in the lifetime of the signal, a particular feature is present, this will be taken into account for the calculation of the Fourier transform, but its specific location on the time axis will be lost. This fact makes it impossible to determine the position or the duration of the lifetime of a single frequency component and it is related to the uncertainty principle in communication theory.

2.4 The Uncertainty Principle in Communication Theory

The scaling property of the Fourier transform described by Eq. (2.11) implies that a signal $s(t)$ and its Fourier transform $\tilde{s}(t)$ can not both be of short 'duration'. The unit impulse $\delta(t)$, which is a signal of zero 'duration' in the time domain, provides a characteristic example of *reciprocal spreading*. Indeed, its Fourier transform is constant (equal to 1) over the whole frequency axis; i.e., the 'duration' in the frequency domain is infinite. This type of uniform spectrum is called *white*, in analogy to white light.

Let us quantify the abstract term 'duration', by defining an effective width and an effective bandwidth in the time and frequency domain respectively. Given a (generally complex) signal $s(t)$, the *effective width* along the time axis of the signal is

$$\Delta t = \left[\frac{\int_{-\infty}^{+\infty} (t - \langle t \rangle)^2 s(t) s^*(t) dt}{\int_{-\infty}^{+\infty} s(t) s^*(t) dt} \right]^{1/2} \tag{2.22}$$

and the *effective bandwidth* along the frequency axis of the signal is

$$\Delta f = \left[\frac{\int_{-\infty}^{+\infty} (f - \langle f \rangle)^2 \tilde{s}(f) \tilde{s}^*(f) df}{\int_{-\infty}^{+\infty} \tilde{s}(f) \tilde{s}^*(f) df} \right]^{1/2} . \tag{2.23}$$

The effective widths of Eq. (2.22) and (2.23) represent standard deviations in time and frequency and they are sometimes referred to as *uncertainties*.

From Eqs. (2.22) and (2.23), it can be easily derived that the *time(width)-bandwidth* or *uncertainty product* $\Delta t \cdot \Delta f$ has to satisfy the uncertainty inequality:

$$\Delta t \cdot \Delta f \geq \frac{1}{4\pi}. \tag{2.24}$$

The time-bandwidth product has a lower bound and this fact prohibits an arbitrarily sharp frequency discrimination from being possible within an arbitrarily short period of time, or vice versa. The inequality of Eq. (2.24) is called the *uncertainty relation* of information theory or the *Gabor-Heisenberg inequality*. It can be noticed that there is a straightforward analogy to the well-known Heisenberg's uncertainty principle found in quantum mechanics; the time-frequency duality corresponds to the position-momentum duality of quantum mechanics [76], [175]. In the context of the theory of communication, the uncertainty relation was rigorously derived by D. Gabor in 1946 [63]. It implies that bandwidth and time-width are irreconcilable quantities. High resolution can not be obtained simultaneously in both the time domain and the frequency domain.

The dimensionless uncertainty product $\Delta t \cdot \Delta f$ is an important parameter in signal processing applications. For example, it can be intentionally increased or decreased (down to its lower bound) according to the specific design requirements (eg. for radar design, design of spread-spectrum systems etc.). In applied signal processing, the uncertainty relation renders the trade-off between temporal and spectral resolutions unavoidable.

There is a case that this trade-off is optimised; indeed, it can be proven that a Gaussian signal (or Gaussian pulse), that is, a signal of the form $\exp[-t^2/(2\sigma^2)]$, exhibits a minimum time-bandwidth product. Gaussian signals are signals of minimum uncertainty , in the sense that $\Delta t \cdot \Delta f = (4\pi)^{-1}$.

The fact that there is an uncertainty principle in both signal theory and quantum theory often leads to misconceptions and there has been a lot of confusion in the past about proper interpretation; therefore, a distinction between the two uses of the uncertainty relation should always be made [151, 38]. In quantum mechanics, it expresses the inherent uncertainty, in a probabilistic sense, related to the measurement of physical quantities. In signal theory, it refers to the mathematical fact that a signal and its Fourier transform can not be made arbitrarily narrow. A further discussion about the relation between signal processing and quantum mechanics will be done in Chapter 3.

2.5 Autocorrelation functions

The *autocorrelation function* $Q_s(t)$ of a signal $s(t)$ is defined by

$$Q_s(\tau) = \int_{-\infty}^{\infty} s(t+\tau/2)s^*(t-\tau/2)dt. \tag{2.25}$$

The autocorrelation function of a signal provides information about the degree of dependence of the value of the signal at some instant in time on its values at other instants. It is used for time-domain analysis.

In the case of random signals, the *power spectral density* (PSD) or simply *power spectrum* corresponds to the energy spectral density (Section 2.3). The power spectral density $S_s(f)$ of a signal $s(t)$ is given by

$$S_s(f) = |\tilde{s}(f)|^2. \tag{2.26}$$

The power spectral density describes the relative amount of energy at various frequencies. The total area under $S_s(f)$ is the energy of the signal. The power spectral density is used for *spectral analysis* (in the frequency domain) and contains no phase information.

The autocorrelation function and the power spectral density function are related according to the *Wiener-Khintchine theorem*:

$$S_s(f) = \int_{-\infty}^{+\infty} Q_s(t)e^{-j2\pi ft}dt; \tag{2.27}$$

that is, the power spectral density $S_s(f)$ of the signal $s(t)$ is the Fourier transform of the signal's autocorrelation function.

Our study so far has been based on the assumption of stationarity. However, this is not the case for many of the signals encountered in every day practice. Physical signals, quite often, are time-varying, that is, *non-stationary*. Because of their time-dependent behaviour, non-stationary signals do not possess an ordinary spectral density and can not be successfully analysed using the ordinary Fourier methods.

2.6 Discussion

In Section 2.3, it was stated that the Fourier transform method is based on the stationarity assumption. It seems that, in general, weakly stationary signals can be successfully represented in the frequency domain by the ordinary spectral density (Section 2.5); but in the case that a signal is only *locally* stationary or generally non-stationary, the ordinary spectral analysis is not sufficient.

It becomes clear that the disadvantages of the Fourier analysis have their greatest effect in the case of random non-stationary signals; the Fourier spectrum is unable to provide the all-essential 'instantaneous' information contained in the signal. The notion of a *time-varying spectrum* can be considered as a generalisation of the ordinary spectrum, preserving all the useful properties of the Fourier transform representation, but also describing the time-varying change in the frequency domain.

Chapter 3

An Introduction to Time-Frequency Signal Analysis

3.1 Introduction

The difficulties of the classical Fourier analysis for the case of non-stationary signals have been presented in the previous chapter. To overcome the problems of the processing of non-stationary signals, alternative methods have been considered. Most of these methods use two-dimensional time-frequency representations. These joint representations describe successfully the time-varying frequency characteristics of a non-stationary signal. They provide a means for isolating the signal features of interest in the time-frequency plane (eg. amplitude and frequency non-stationarities in harmonic signals) and they are particularly suitable for applications in random and/or non-stationary signal analysis. Recently, time-frequency representations have found applications in areas as diverse as speech analysis/synthesis, radar, geophysics, musical voice synthesis, sonar, image processing, audio engineering, biology and biomedicine.

Historically, the first ideas toward time-frequency analysis are found in the classic works of D. Gabor [63] and J. Ville [173], who pointed out the analogy between communication theory and quantum mechanics. In Gabor's pioneering paper, the *uncertainty relation* of communication theory is rigorously derived,

the *"instantaneous frequency"* is suggested as a useful concept, the *Gaussian expansion* (later to be known as the Gabor expansion) in terms of elementary signals is introduced and a predecessor to the *analytic signal* is presented. This Gaussian expansion, referred to as "information diagram" in Gabor's paper, was chronologically the first joint time-frequency signal representation.

It is clear that concepts of instantaneous information (such as instantaneous frequency or instantaneous power) are very important in time-frequency analysis. The notion of "instantaneous frequency" was further studied by J. Ville [173]. An early definition of the instantaneous frequency describes it as the rate of change of the phase of a time-varying signal, which was found to be equivalent to the derivative of the phase of Ville's analytic form. Later, in the light of the formulated joint time-frequency representations, the instantaneous frequency was defined as the average frequency at a particular point in time (see Section 3.2). Linearity of the instantaneous frequency is a highly desirable property in time-frequency signal analysis.

3.2 A Short Review of Time-Frequency Representations

Joint time-frequency representations (sometimes referred to as "conjoint" or "time-scale" representations) map a one-dimensional signal $s(t)$ into a two-dimensional function $Y(t, f)$ in order to extract meaningful information. They provide a more complete description of a non-stationary signal than the traditional (single-domain) Fourier representation; the one-dimensional signal representations (time description $s(t)$ or Fourier transform $\tilde{s}(f)$) are just special cases of a joint representation. Two of the most popular time-frequency methods used in modern digital spectral analysis - which are conceptually close to the traditional Fourier transform - are the Short-Time Fourier Transform and the Wigner-Ville method.

The *Short-Time Fourier Transform* (STFT) is a complex-valued representation. It performs local spectral analysis using a short window centred at time t. A local spectrum is thus obtained which describes the frequency content of

the signal at time t. The window is shifted covering the complete time domain of the signal and in this way, the Short-time Fourier transform provides a two-dimensional local spectrum description. The notion of instantaneous frequency, as proposed by J. Ville, can be applied.

The uncertainty principle presents a fundamental problem to Short-time Fourier transform analysis. Using a short window (high resolution in time) automatically means that the frequency resolution of the local spectrum will be low, and vice versa. The two requirements of a short window in the time domain and of a narrow bandwidth in the frequency domain are in contradiction. A trade-off has to be made between the frequency resolution and the observation time (length of data window which determines the time resolution) and this is a major disadvantage. The squared magnitude of the Short-time Fourier transform offers a real-valued alternative and is sometimes referred to as the *spectrogram* or equivalently the *periodogram*.

The second approach is the *Wigner-Ville* or *Wigner Distribution function* method. E.P. Wigner first used this representation in quantum mechanics [188]. The Wigner Distribution function is a two-dimensional real-valued function of time and frequency and was first applied to signal analysis by J. Ville [173]. The Wigner function representation overcomes the drawbacks of the Short-time Fourier transform method. However, the fundamental uncertainty principle of signal theory is incorporated in the mathematical structure of the Wigner distribution function and limits its resolutional ability. The Wigner-Ville technique will be discussed extensively in the next chapter.

The Wigner distribution function belongs to a family of energetic time-frequency distributions known as the Cohen's generalised class first introduced in an important paper by Cohen in 1966 [37]. Time-frequency distributions of the Cohen's class are bilinear functions of time and frequency which are designed to satisfy certain desirable properties (such as the time and frequency marginal energy distributions and reduced interference). They share the same general formulation and they are uniquely characterised by a two-dimensional function referred to as the *time-frequency kernel* [35]. The properties of a time-frequency distribution are directly related to conditions of the characteristic kernel. Due to

its unique properties, the Wigner distribution function is the ideal time-frequency distribution in many respects (see Section 4.2). Other members of Cohen's general class of joint energy representations which are of current interest are:

i the Page distribution [120],

ii the Rihaczek distribution [131],

iii the Choi-Williams (or exponential) distribution [31],

iv the Born-Jordan distribution [38],

v the cone-kernel distribution [200], and

vi the minimum variance distribution [75].

The spectrogram is also a special case in this family. A detailed review of time-frequency distributions of the Cohen's general class can be found in [38].

Other time-frequency representations, which do not use the ordinary harmonic analysis, are the Gabor transform, the wavelet transform, and the Bargmann representation. These methods are based on analytic functions and their potential for signal processing applications is significant because of the powerful analytic properties.

The Gabor transform and the wavelet transform decompose a signal in terms of alternative orthogonal basis functions. These functions are localised in time and frequency. The Gabor transform uses a Gaussian basis and the wavelet transform uses a wavelet basis consisting of special functions called wavelets. Both methods are particularly suitable for non-stationary signal analysis. Although these methods are mathematically complex, the numerical algorithms involved are very fast. The Gabor transform was first introduced in the early paper of D. Gabor back in 1946 [63] , while the use of wavelets originated from the analysis of earthquake records [69]. These methods are now significant tools in signal analysis and have found important applications in speech, random vibration and radar signal analysis, and more recently in image processing. Using these methods, the major disadvantage of Fourier transform techniques is overcome by breaking a

signal down into well-localised elements. In recent years, the wavelet analysis has enjoyed popularity and has been extensively studied with a vast and still growing rapidly bibliography [46, 47, 48, 110, 117].

Another representation used in quantum mechanics is the Bargmann analytic representation. In the context of signal analysis, the Bargmann analytic function has not been used so far, although it provides an alternative time-frequency representation and has been successfully applied in other fields.

In the following chapters, the Wigner-Ville method, the Gabor transform and the Bargmann representation are presented and examined from a signal theoretic point of view. The common mathematical background of these methods lies on the theory of quantum mechanics and here the potential of each method for signal processing applications is explored. Special emphasis is given to practical applications in optical signal analysis. The use of these methods as signal synthesis aids and as diagnostic tools for real-life random processes will be demonstrated. Furthermore, relations between the various time-frequency representations will be studied and some useful conclusions derived.

3.3 Signal Processing and Quantum Mechanics

From our discussion on the uncertainty principle in signal theory (Section 2.4) as well as the 'mathematical origin' of the various time-frequency representations, it is clearly indicated that there is a formal *mathematical analogy* between signal analysis and modern quantum theory. At an early time, the original papers of Gabor and Ville pointed out the quantum-mechanical influence on the work on time-frequency methods.

The similarities between the two different fields originate from the fact that, in quantum theory, the probability associated to momentum is given by the squared modulus of the Fourier transform of the wave function. The time and frequency pair of signal theory can be thus associated with the position and momentum pair of quantum mechanics correspondingly. Additionally, the same kind of association can be made between the signal and the wave function as well as between the signal energy and the probability for finding the particle at

a certain position. The time-frequency space corresponds to the so-called *phase space* in quantum mechanics and sometimes the latter is used in the context of signal processing as well. For these reasons, between the two fields there is a very good mathematical correspondence.

Despite this formal analogy, there exist significant fundamental differences. The quantum-mechanical theory is inherently probabilistic, while in signal theory this is not generally the case; only a stochastic signal can be considered in a probabilistic sense. Another important difference is that the physical quantities of quantum mechanics are described by operators instead of functions. This is the reason why signals do not suffer quantisation. That said, there is a great similarity between the theory of hermitian operators in quantum mechanics and the so-called *hermitian representation* of square-integrable signals. It has been known that many of the properties of time-frequency representations can be derived from an hilbertian condition [58].

Even though their conceptual differences are important, the mathematical analogies between signal theory and single-particle (non-relativistic) quantum mechanics can often be quite useful and the two fields may share the same numerical techniques, but not to an unlimited extend. Sometimes, interpretation of the formulae can be dramatically different. One has to be cautious in transcribing quantum-mechanical relations to the language of signals since this may yield results which are totally meaningless in a signal-theoretical sense.

3.4 The Notion of the Analytic Signal

For the calculation of time-frequency representations, it is generally convenient to use not the original real signal but the so-called *analytic signal* (or *pre-envelope*) associated with the real signal (the idea was originally proposed by J. Ville). The analytic signal was first applied in radar signal analysis and later on, has been used as a useful theoretical tool in various time-frequency methods. The following analysis considers only one-dimensional signals.

Let $u(t)$ be a real signal in time. The corresponding analytic signal is defined

as:

$$s(t) = u(t) + jv(t), \tag{3.1}$$

where $v(t)$ is given by the *Hilbert transform* of $u(t)$. It is common practice that the total energy in the signal is normalised:

$$\int_{-\infty}^{\infty} |s(t)|^2 dt = 1. \tag{3.2}$$

It is convenient to employ the normalising conventions of the quantum mechanical theory, since this enables the direct mathematical analogy between signal processing and quantum mechanics to be easily identified.

In his early paper, Gabor had suggested a different complex form of the signal which is known as the *exponential* or *quadrature representation*. This provides a good approximation of the Hilbert-transform analytic representation, particularly if the real signal is narrowband; that is, it contains frequencies only in narrow bands about a certain frequency $\pm f_0$. The Hilbert-transform signal $s(t)$ of Eq. (3.1) is called the analytic signal since the generalised signal $s(z)$ is an analytic function (the complex number z lies in the upper half of the complex plane and $z_R \equiv \mathrm{Re}z$ is the time variable); that is, it satisfies the important *Cauchy-Riemann* equations:

$$\frac{\partial u}{\partial z_R} = \frac{\partial v}{\partial z_I}, \tag{3.3}$$

$$\frac{\partial u}{\partial z_I} = -\frac{\partial v}{\partial z_R}, \tag{3.4}$$

where z_I is the imaginary part of z. In fact, the Hilbert-transform signal of Eq. (3.1) is the *only* complex signal that satisfies the requirement of analyticity.

This complex representation consists in working solely in terms of the positive frequencies [189]; as described by Gabor [63], this can be achieved by removing the amplitudes belonging to negative frequencies from the spectrum of the real signal and multiplying the amplitudes of positive frequency by 2. In this way, the total energy of the original real signal is preserved. This process is equivalent to the process described by Eq. (3.1). In terms of the previous definition of the analytic signal, the concept of instantaneous frequency can be well described by the phase of the analytic signal, particularly for narrowband signals.

There are several advantages in using the analytic signal for applications of time-frequency analysis:

- The instantaneous frequency can be defined in terms of the analytic signal.
- Aliasing in discrete implementations is avoided and a sampling rate equal to the standard Nyquist rate is maintained.
- Interference terms between positive and negative frequencies are eliminated.
- Information in the negative frequency band of real signals is redundant.
- Calculations are more straightforward.

Very often the very first step to the calculation of a time-frequency representation of a signal is the required calculation of the associated analytic form. The analytic signal approach leads to a convenient implementation since the calculation uses the Hilbert transform.

The Hilbert transform of the signal $u(t)$ is defined by

$$v(t) = \frac{1}{\pi} P \int_{-\infty}^{\infty} \frac{u(\alpha)}{t-\alpha} d\alpha, \tag{3.5}$$

where P stands for the Cauchy principal value of the integral at $\alpha = t$. In the context of linear system theory, Hilbert transform represents the response (to the real signal $u(t)$) of the so-called *quadrature filter*. This filter is described by the transfer function:

$$H(f) = -j \operatorname{sgn} f, \tag{3.6}$$

where f denotes the variable in the frequency space. The corresponding impulse response is equal to $1/\pi t$ and it follows that the Hilbert transform can be given by the convolution:

$$v(t) = u(t) * \frac{1}{\pi t}, \tag{3.7}$$

which enables us, by Fourier transforming both sides of Eq. (3.7), to get a simple expression of the Fourier transform of $v(t)$:

$$\tilde{v}(f) = -j\tilde{u}(f) \operatorname{sgn} f, \tag{3.8}$$

where the tilde denotes the Fourier transform operation. The inverse of the Hilbert transform of Eq. (3.5) is:

$$u(t) = -\frac{1}{\pi} P \int_{-\infty}^{\infty} \frac{v(\alpha)}{t-\alpha} d\alpha. \tag{3.9}$$

From Eqs. (3.1), (3.8), the Fourier transform of the analytic signal can be obtained:

$$\tilde{s}(f) = \begin{cases} 2\tilde{u}(f) & , \quad f > 0; \\ \tilde{u}(f) & , \quad f = 0; \\ 0 & , \quad f < 0. \end{cases} \tag{3.10}$$

The imaginary part $v(t)$ of the analytic signal is sometimes called the *quadrature signal*, because its frequency components are in phase quadrature with those of the real signal $u(t)$ (i.e. their phase difference is 90^o).

Practical applications usually require discretisation of the original continuous-time signal (see Section 3.3). The discrete-time analytic signal of a finite discrete signal $u[n]$ is of the form:

$$s[n] = u[n] + jv[n], \tag{3.11}$$

where the imaginary part $v[n]$ is given by the Discrete Hilbert transform of $u[n]$. From the previous analysis, it is evident that the Discrete Hilbert transform can be computed using powerful FFT algorithms. In processing applications, after analysis has been carried out using the Hilbert transform representation, the real signal can be recovered by taking the real part of the resulting analytic signal. Numerical algorithms are presented in Appendix B.

3.5 Application in Optical Signal Processing

As a real-life example, the analytical signal representation of a given real signal $u(t)$ (Fig. 1) was calculated. This is an optical signal occurring when monitoring a power switch (see Appendix A). Such signals are obviously highly non-stationary. They provide useful information about the condition of power electronic devices and can be used for optical monitoring and maintainance management of systems. For numerical implementation, the discrete-time version of the signal was used

(see Eq. (3.11)). The given signal was sampled at a rate of $40kHz$ and contains 2,380 points.

The first step of the analysis was the calculation of the Fourier transform of the signal $u(t)$ using an FFT algorithm. The modulus of the Fourier transform of $u(t)$ is shown in Fig. 3.4. It is evident that $u(t)$ can be considered as a narrowband signal. Thus, we are able to evaluate the analytic form of the signal using the method described earlier.

Using Eq. (3.8), we calculated the Fourier transform of the Hilbert transform of the original signal (see Appendix B). The Hilbert transform $v(t)$ was then derived by an inverse FFT. The Hilbert transform $v(t)$ is the imaginary part of the analytic signal and is shown in Fig. 3.2. Given that the real part is the original signal $u(t)$, we can easily obtain the modulus of the analytic form $s(t)$ of $u(t)$ (Fig. 3.3).

The modulus of the Fourier transform of the analytic signal $s(t)$ is illustrated in Fig. 3.5 (where, for the sake of detail, the dc contribution has been omitted).

A comparison between Fig. 3.4 and Fig. 5.5 reveals that the analytic signal has a one-sided spectrum that consists only of the positive frequencies of the real signal which have double amplitudes.

3.6 Discussion

Time-frequency representations and the concept of the analytic signal have been discussed. Joint time-frequency representations provide the means to deal with 'traditional' problems of signal analysis. Time-frequency analysis has a preference for analytic signals because, in this way, the instantaneous frequency is defined. The analytic signal can be generally applied to narrowband signals and provide information about the instantaneous characteristics of signals. The above analysis will become very useful for the methods presented in the chapters that follow.

Figures

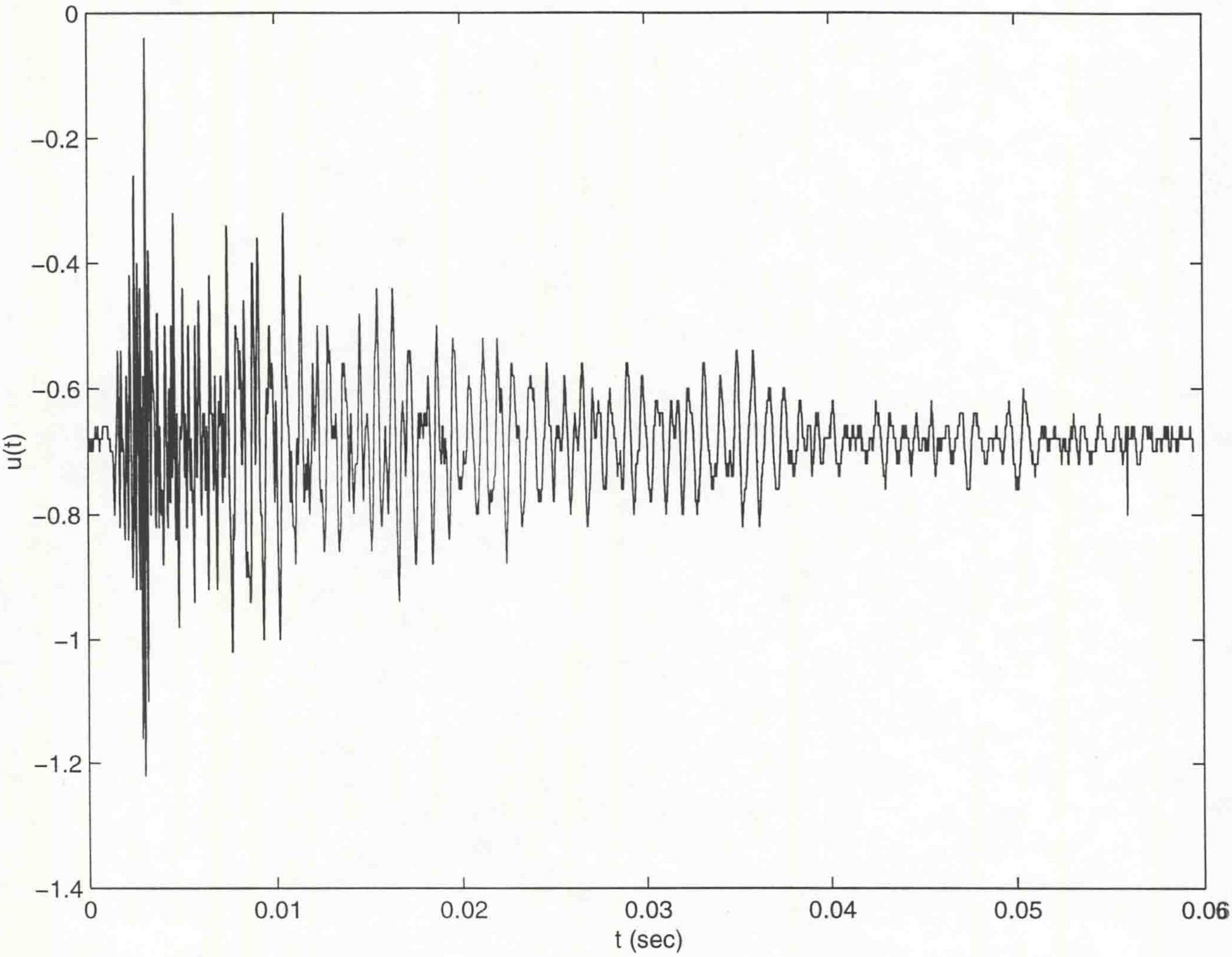

Figure 3.1: An optical signal ($u(t)$) taken from the emission of a power switch.

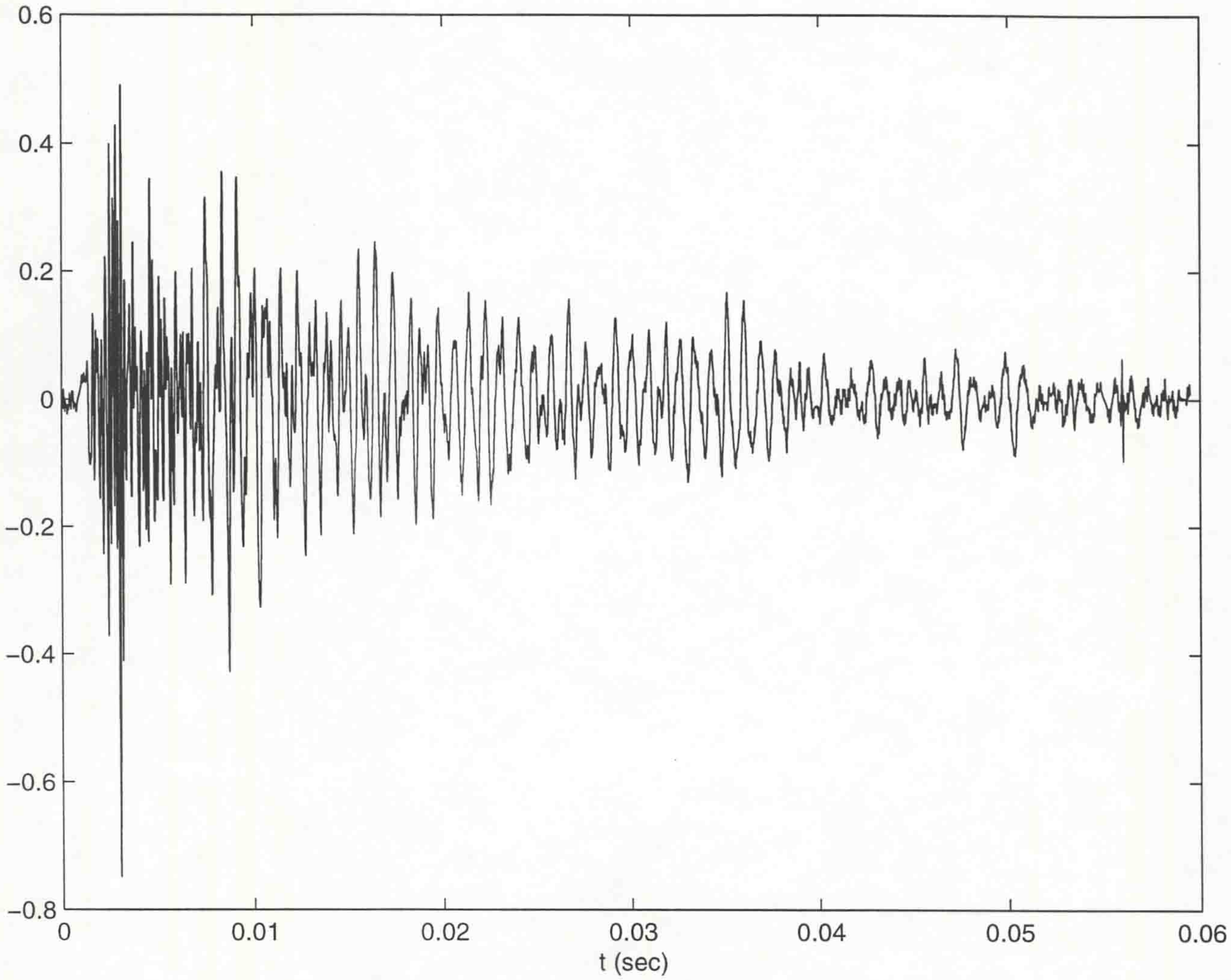

Figure 3.2: The imaginary part $v(t)$ of the analytic form $s(t)$ of the given real signal $u(t)$; that is, the Hilbert transform of $u(t)$.

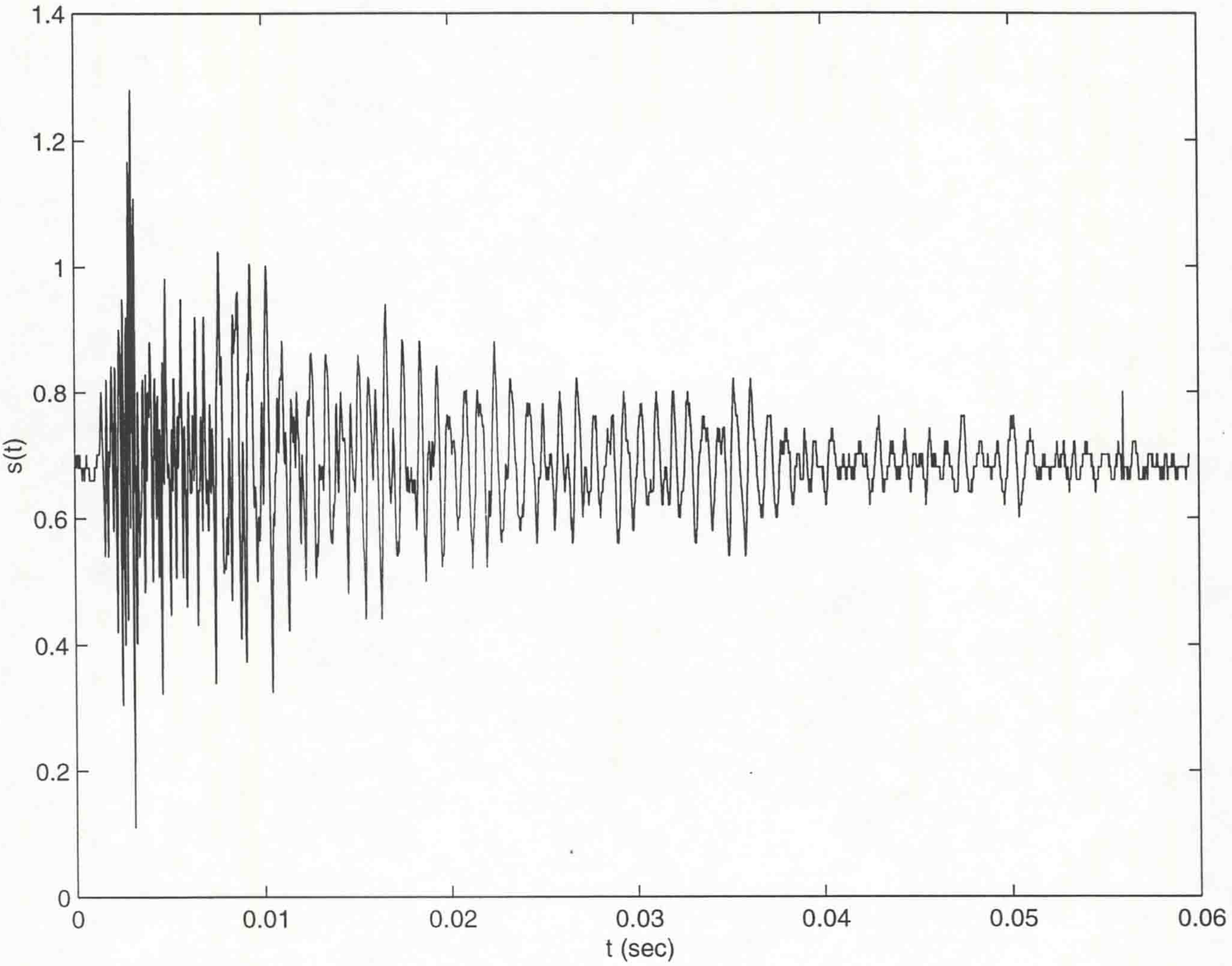

Figure 3.3: The modulus of the analytic signal $s(t)$ corresponding to the real signal $u[n]$.

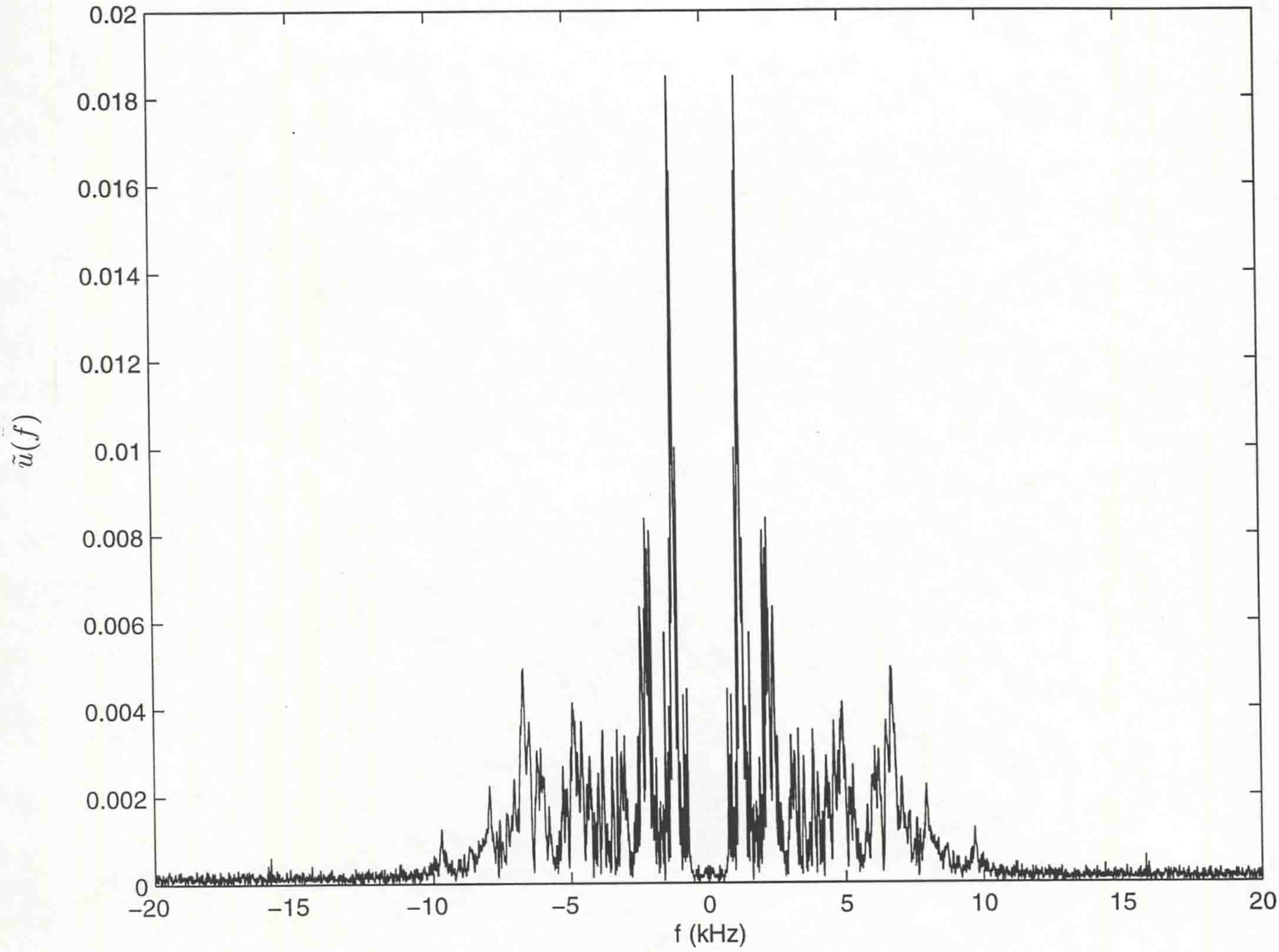

Figure 3.4: The modulus of the Fourier transform of the real signal $u(t)$.

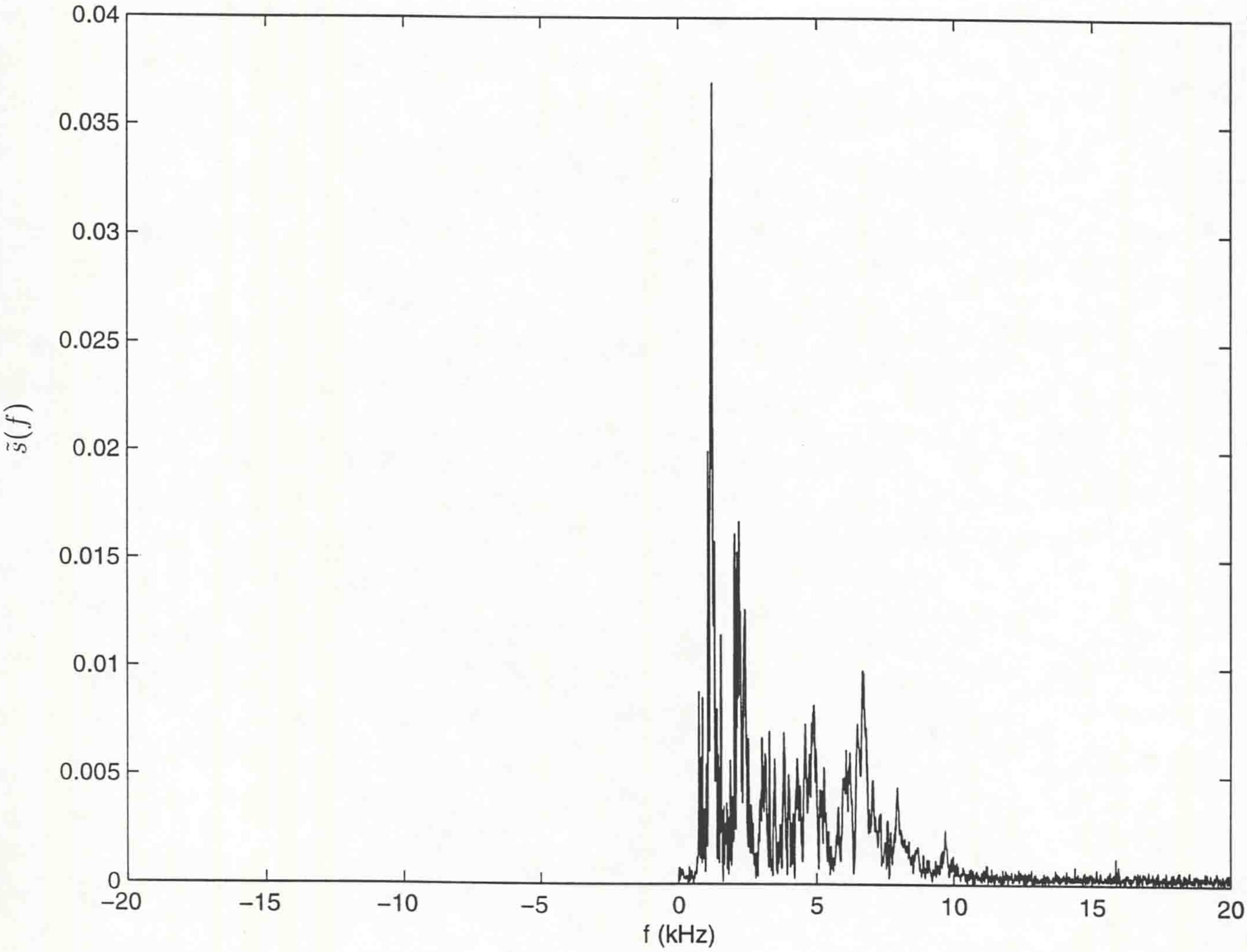

Figure 3.5: The modulus of the Fourier transform of the analytic signal $s(t)$.

Chapter 4

The Wigner Distribution Function Representation and Applications in Optical Signal Processing

4.1 Introduction

Let $u(t)$ be a real square-integrable signal in time. As described earlier, the corresponding analytic signal is given by

$$s(t) = u(t) + jv(t), \tag{4.1}$$

where $v(t)$ is given by the Hilbert Transform of $u(t)$, as mentioned earlier (Chapter 3). As in previous chapters, the total energy in the signal is usually considered to be normalised:

$$\int_{-\infty}^{+\infty} |s(t)|^2 dt = 1. \tag{4.2}$$

The *Wigner* (or *Wigner-Ville*) distribution function is a bilinear (quadratic) signal representation. It was first introduced by Wigner [188] in 1932 within the context of quantum mechanics and soon became a representation of great significance that provided insight into the connection between quantum and classical

mechanics. It was later proposed by Ville [173] in the context of signal theory and recently became very popular with applications in many areas of signal processing. It is suitable for representing a signal in both time and frequency domains (or, in the case of images, in the spatial and spatial frequency domains) and its popularity is, to a large extend, due to the fact that the Wigner Distribution Function (WDF) possesses a plethora of attractive properties.

The Wigner representation is unique and theoretically optimal in the sense that it satisfies a maximum number of desirable mathematical properties and features optimal time-frequency concentration. As mentioned earlier, the Wigner-Ville representation is the prominent member of Cohen's generalised class of joint representations, associated with the simplest kernel (equal to unity). In the context of signal processing, the Wigner distribution function provides an accurate characterisation of the energy density distribution in the time-frequency plane and it is a powerful tool for local frequency analysis since it describes the dynamics of change in the frequency components through the signal's lifetime.

The cross-Wigner distribution function of two signals $f(t)$ and $g(t)$ is given by

$$W_{f,g}(t,f) = \int_{-\infty}^{+\infty} e^{-j2\pi f\tau} f(t+\tau/2) g^*(t-\tau/2) d\tau. \tag{4.3}$$

The auto-Wigner distribution function (AWDF) of $s(t)$ is defined as

$$W_s(t,f) = \int_{-\infty}^{+\infty} e^{-j2\pi f\tau} s(t+\tau/2) s^*(t-\tau/2) d\tau. \tag{4.4}$$

The analogy to single-particle non-relativistic quantum mechanics is straightforward (the time and frequency variables of signal theory correspond to the position and momentum variables of quantum mechanics). At this point, it would be worth to note that the word "distribution" here is not used in the strict probabilistic sense, although for stochastic non-stationary signals this would be exactly the case. In general, for time-frequency analysis, "distribution" means *intensity* or *energy density* and it may have negative values, in contrast to the standard terminology of probability theory. In the following sections, WDF will always denote the auto-WDF, unless it is otherwise stated.

According to Eq. (4.4) and Eq. (2.25), the WDF is related to the *instantaneous* autocorrelation function $R_s(\tau;t)$ of $s(t)$ (see Chapter 2) defined by

$$R_s(\tau,t) = s(t+\tau/2)s^*(t-\tau/2). \tag{4.5}$$

The Fourier transform of $R_s(\tau,t)$ provides the instantaneous spectral density function

$$D_s(f;t) = \int_{-\infty}^{+\infty} e^{-j2\pi f\tau} R_s(\tau,t)d\tau \equiv W_s(t,f). \tag{4.6}$$

It is clear that the Wigner function of a signal can be viewed as an instantaneous spectral density.

An interesting problem in signal processing would be to identify a signal with a *rotationally invariant* WDF. This case corresponds to a uniform 'distribution of uncertainty' in the time-frequency plane. Drawing the analogy to the well-known solution of quantum mechanics (number eigenstates), the corresponding signal waveform is given by the following relation [98, 78]:

$$h_n = 2^{1/4}(2^n n!)^{-1/2}\exp(-\pi t^2)H_n(\sqrt{2\pi}t)\ , \quad n = 0,1,... \tag{4.7}$$

where $H_n(t)$ is the nth-order Hermite polynomial:

$$H_n(t) = (-1)^n \exp(t^2/2)\frac{d^n}{dt^n}\exp(-t^2/2)\ . \tag{4.8}$$

The WDF of these *Hermitian signals* has a rotational symmetry and it is given by:

$$W_h^{(n)}(t,f) = (2\pi)^{-1/2}(-1)^n e^{-2\pi(t^2+f^2)}\mathbf{L}_n[4\pi(t^2+f^2)], \tag{4.9}$$

where $\mathbf{L}_n$ is the nth-order Laguerre polynomial [1]:

$$\mathbf{L}_n(t) = \sum_{l=0}^{n}\frac{n!(-t)^l}{(n-l)!l!}\ . \tag{4.10}$$

The Hermitian signals $\{h_n\}$ form a complete orthonormal basis which can be useful in signal analysis.

The potential fields of application of the WDF in a signal theoretical context are numerous: signal detection and classification, time-varying filter design, Fourier and ray optics, loudspeaker design, radar Doppler theory, texture analysis, sonar, biomedicine etc. The WDF representation can be happily used in

conjunction with modern signal estimation techniques [129] (especially in the non-stationary case). In this chapter, application of the WDF in the processing of time-varying optical signals will be presented.

There are two ways to evaluate the WDF of an optical signal (the exact evaluation being generally impossible):

1. Purely optical means to obtain an approximation of Eq. 4.4. Fourier methods are the foundations of the modern optical system theory. The WDF representation has been applied to provide an alternative way of optical generation and analysis yielding significant results [15, 11]. It has successfully led to the connection between different viewpoints of optical theory.

2. Discretisation of the analogue signal. For practical implementation of real-life signals, one usually has to deal with digital or digitised data. For this reason, actual signals can be analysed using the Discrete Wigner distribution function (DWDF) which will be introduced in a later section.

The following sections will concentrate on the application of the WDF in the processing of sampled optical signals. Purpose-developed software is found in Appendix B. The interest in the employed techniques is demonstrated by various results. Several types of optical signals are analysed using the Wigner Distribution Function representation. The aim of this analysis is the characterisation and interpretation of these signals and the extraction of meaningful features. The analysis is restricted to one-dimensional signals. In the following section, some known properties of the WDF are reviewed briefly to provide understanding of the signal representation application.

4.2 Properties of the Wigner Distribution Function

The (auto)Wigner Distribution Function has many important properties which are very useful for signal analysis [35, 193, 81]. The basic properties of the Wigner Function are summarised as follows:

I *Unicity.* The Wigner representation is unique in the sense that it is the only Time-Frequency representation which provides:

- the ordinary spectrum if the signal is stationary,
- time-frequency linearity, and
- linear modulation and filtering.

II If $\tilde{s}(f)$ is the Fourier transform of $s(t)$, then:

$$W_{\tilde{s}}(f,t) = \int_{-\infty}^{+\infty} e^{j2\pi\phi t}\tilde{s}(f+\frac{\phi}{2})\tilde{s}^*(f-\frac{\phi}{2})d\phi \tag{4.11}$$

and

$$W_{\tilde{s}}(f,t) = W_s(t,f). \tag{4.12}$$

Eqs. (4.11), (4.12) show the *symmetry* between the time and the frequency domain.

III The Wigner function is always a *real-valued* function:

$$W_s(t,f) = W_s^*(t,f). \tag{4.13}$$

IV For a real signal $u(t)$, the WDF is an *even* function of frequency:

$$W_u(t,f) = W_u(t,-f). \tag{4.14}$$

V *Time Shift.* If $g(t) = f(t-t_0)$, then:

$$W_g(t,f) = W_s(t-t_0,f). \tag{4.15}$$

This is called the shift property of the WDF.

VI *Frequency Shift.* If $g(t) = s(t)e^{j2\pi f_0 t}$, then:

$$W_g(t,f) = W_s(t,f-f_0). \tag{4.16}$$

This is known as the modulation property of the WDF.

VII The integration of the WDF with respect to frequency gives the *instantaneous signal power*:

$$\int_{-\infty}^{+\infty} W_s(t,f)df = |s(t)|^2. \tag{4.17}$$

VIII The integration of the WDF with respect to time provides the *power density spectrum* of the signal:

$$\int_{-\infty}^{+\infty} W_s(t,f)dt = |\tilde{s}(f)|^2. \tag{4.18}$$

IX The first-order moment of the WDF with respect to frequency gives the *instantaneous frequency* $\phi(t)$ of the signal:

$$\phi(t) = \int_{-\infty}^{+\infty} fW_s(t,f)df. \tag{4.19}$$

X The first-order moment of the WDF with respect to time gives the *group delay* $\tau(f)$:

$$\tau(f) = \int_{-\infty}^{+\infty} tW_s(t,f)dt. \tag{4.20}$$

XI *Moyal's formula.* The integral of the square of the WDF gives the square of the total energy of the signal:

$$\int_{-\infty}^{+\infty}\int_{-\infty}^{+\infty} |W_s(t,f)|^2 dtdf = \left|\int_{-\infty}^{+\infty} |s(t)|^2 dt\right|^2. \tag{4.21}$$

Moyal's formula is the analogon to Parseval's theorem.

XII *Convolution property.* If $s(t) = g(t) * h(t)$, then:

$$W_s(t,f) = W_g(t,f) * W_h(t,f), \tag{4.22}$$

where the convolution operation acts with respect to time.

XIII *Windowing property.* If $s(t) = g(t)h(t)$, then:

$$W_s(t,f) = W_g(t,f) * W_h(t,f), \tag{4.23}$$

where the convolution operation acts with respect to frequency.

XIV *Negativity.* The WDF is not always positive. The fact that it can take negative values as well means that it does not provide a 'true' energy density. This behaviour of the WDF is connected to the uncertainty principle in signal theory (Section 2.3). The only signals that achieve an *all-positive* WDF are Gaussian signals, which are minimum uncertainty signals. It can be easily proved that the WDF of a Gaussian signal is a two-dimensional Gaussian function. In general, the negativity of the WDF does not present a significant problem. Indeed, suitable averages of the WDF, over carefully chosen regions of the time-frequency plane (the area of which is in accordance with the uncertainty principle) are shown to result only in positive values. The uncertainty in a time-frequency representation ("representational uncertainty") can not be easily defined in a quantitative way. To deal with this problem, Jacobson and Wechsler [81] have suggested that joint entropic measures of uncertainty should be used.

XV For the special case $f = 0$, from Eq. 4.4: $W(t, f = 0)$ is equal to the *autocorrelation function* $Q_s(t)$ (defined in Eq. (2.25)).

XVI The integral of the WDF over the whole T-F plane gives the *total energy* of the signal:

$$\int_{-\infty}^{+\infty}\int_{-\infty}^{+\infty} W_s(t,f)dt\,df = \int_{-\infty}^{+\infty} |s(t)|^2 dt. \tag{4.24}$$

XVII The *absolute value* of the WDF never exceeds 1:

$$-1 \leq W_s(t,f) \leq 1 \tag{4.25}$$

(considering the previous normalisation of the signal's energy).

The last two properties of the (auto)Wigner distribution function are fundamental, since they lead to its interpretation as a pseudo-distribution of the energy of the signal in the time-frequency plane.

4.3 The Ambiguity Function and its Relation to the WDF

The *ambiguity function* $A_s(\tau, \phi)$ of a signal $s(t)$ with total energy equal to 1 is given by

$$A_s(\tau,\phi) = \int_{-\infty}^{+\infty} s(t+\tau/2)s^*(t-\tau/2)\exp(-j2\pi\phi t)dt = A_{\tilde{s}}(\phi,\tau) =$$

$$= \int_{-\infty}^{+\infty} \tilde{s}(f+\phi/2)\tilde{s}^*(f-\phi/2)\exp(j2\pi\tau f)df \quad . \tag{4.26}$$

In the literature of radar signal theory, the ambiguity function is sometimes described as the complex or time-frequency autocorrelation function, the delay-Doppler ambiguity function, the radar uncertainty function or the matched-filter response function. The connection between ambiguity functions and Wigner distribution functions has been first brought forward by Klauder [98]. He pointed out the analogy to the uncertainty principle of quantum theory. The ambiguity function is the analogon of the *Weyl function* in quantum mechanics.

It can be proved that the the ambiguity function is the (double) Fourier transform of the WDF:

$$A_s(\tau,\phi) = \int_{-\infty}^{+\infty}\int_{-\infty}^{+\infty} e^{-j2\pi(\phi t - f\tau)} W_s(t,f)dtdf. \tag{4.27}$$

The proof is based on three properties of the Fourier transform: the complex conjugate, the duality and the convolution theorem (Section 2.3). Using the function $R_s(\tau, t)$ defined in Eq. (4.5) and its symmetrical function

$$P_s(\phi, f) = \tilde{s}(f+\phi/2)\tilde{s}^*(f-\phi/2), \tag{4.28}$$

we have

$$A_s(\tau,\phi) = \tag{4.29}$$

$$\int_{-\infty}^{+\infty} e^{-j2\pi\phi t} R_s(\tau,t)dt =$$

$$\int_{-\infty}^{+\infty} e^{j2\pi f\tau} P_s(\phi,f)df =$$

$$\int_{-\infty}^{+\infty}\int_{-\infty}^{+\infty}\int_{-\infty}^{+\infty} e^{j2\pi\phi t}e^{-j2\pi\phi t}\left\{e^{j2\pi f\tau}P_s(\phi,f)\right\}df\,dtd\phi =$$

$$\int_{-\infty}^{+\infty}\int_{-\infty}^{+\infty} e^{-j2\pi(\phi t-f\tau)}\left\{\int_{-\infty}^{+\infty} e^{j2\pi\phi t}P_s(\phi,f)d\phi\right\}dtdf =$$

$$\int_{-\infty}^{+\infty}\int_{-\infty}^{+\infty} e^{-j2\pi(\phi t-f\tau)}\left\{\int_{-\infty}^{+\infty} e^{-j2\pi f\tau}R_s(\tau,t)d\tau\right\}dtdf,$$

which, with the use of Eq. (4.5), results in the expression of Eq. (4.27). Consequently, the properties of the ambiguity function can be easily derived by combining the properties of the WDF (Section 4.2) and the properties of the Fourier transform (Section 2.3).

Ambiguity function representation has become very popular in radar theory. Its important application as a signal design criterion in mathematical radar theory was first presented by P.M. Woodward [189]. In radar theory, the pair (τ,ϕ) represents the range (time) and velocity (Doppler frequency) pair of variables. High range resolution and high velocity resolution are irreconcilable requirements (uncertainty relation in radar signal theory [19]) and signal design for specified tasks under certain conditions can be done successfully using the ambiguity function which characterises the trade-off between the resolution in the range domain and the resolution in the velocity domain [7, 171, 52]. A detailed study of the ambiguity function is presented in [132].

Three important general properties of the ambiguity function are:

I The ambiguity function reaches its maximum value at the origin:

$$|A_s(\tau,\phi)| \leq A_s(0,0) = 1 \quad . \tag{4.30}$$

II The volume under $|A_s(\tau, \phi)|$ is unity:

$$\int_{-\infty}^{+\infty}\int_{-\infty}^{+\infty} |A_s(\tau, \phi)| d\tau d\phi = |A_s(0,0)|^2 = 1, \tag{4.31}$$

which corresponds to the total signal energy. This equation is known as the radar uncertainty principle and it shows that the ambiguity function can not be concentrated arbitrarily close to the origin.

III It is very interesting that for signals that are odd or even functions of time ($s(t) = s(-t)$ or $(s(t) = -s(-t))$, the ambiguity function and the WDF are the same except for a scaling factor:

$$W_s(t, f) = \pm 2 A_s(2f, 2t) \quad . \tag{4.32}$$

The scaling factor of 2 appears as a consequence of the definitions of Eqs. (4.4), (4.26) we used.

From Eq. (4.26) it is obvious that the ambiguity function is a (complex-valued) function of correlation lags. In contrast, the Short-Time Fourier transform, the WDF representation and the Gabor transform can all be viewed as functions of phase-space variables. The ambiguity function provides a "correlative" point of view, whereas the three aforementioned time-frequency representations provide an "energetic" point of view.

4.4 The Wigner Distribution Function and its Applications in Signal Analysis and Synthesis

In this section, practical implementation of the WDF with computer algorithms (see Appendix B) is discussed and inherent problems of the representation are examined. Applications in the areas of signal analysis and synthesis are also considered.

To apply the WDF representation to digital data, a discrete version of the Wigner distribution is needed. Historically, the adaption of the WDF methods

for discrete-time signal processing is due to Claasen and Mecklenbräuker (1980). A consistent definition of the Discrete Wigner Distribution Function (DWDF) is found in their classic paper [35]. If $s[n]$ represents a finite discrete-time (generally complex) signal (or a digital image in a one-dimensional space), the DWDF can be defined by

$$W[n,\theta] = \frac{1}{N}\sum_{k=0}^{N-1} e^{-j4\pi k\theta/N} s[n+k]s^*[n-k], \tag{4.33}$$

where N is the number of points of the digital signal $s[n]$ and $k = 0, 1, 2, ..., N-1$. Not all the properties of the continuous WDF are preserved by discretisation, due to the aliasing effects occurring in the discrete case. The above definition satisfies the following criteria:

- Simplicity;
- Preservation of as many of the properties of the continuous WDF as possible;
- Simple description of the relationship between the continuous WDF of a continuous-time (analogue) signal and the DWDF of the discrete-time signal obtained by sampling the continuous-time signal.

A major problem in practical applications is presented by *interference* or *cross terms* in the WDF of real signals. Interaction between *aliasing* positive and negative frequency components generate unwanted peaks between the actual frequency components. Various methods have been suggested to reduce these interference terms. Most of these methods consider attenuation of these terms using a two-dimensional "smoothing kernel" [5, 79]). Another approach is the oversampling of analogue signals. Since the DWDF of Eq. (4.33) has a 'periodicity' of $N/2$ on the frequency axis, the Nyquist criterion for the discrete real signal is not strong enough for its DWDF. Interpolation with additional data points or oversampling at twice the Nyquist rate or higher provide a satisfactory remedy. An alternative way to avoid aliasing is to apply the WDF representation to the analytic signal associated with the real signal rather than to the real signal itself. Interference is avoided by elimination of the negative frequencies [193].

The discrete-time(space) analytic signal of the discrete-time(space) real signal $u[n]$ is of the form: $s[n] = u[n]+jv[n]$, where the associated imaginary part $v[n]$ is given by the Discrete Hilbert transform of s[n]. The analytic signal approach leads to a convenient implementation since the calculation uses the Hilbert transform (Chapter 3). Usually the Discrete Hilbert transform can be computed very fast by using powerful FFT algorithms. The advantages of using the analytic signal are extensively discussed in Section 3.4.

The formulation of the DWDF (Eq. (4.33)) is similar to the Discrete Fourier Transform of the discrete time(space)-dependent correlation function $R_k[n]$, which is a complex function of two variables and can be calculated using cross-multiplication:

$$R_k[n] = s[n+k]s^*[n-k], \tag{4.34}$$

where $s[n]$ is the analytical signal corresponding to the original real signal $u[n]$ and by convention $s[m] = 0$ for $m < 0$ and $m > N-1$. This means that the calculation of the DWDF can be carried out simply by using an FFT algorithm. The use of an FFT actually makes the calculation faster to execute than a straightforward calculation of the sum of Eq. (4.33). However, preliminary processing of the data to obtain the analytic signal is required.

So the procedure for the evaluation of the DWDF is:

1. Pre-processing: Discrete Hilbert transform of the data. Calculation of the analytic form. Efficient ways to calculate the DHT are presented in Chapter 3.

2. Time-dependent correlation function $R_k[n]$ of the analytic signal is calculated using Eq. 4.34.

3. DWDF is calculated by means of the adapted FFT of the correlation function (Eq. (4.33)).

Sometimes the negativity of the DWDF makes it unsuitable for certain applications. In such cases, the removal of the negative values in a consistent way

is attractive, usually by taking a suitable sliding averaging window $V[n, \theta]$ to smooth the WDF. This all-positive version of WDF is usually referred to as the *pseudo*-Wigner distribution function.

The WDF representation can be successfully applied to signal *synthesis* [21, 137]. A simple synthesis algorithm based on Eq. (4.17) has been developed (Appendix B). The original signal is reconstructed from its evaluated WDF. This can be helpful in order to check if the WDF is accurately evaluated. Reconstruction of the spectrum of the signal can be achieved by an analogous process based on Eq. (4.18).

Using this method, the modulus of the analytic form can be estimated accurately. The WDF is a real-valued function and from its definition (Eq. (4.4)), it is clear that it retains no phase information. This means that the sign of the reconstructed (real) signal can not be recovered. However, this is not important in certain applications, like radar signal design. Sometimes, it is useful to select a set of phase terms which are as close as possible to those of the original signal.

The general synthesis procedure includes the following stages:

1. Calculation of the WDF of the signal $s[n]$: $W[n, \theta]$ (signal analysis).
2. Filtering. Modification of the WDF by means of a time-dependent filter function $H[n, \theta]$ designed to retain desirable signal components and suppress noise: $Y[n, \theta] = H[n, \theta]W[n, \theta]$.
3. Evaluation of the new version of signal from modified WDF $Y[n, \theta]$ (signal synthesis).

Generally, the modified WDF $Y[n, \theta]$ is not a valid WDF. This problem is a subject of further investigation.

4.5 Implementation of the Method Using Optical Signals

Algorithms for the required calculations were developed (Appendix B) and various signals of experimental interest were examined in the light of the WDF representation. Here, the processing of several examples of time-varying signals encountered in experimental optics will be presented.

The calculations were carried out using the techniques described in Section 4.4. The results for the WDF evaluation have been verified using the synthesis algorithm (Appendix B) to reconstruct successfully the initial signal from the evaluated WDF. Moreover, the developed signal processing software was thoroughly tested using the theoretical results (for example, the fact that WDF is a real function).

4.5.1 Two Interesting Cases

A Kronecker delta function (unit impulse) is an example which provides a good understanding of the Time-Frequency representation (see Section 2.4). A 3-D graph of the DWDF for the function $\delta[n-60]$ is given in Fig. 4.1. As can be noticed, the Wigner distribution function is mainly concentrated on a single point in time domain, whilst the spectrum at this point is similar to a white spectrum.

The signal $l(t)$ of Fig. 4.2 is a typical non-stationary noise signal (this type of noise frequently appears in biomedical engineering and is known as *Lanshammar's* noise). A 3-D graph of its WDF can be found in Fig. 4.3, where as in Fig. 4.4 a contour map of the same WDF is illustrated. It is interesting to see the detail in which the WDF representation describes the intrinsic randomness of the signal.

4.5.2 The WDF of an Electric Arc Signal

Examples of real-life optical signals related to the optical emission of an electric arc plasma, were supplied by the Optics Laboratory in the Department of Electrical Engineering and Electronics, the University of Liverpool. Signals of

this nature exhibit high nonstationarity and a random behaviour, and are very important in arc monitoring applications [134, 94]. The signal $u(t)$ of Fig. 4.5 was obtained from the output of an optical fibre particle concentration monitor or, simply, powder monitor (see Appendix A). Its magnitude is a function of time and it is expressed in units of dominant wavelength. The illustrated version of the signal has a mean equal to zero.

The imaginary part and the modulus of the corresponding analytic form $s(t)$ are shown in Figures 4.6 and 4.7 respectively. The analytic signal has a total energy equal to one. As mentioned earlier (Chapter 3), the concept of the analytic signal $s(t)$ is applicable in the case of band-limited or relatively narrowband signals. It is known that the analytic signal has a one-sided Fourier transform which is nonzero only in the positive axis. The Fourier transform of $s(t)$, illustrated in Fig. 4.8 (real part only), is confined to a narrow interval of frequency. It is seen that $s(t)$ can be considered narrowband.

In order to investigate the potential of these signals for condition monitoring and fault diagnosis in electric arc systems, seven different signals $u_i(t), (i = 1, ..., 7)$ of the same type were considered (Figs. 4.9-15). The illustrated versions of the signals have their energy normalised to unity and zero mean. The signals $u_4(t), u_5(t), u_6(t)$ and $u_7(t)$ correspond to the same value of the fault current (14.9 kA) (see figure captions in Figs. 4.9-4.15).

The WDF representations of each one of the signals $u_i[n]$ are illustrated in the contour maps of Figures 4.16-22 respectively. The detailed structure of these signals in the time-frequency plane can be clearly seen. Comparing the contour maps corresponding to the same current ($14.9kA$), it is evident that along the frequency axis, the DWDF is concentrated in a relatively small region near zero frequency; this is another strong indication that our signal is approximately narrowband. More specifically, we can see that the largest part of the frequency content of the signal lies around 0.25 kHz. In this frequency range, three distinct highly concentrated areas successively in a descending order of intensity can be noticed.

It is evident that the interpretation of the WDF maps can sometimes be tricky and requires examination of an adequate amount of data. However, as it

was demonstrated above, the WDF representation offers a new insight and reveals important time-varying features of the signal. In optical monitoring applications (for example, in power electronics), careful investigation using the WDF promises to yield valuable information about the condition of the equipment, lead to efficient techniques for problem identification and diagnosis (eg. for production of better equipment-damage maps), and improve system control.

In a similar way, the method can also be used for extraction of useful information from mechanical vibrations (time-frequency analysis of acoustical signals).

4.6 Discussion

The Wigner distribution function describes the energy density of a signal in both time and frequency in a probabilistic way. The WDF representation has proved to be a powerful tool in the area of signal processing.

Here, the potential of this representation for applications in signal synthesis, optical signal analysis and classification has been demonstrated, highlighting its use as a diagnostic tool in important applications where condition monitoring of electrical and mechanical systems is needed (eg. arc plasma processing, monitoring of high voltage switch gear, mechanical vibration analysis etc.). The main original aspects of this work are the use of the Wigner function in the context of optical signal processing and optical monitoring, the WDF analysis for fault diagnosis and the development of robust computer algorithms for WDF analysis and synthesis.

Compared to other signal analysis methods, the WDF representation is highly informative; actually, it provides more information than required for a complete reconstruction of the signal being analysed ($N^2/2$ data points of WDF for a digital signal of N data points). Depending on the specific application, this could be viewed as an advantage or a disadvantage. Its potential for the extraction of meaningful features present in a signal is quite substantial.

A major disadvantage of the WDF representation, though, is arguably that the computation takes a long time to complete. Another disadvantage of the

WDF is its intrinsic negativity.

Further work for WDF analysis of two-dimensional images is recommended. The evaluation of a suitably defined Discrete Wigner distribution function for a two-dimensional image and the use of this function as a tool for image analysis or synthesis still present a major challenge [11, 130, 202, 203, 201].

Figures

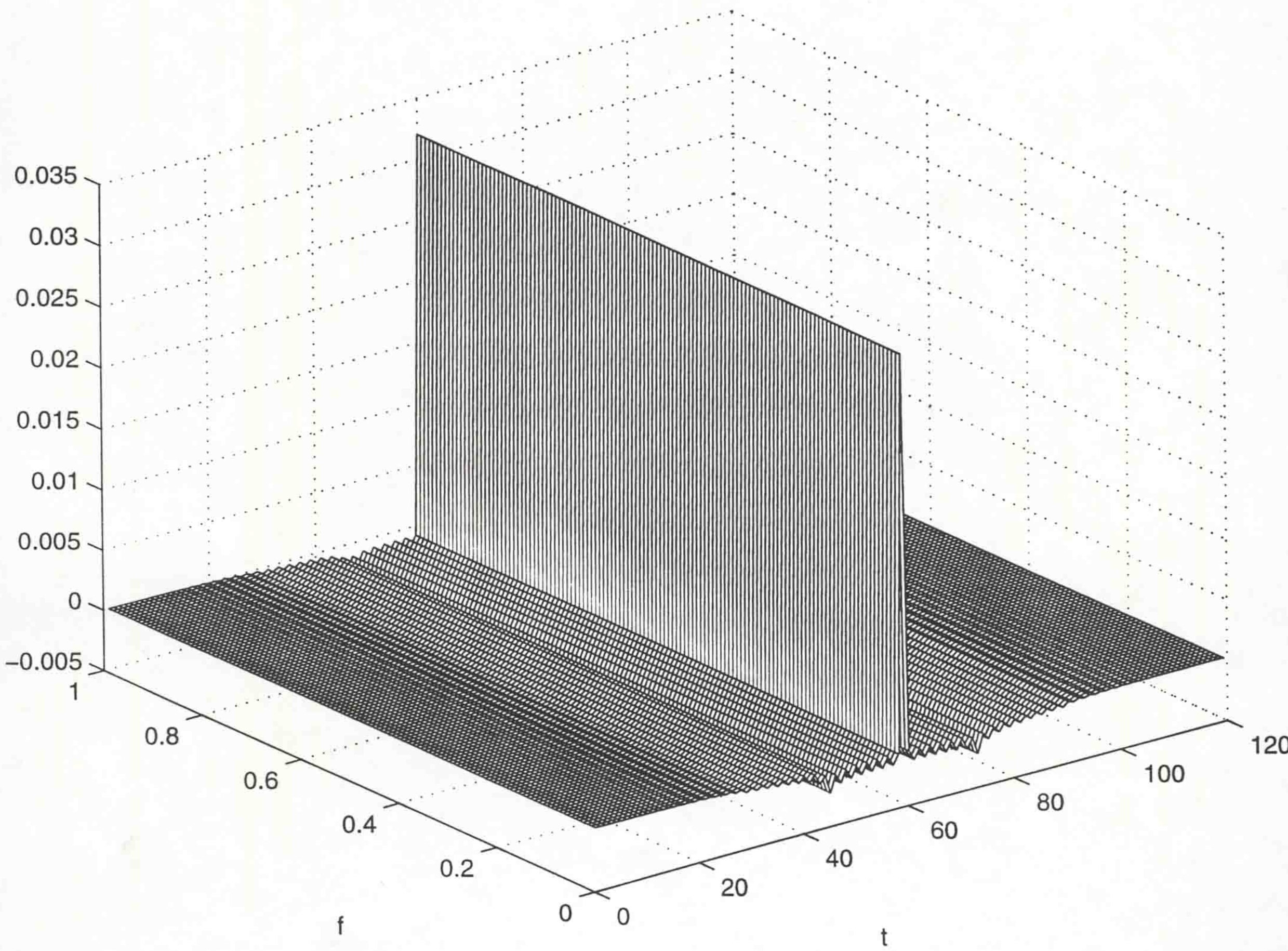

Figure 4.1: The Wigner distribution function of the pulse $\delta[n - 60]$.

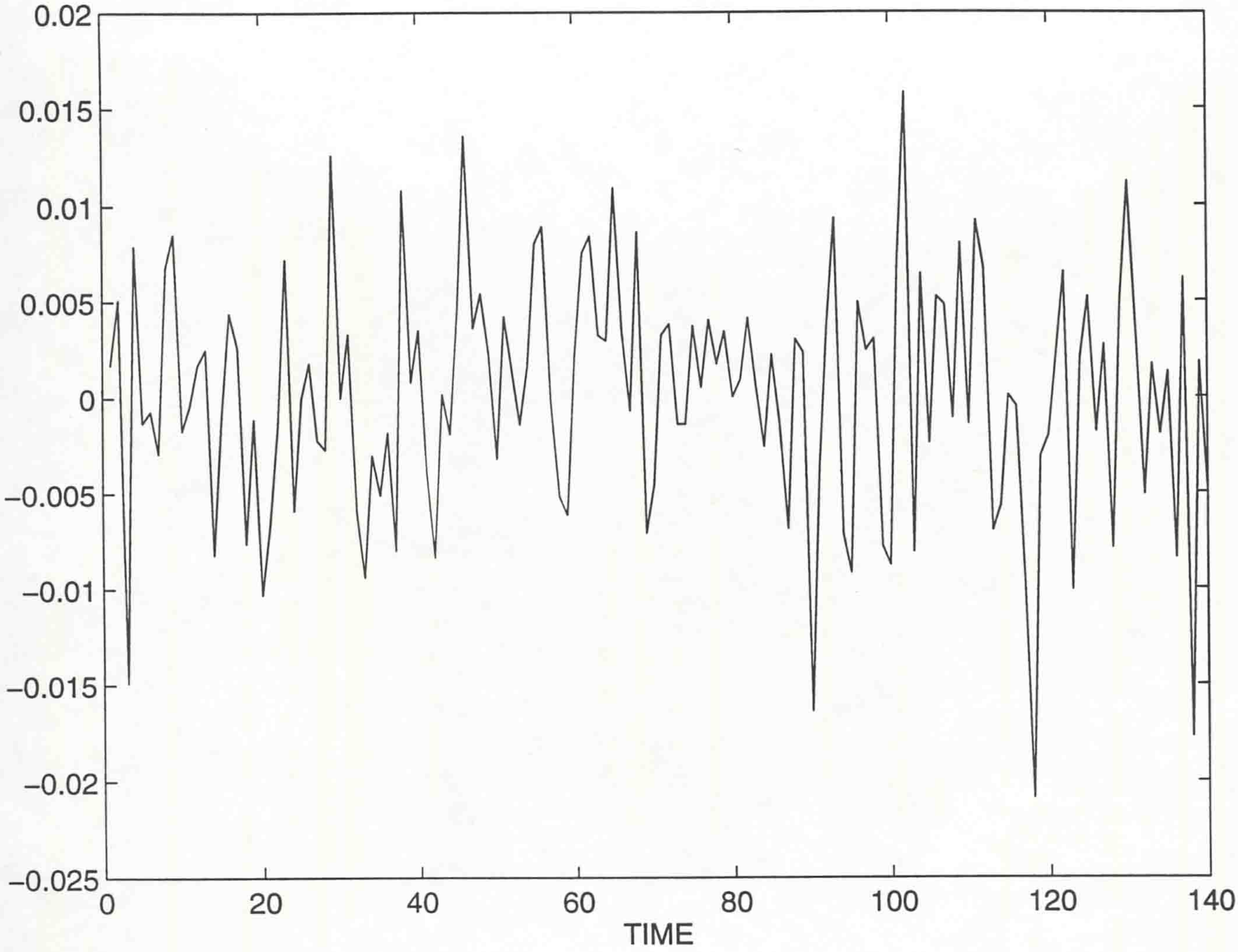

Figure 4.2: An example of Lanshammar's noise ($l(t)$).

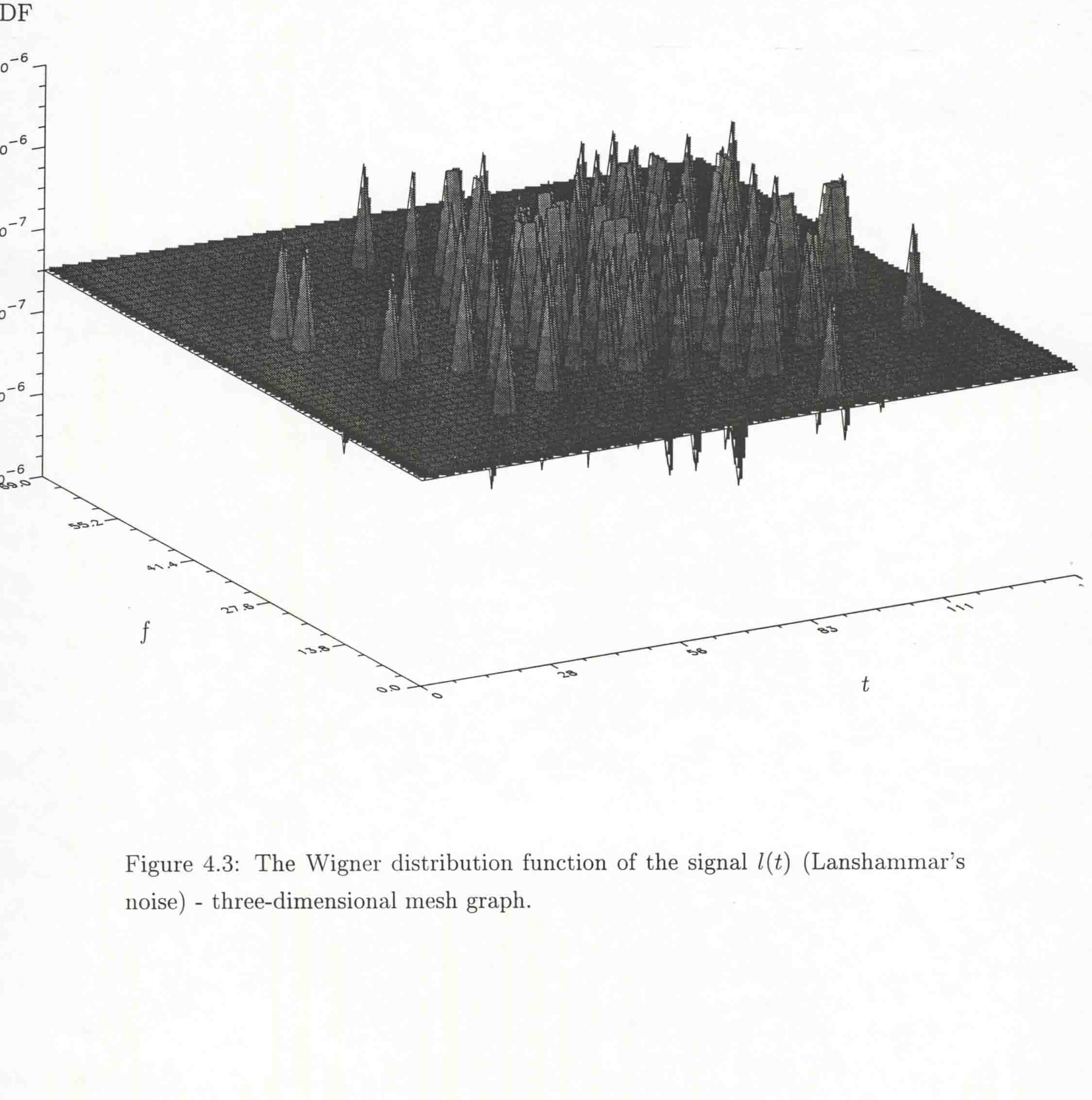

Figure 4.3: The Wigner distribution function of the signal $l(t)$ (Lanshammar's noise) - three-dimensional mesh graph.

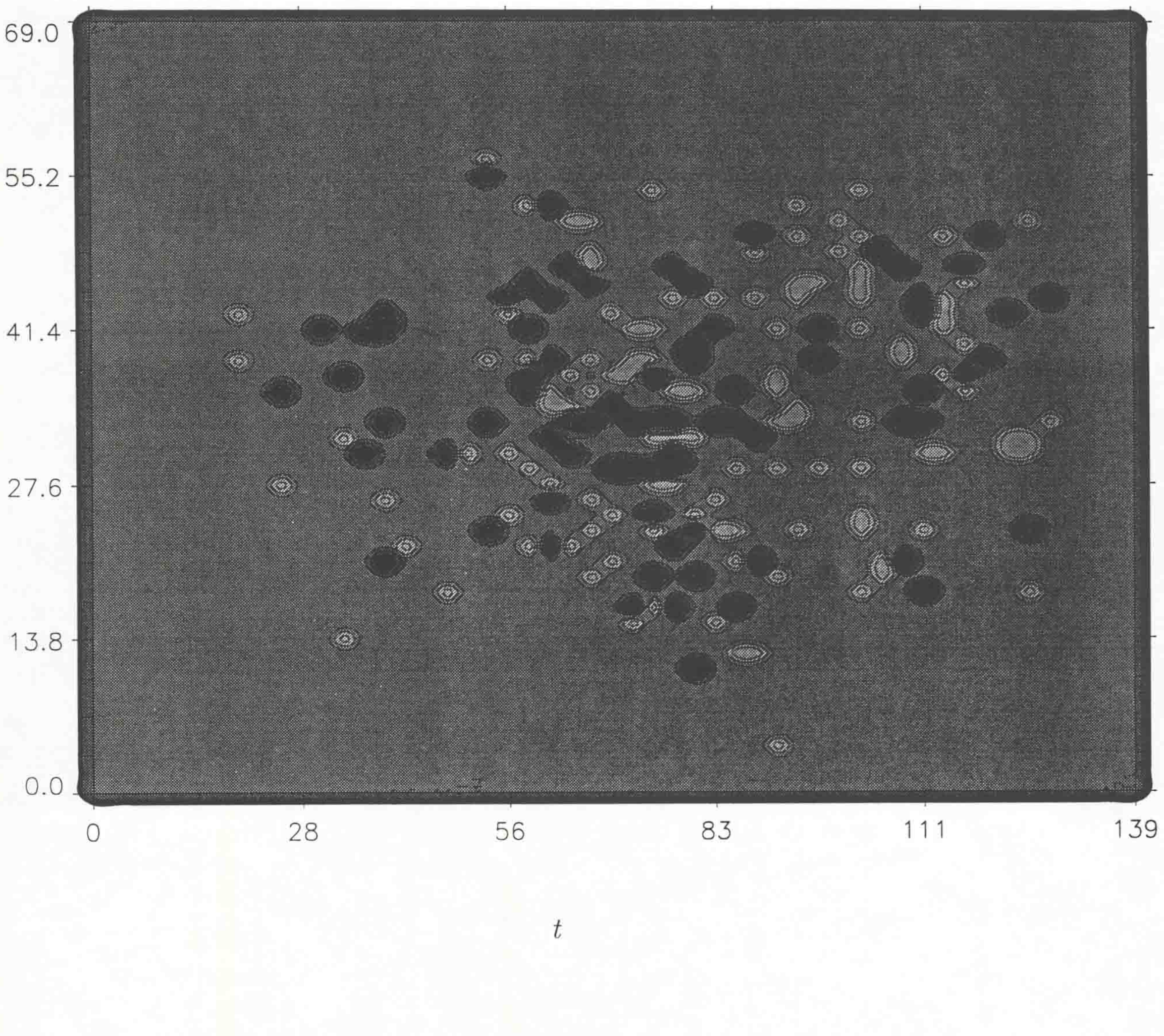

Figure 4.4: The Wigner distribution function of the signal $l(t)$ (Lanshammar's noise) - contour plot.

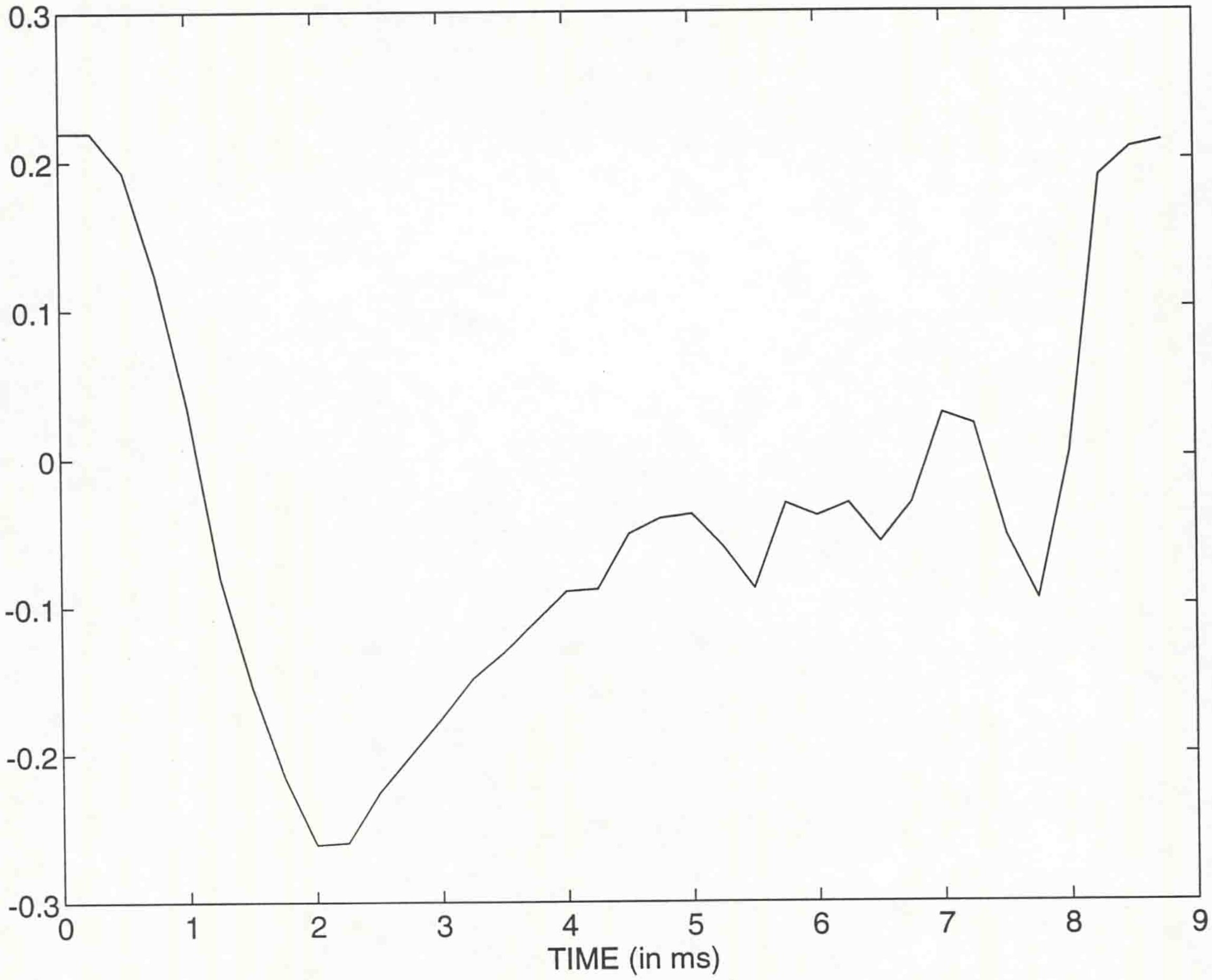

Figure 4.5: An electric arc signal ($u(t)$) obtained from the output of a powder monitor of electric arc plasma in the form of dominant wavelength as a function of time.

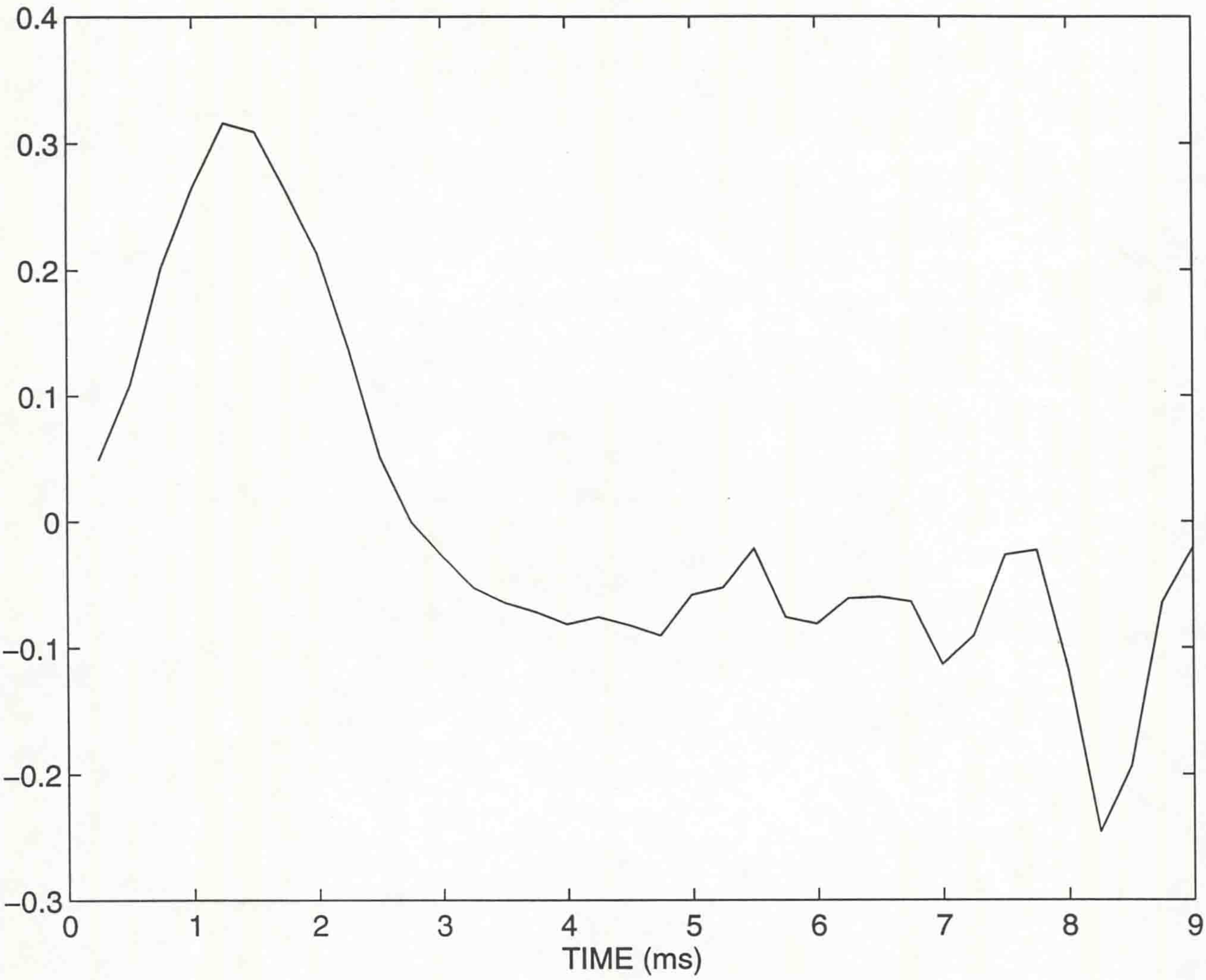

Figure 4.6: Imaginary part of the analytic form of the electric arc signal $u(t)$.

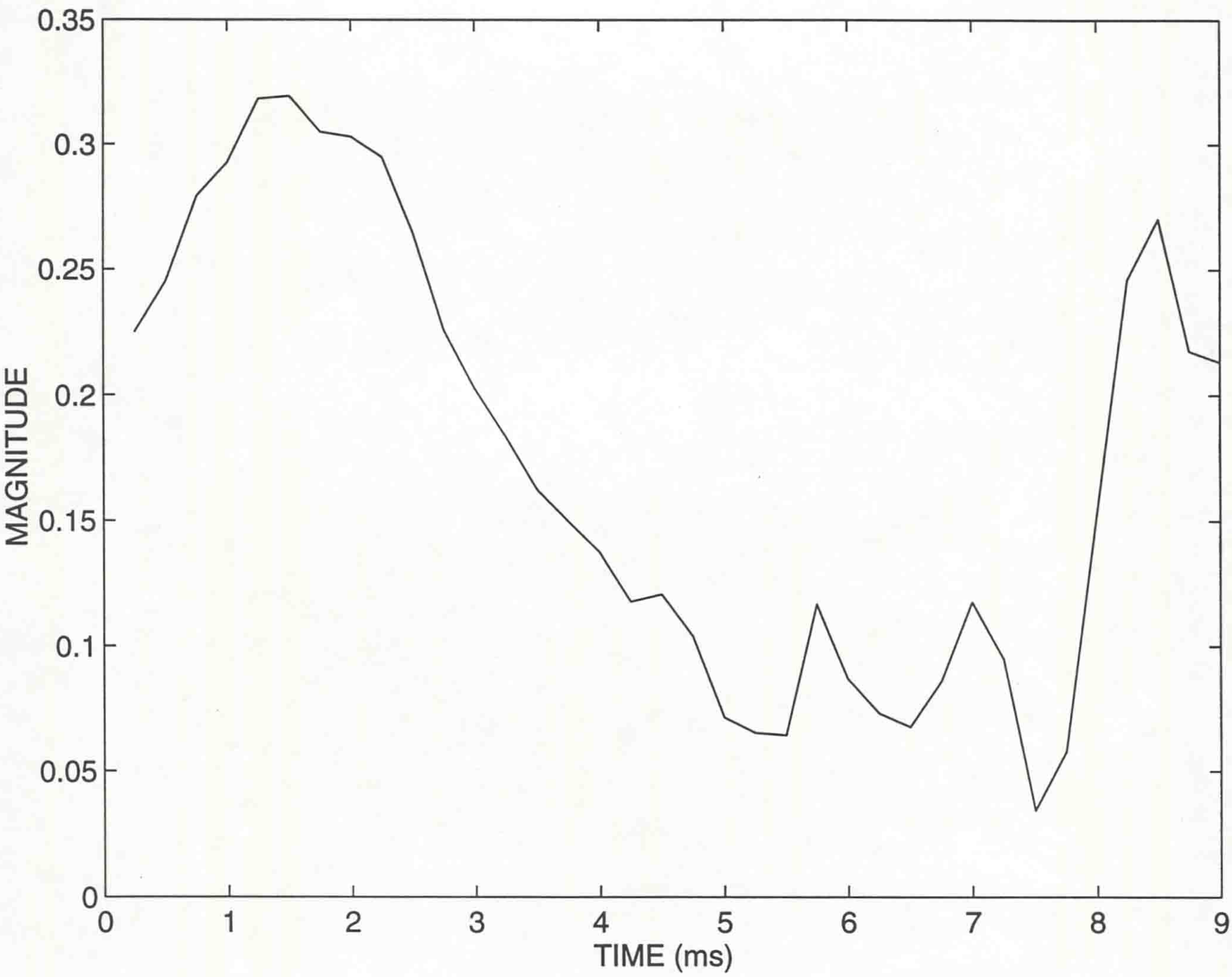

Figure 4.7: Modulus of the analytic form of electric arc signal $u(t)$.

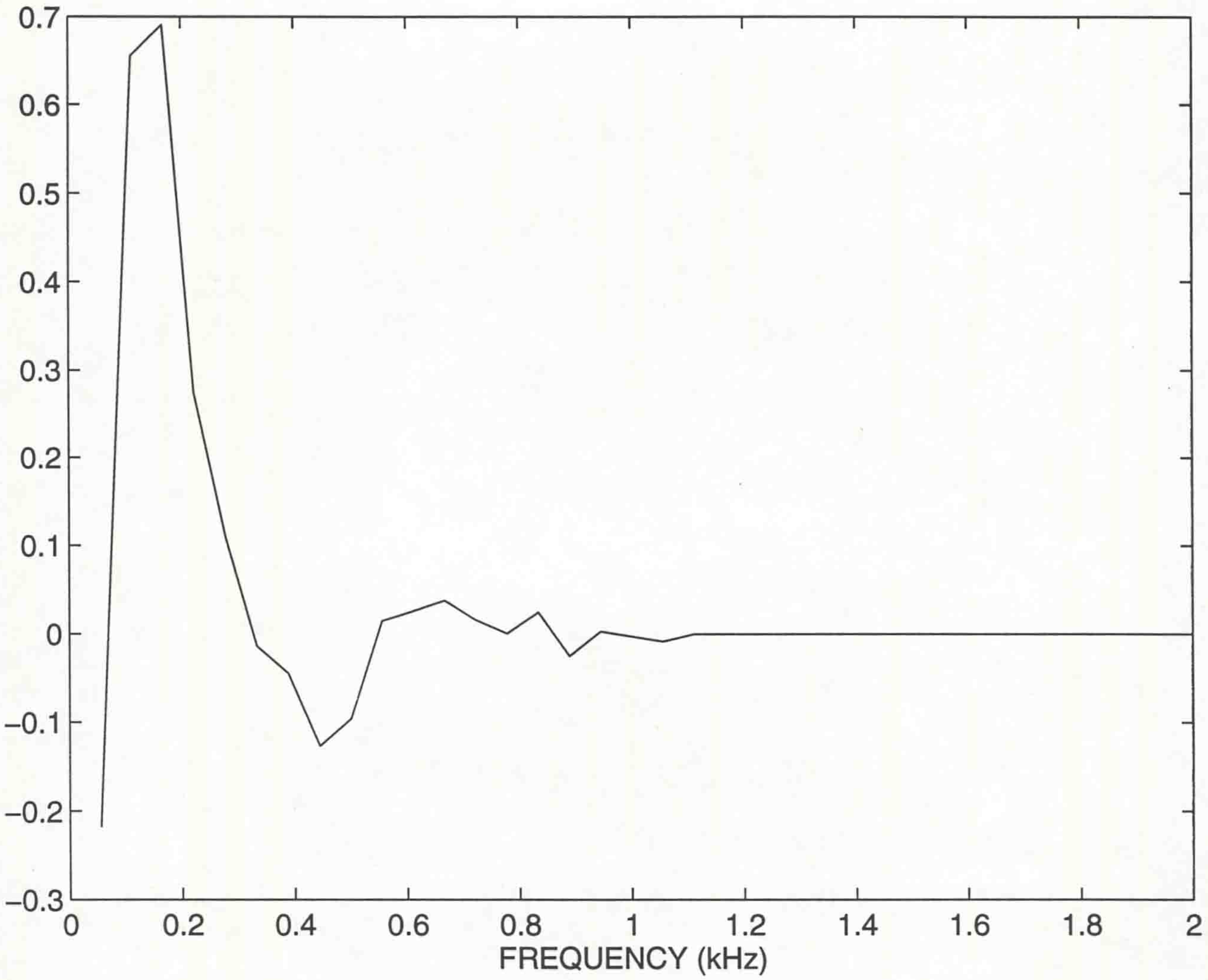

Figure 4.8: Real part of the Fourier transform of the analytic form of electric arc signal $u(t)$.

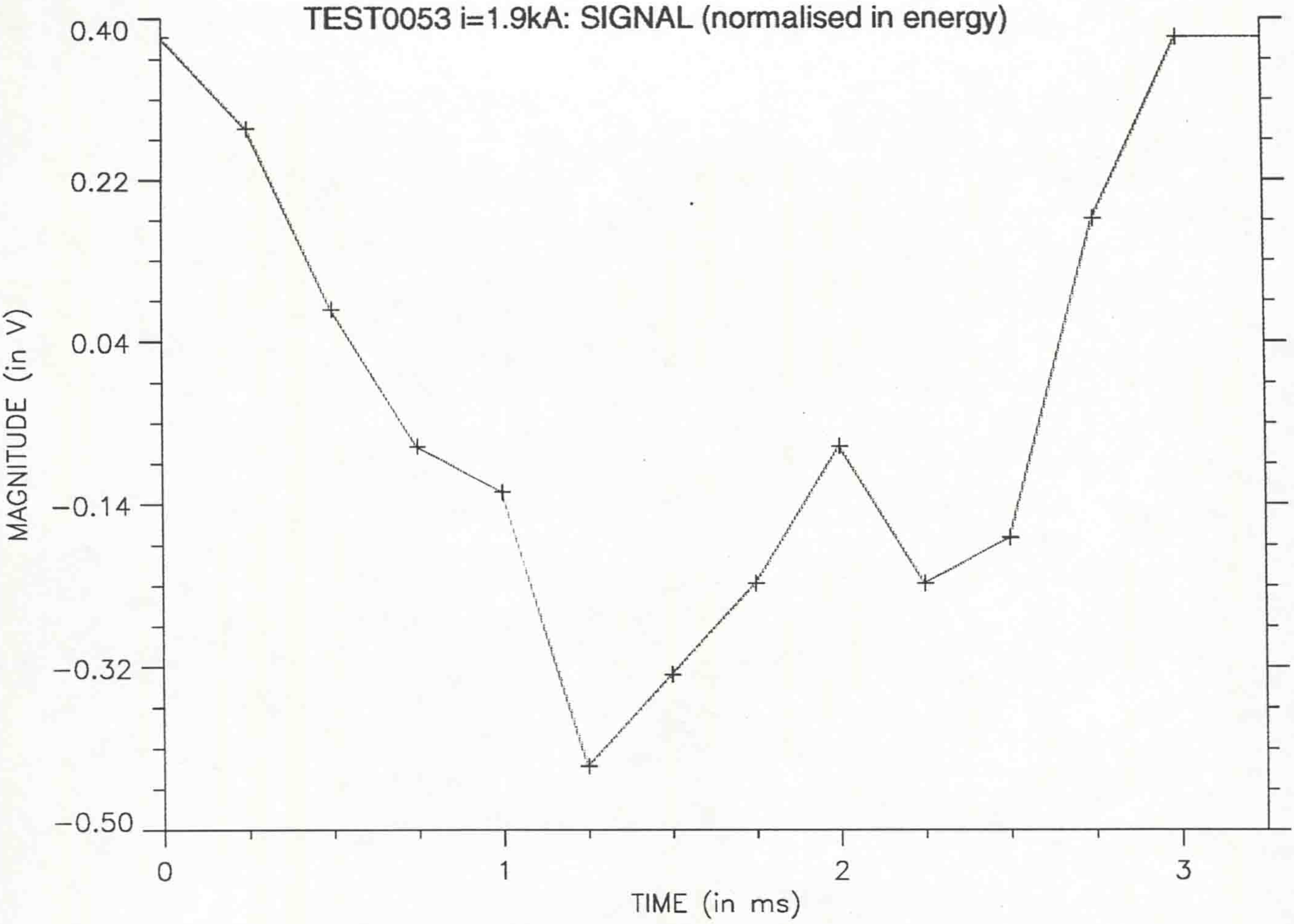

Figure 4.9: Electric arc signal $u_1(t)$, corresponding to an electrical current of $1.9kA$ at the powder monitor.

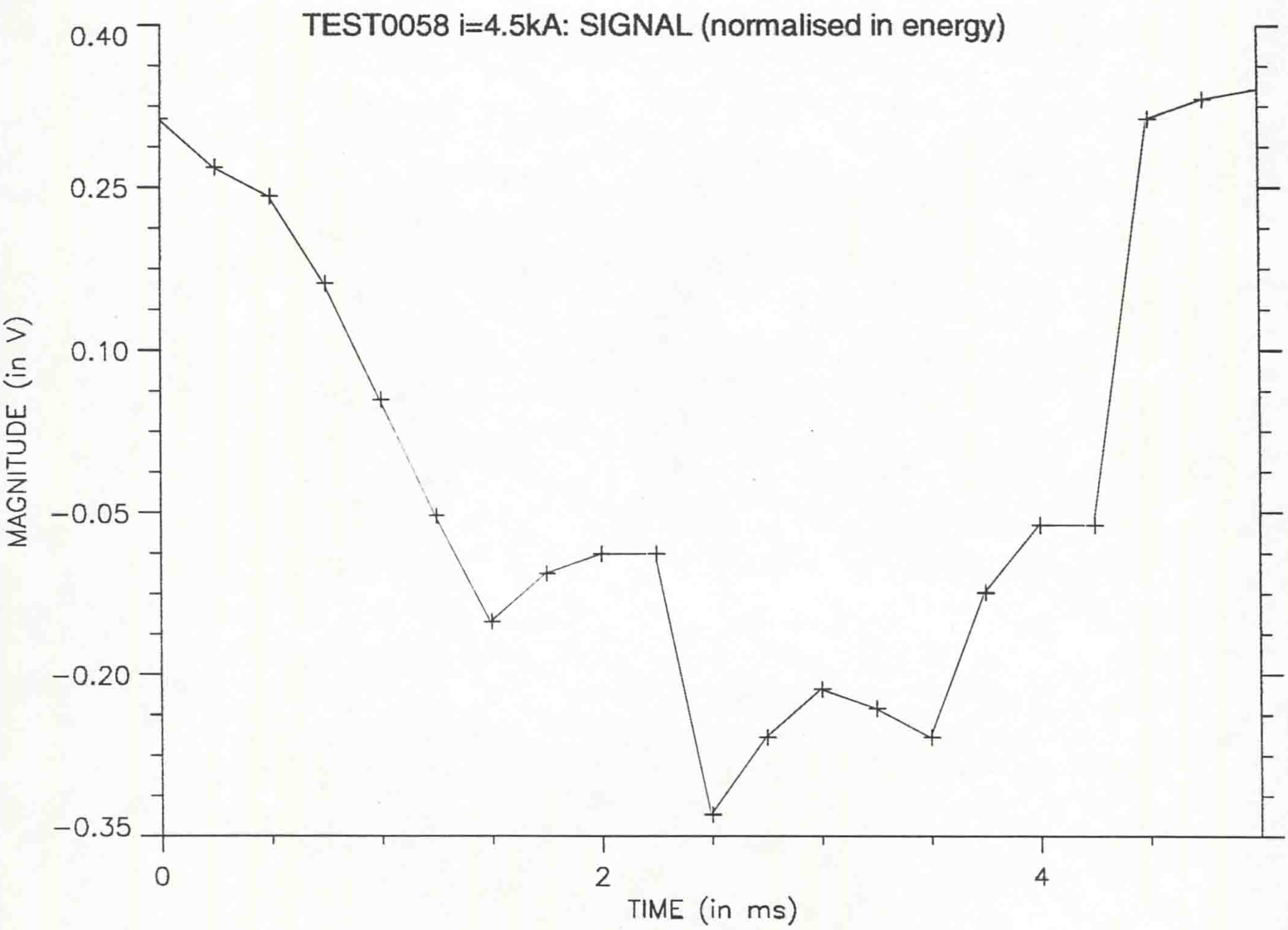

Figure 4.10: Electric arc signal $u_2(t)$, corresponding to an electrical current of 4.5 kA at the powder monitor.

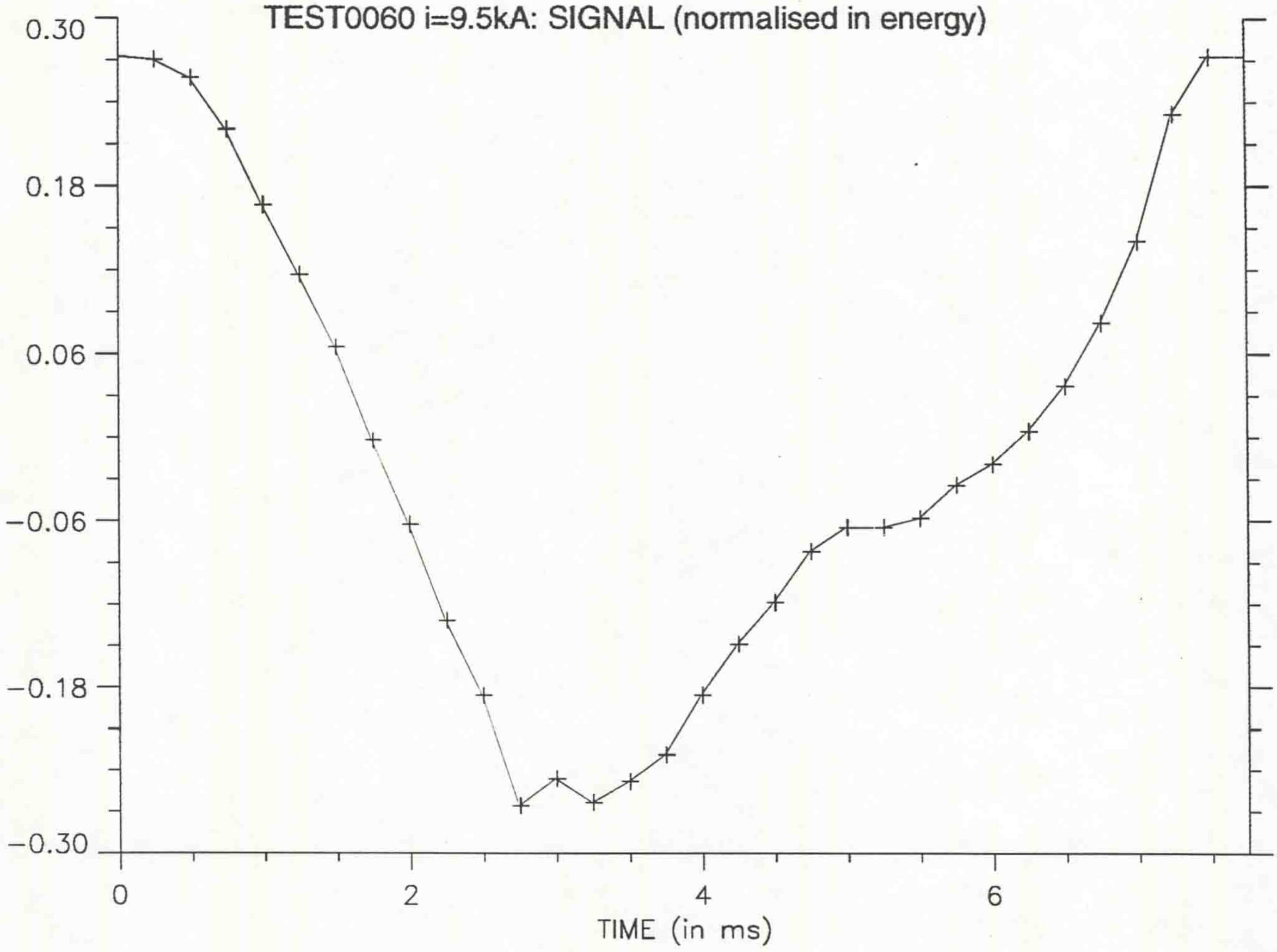

Figure 4.11: Electric arc signal $u_3(t)$, corresponding to an electrical current of 9.5 kA at the powder monitor.

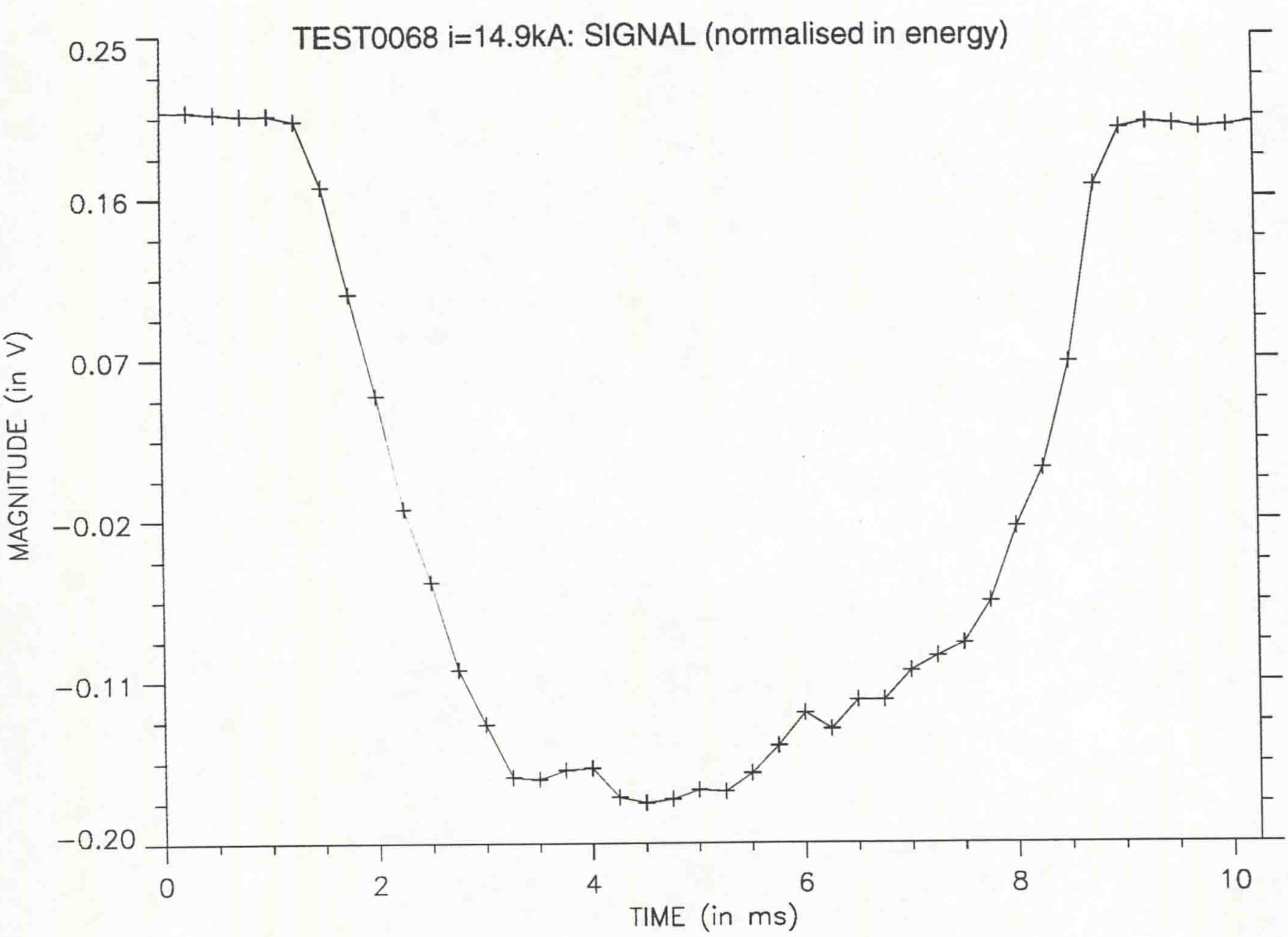

Figure 4.12: Electric arc signal $u_4(t)$, corresponding to an electrical current of 14.9 kA at the powder monitor.

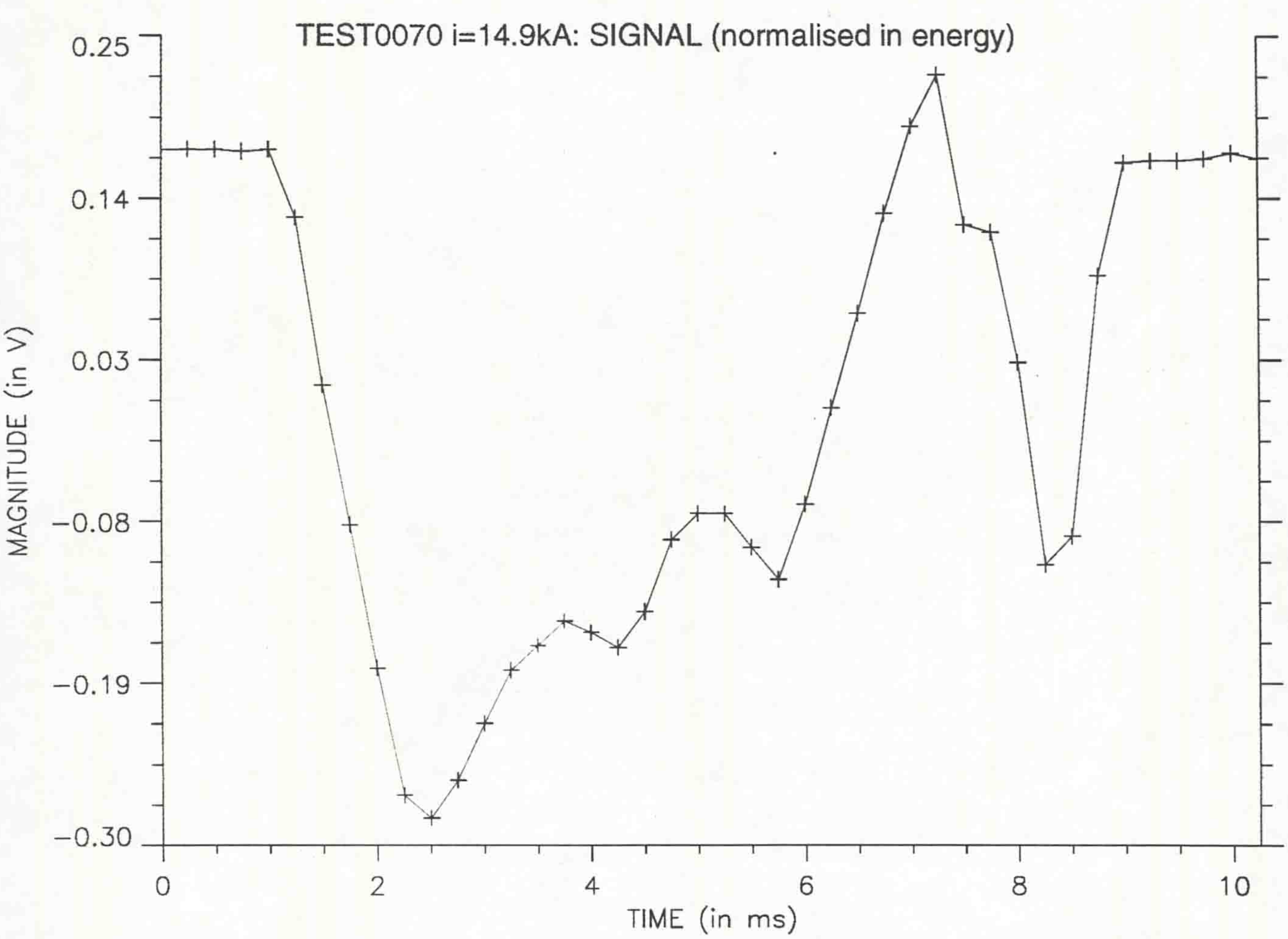

Figure 4.13: Electric arc signal $u_5(t)$, corresponding to an electrical current of 14.9 kA at the powder monitor.

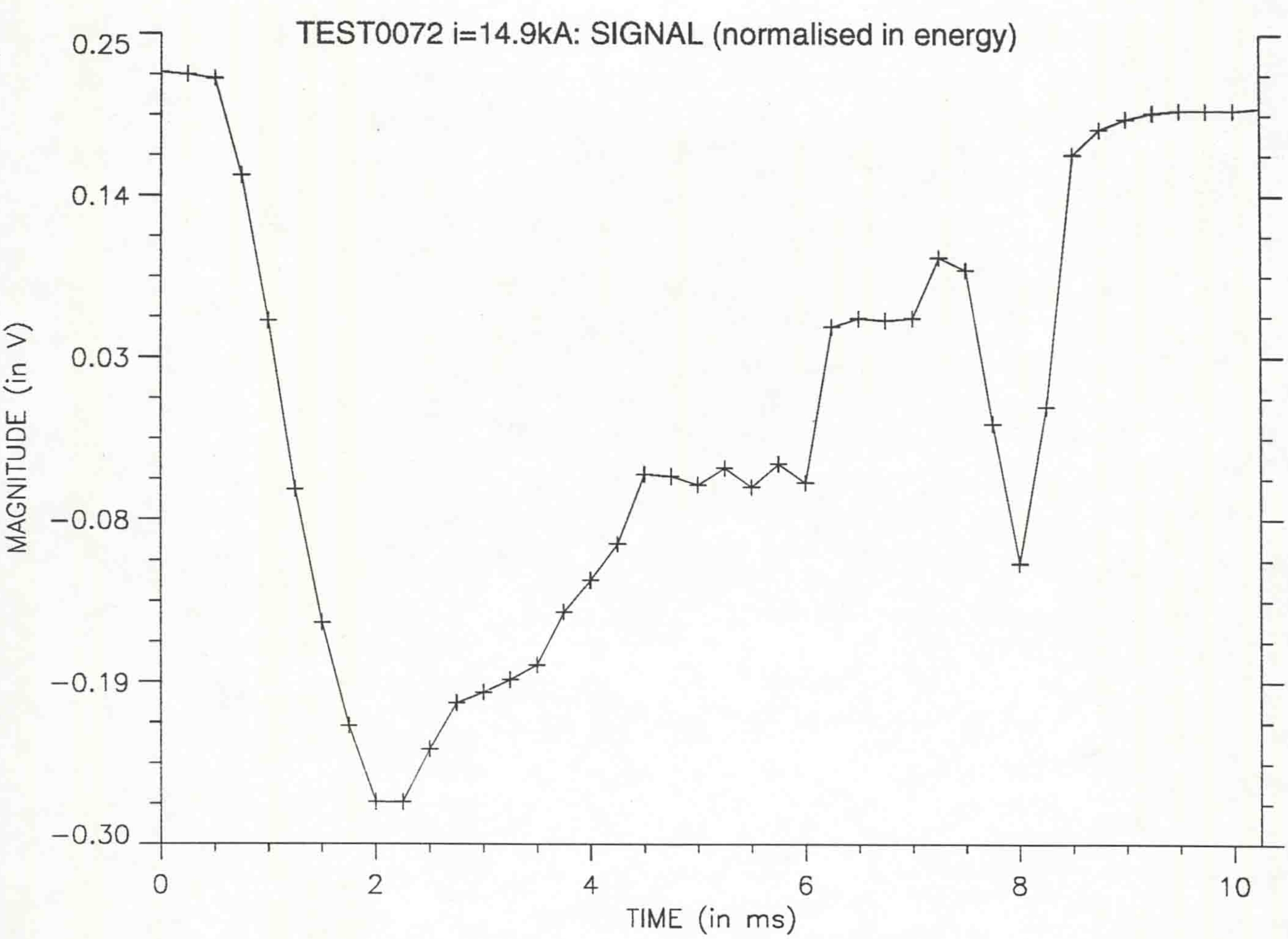

Figure 4.14: Electric arc signal $u_6(t)$, corresponding to an electrical current of 14.9 kA at the powder monitor.

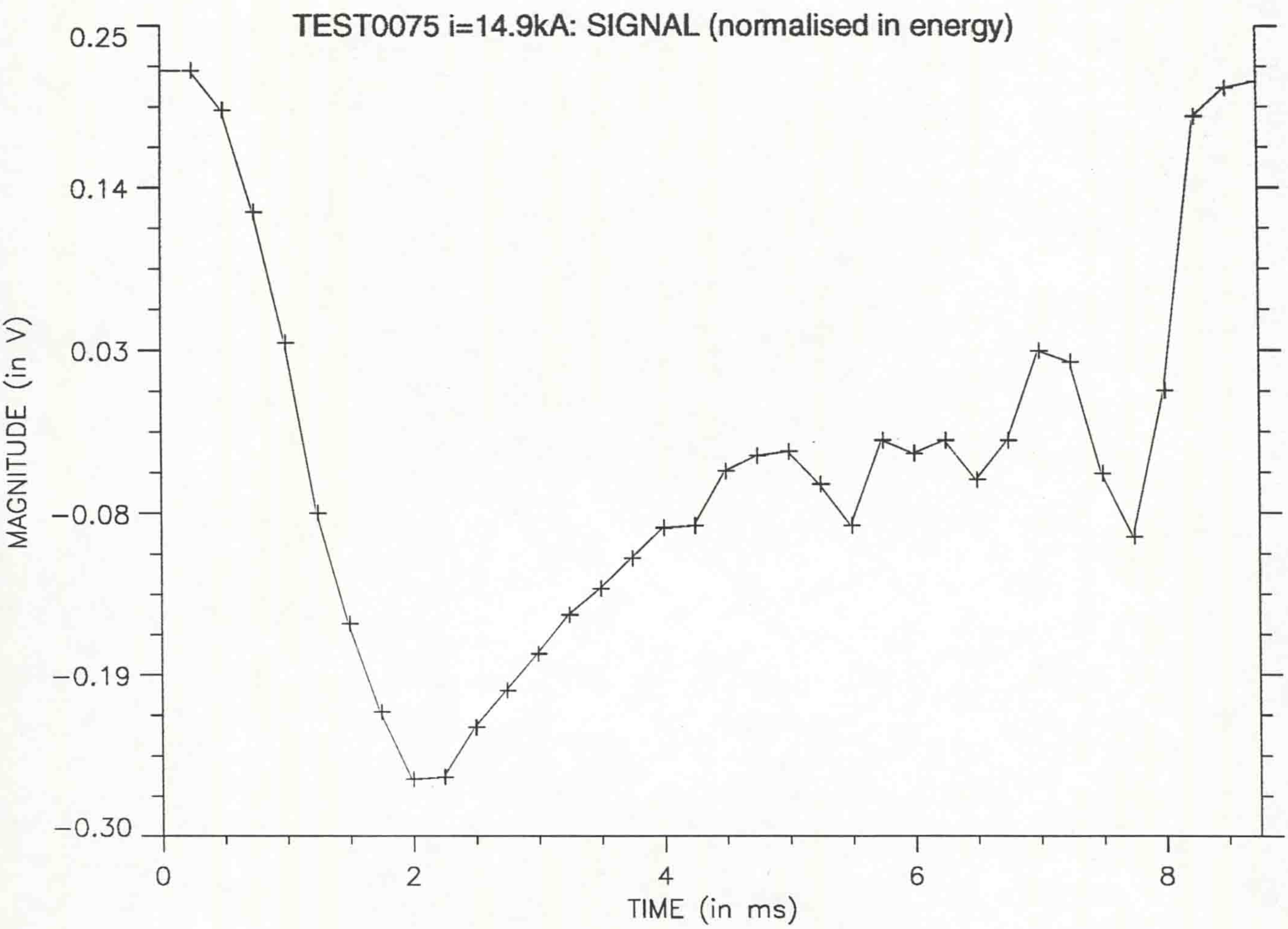

Figure 4.15: Electric arc signal $u_7(t)$, corresponding to an electrical current of 14.9 kA at the powder monitor.

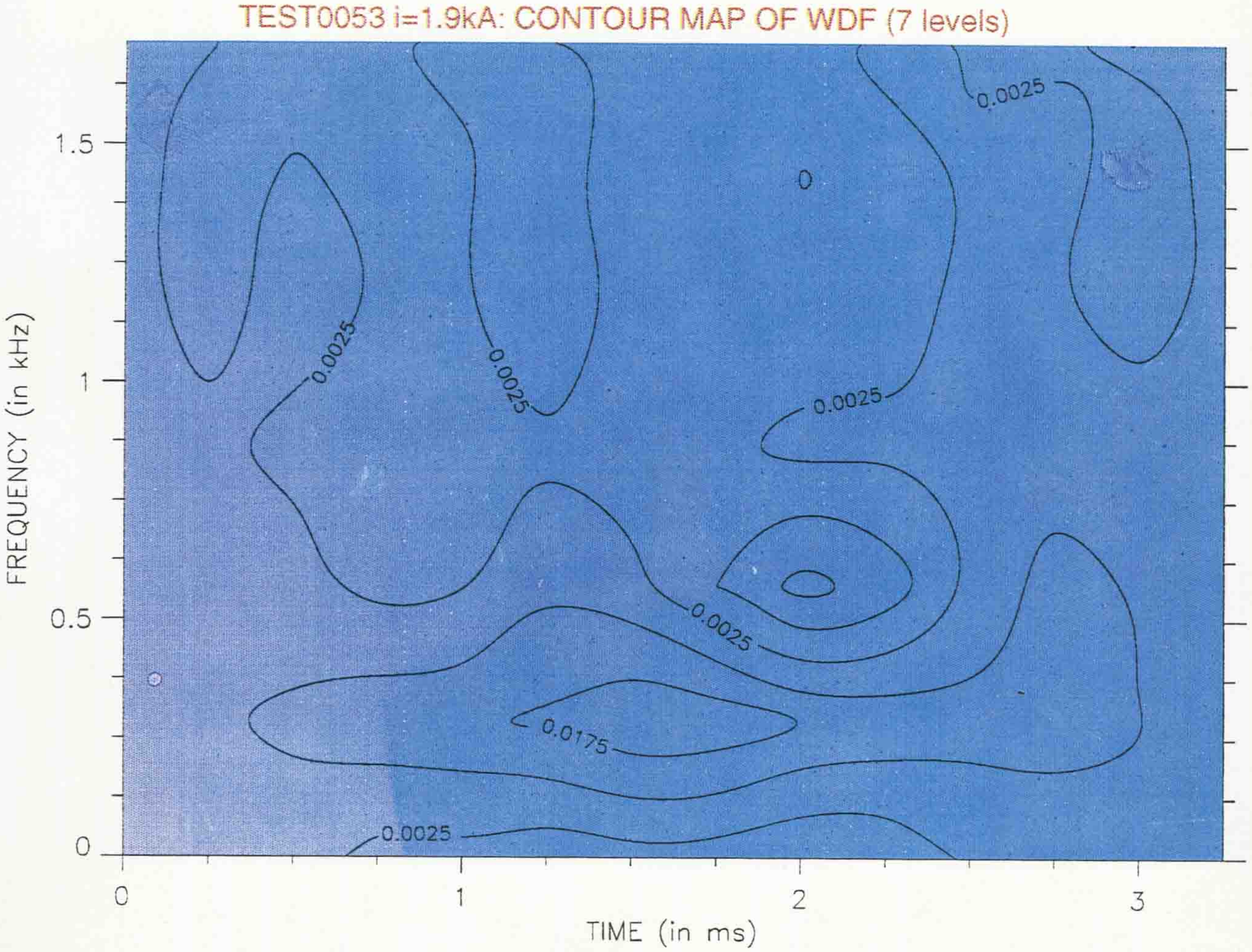

Figure 4.16: The Wigner distribution function of the electric arc signal $u_1(t)$.

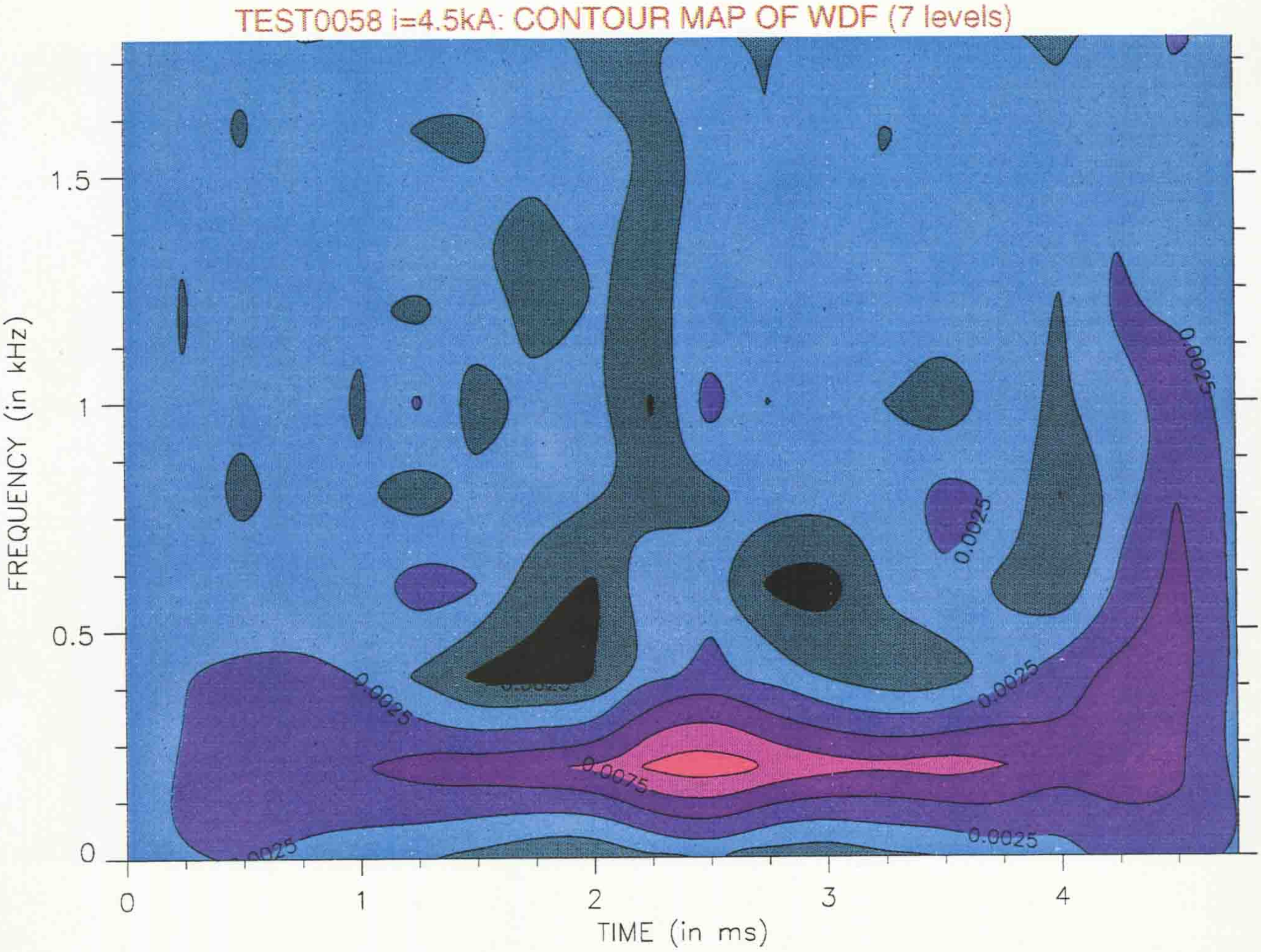

Figure 4.17: The Wigner distribution function of the electric arc signal $u_2(t)$.

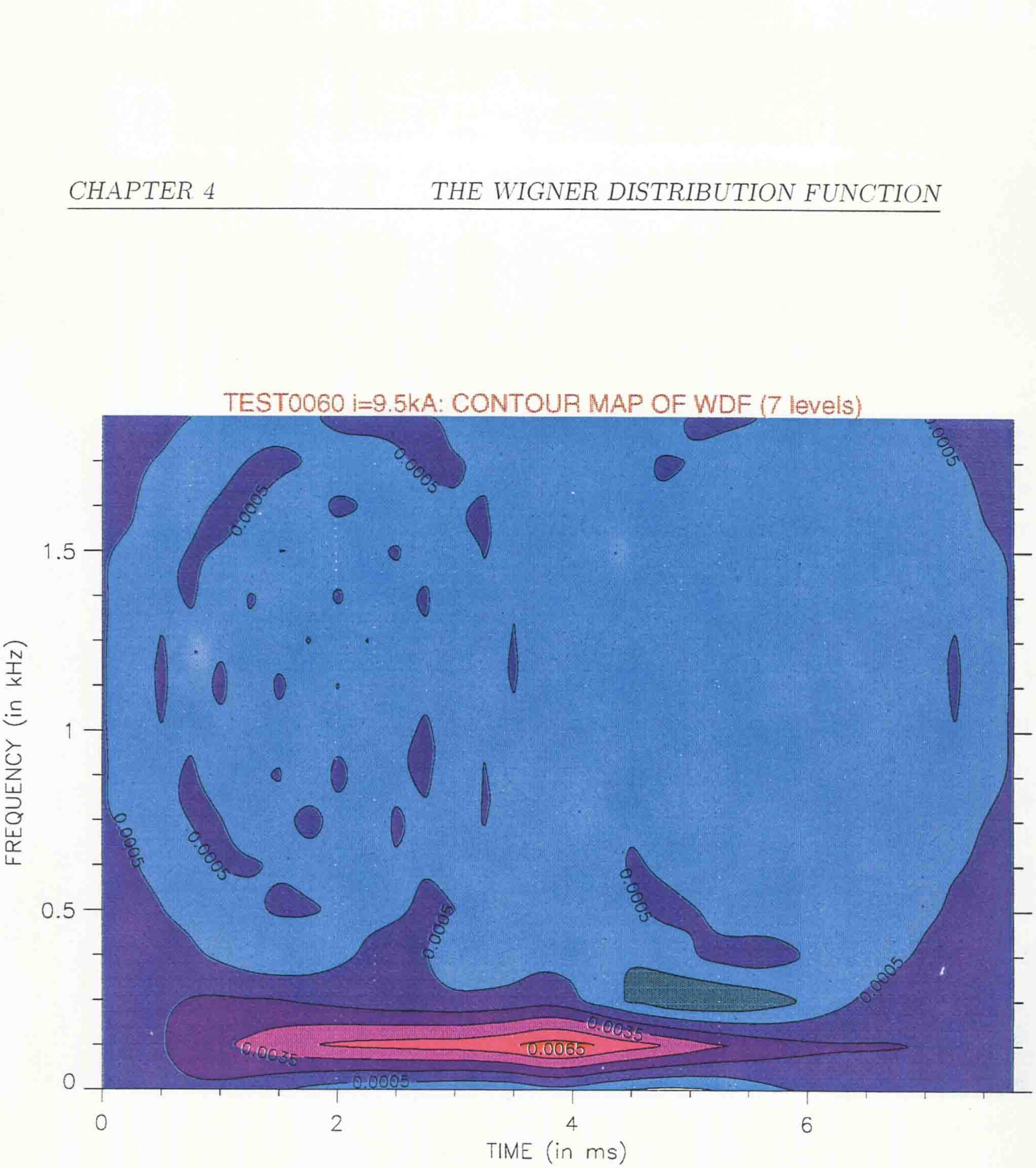

Figure 4.18: The Wigner distribution function of the electric arc signal $u_3(t)$.

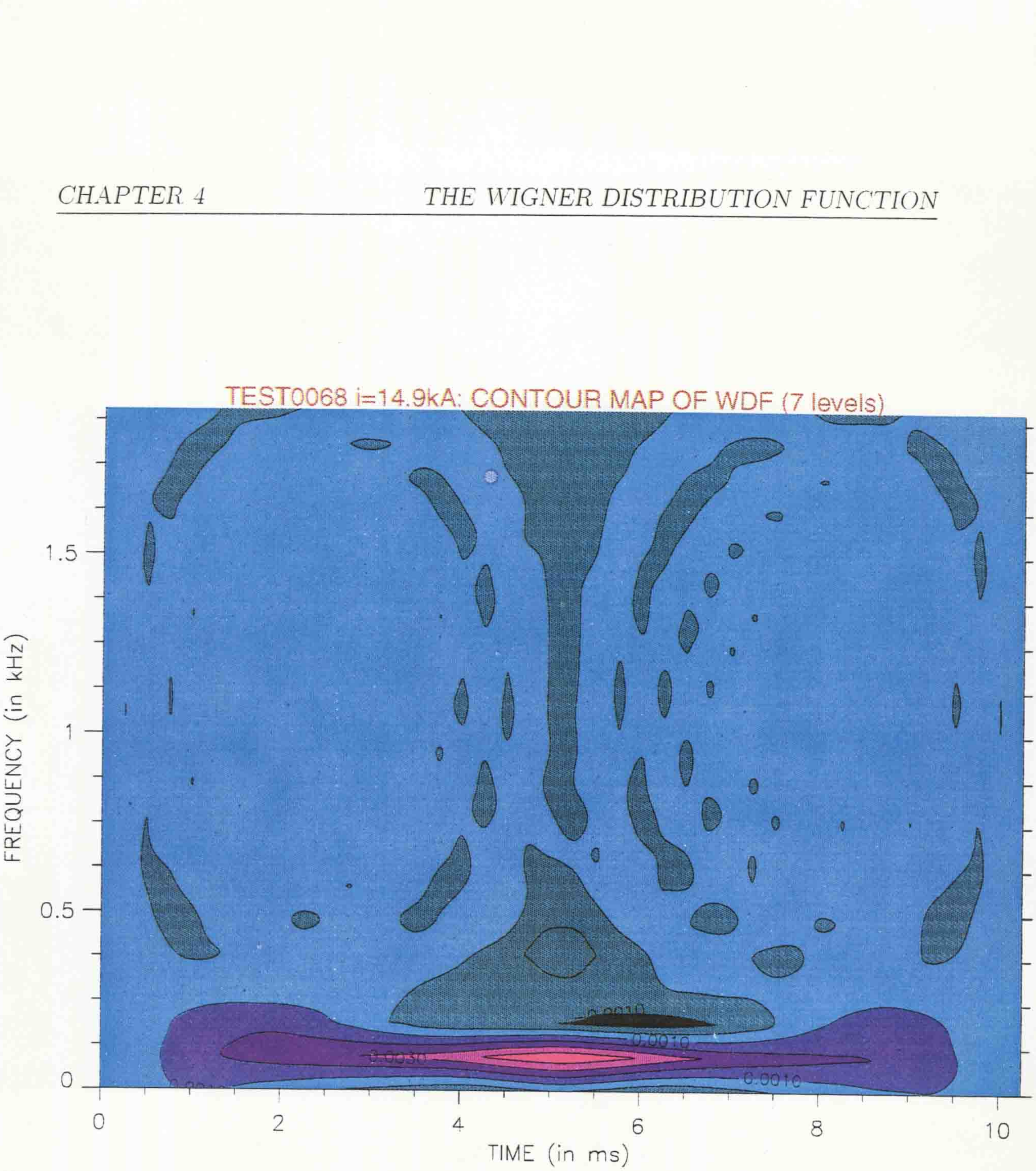

Figure 4.19: The Wigner distribution function of the electric arc signal $u_4(t)$.

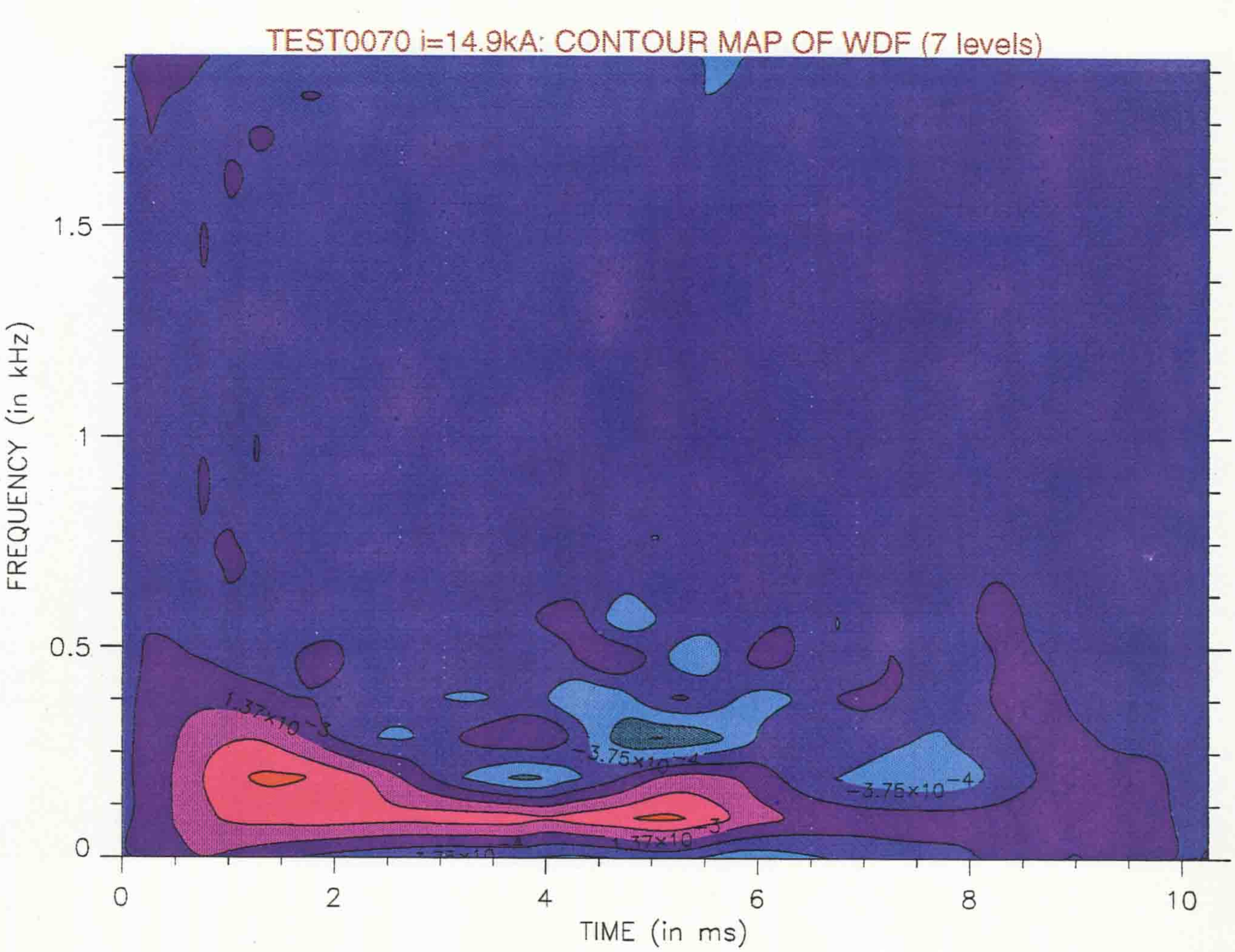

Figure 4.20: The Wigner distribution function of the electric arc signal $u_5(t)$.

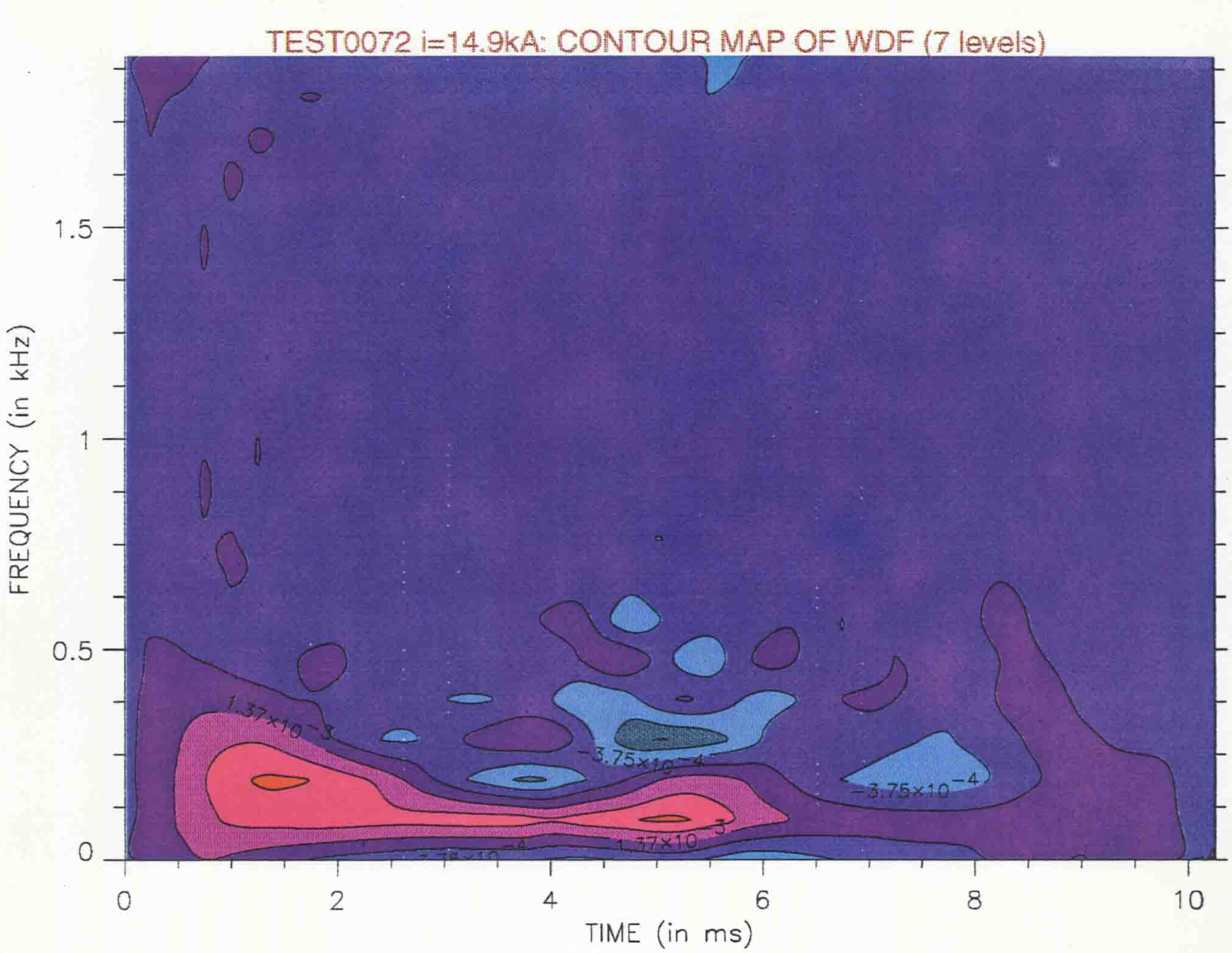

Figure 4.21: The Wigner distribution function of the electric arc signal $u_6(t)$.

Figure 4.22: The Wigner distribution function of the electric arc signal $u_7(t)$.

Chapter 5

The Gabor Expansion of a Signal Using a 'Truncated' von-Neumann Lattice

5.1 Introduction

The expansion of an arbitrary signal in terms of Gaussian signals - known as the *Gabor transform* or the *Gaussian expansion* - is due to D.Gabor. Since the approximate expansion he introduced in his classic monograph [63], later exact expansions were found [76, 118] and studied extensively [16, 82, 57, 161, 187, 192, 170, 204]. A considerable amount of work has been done on the existence, the completeness and the uniqueness of the Gabor transform [82, 16]. It is now known that Gabor expansions exist for any reasonable signal.

The Gabor representation is a joint representation in both time and frequency and its energy spectrum is a special case of Cohen's generalised class of time-frequency representations, related to the representation of a spectrogram using a gaussian window (Section 3.2) [81, 38]. From a mathematical point of view this expansion is similar to the expansion of an arbitrary quantum state in terms of coherent states (the analogue of Gaussian signals) in quantum mechanics and quantum optics [77, 99, 108, 125, 164]. A signal is represented by a superposition

of time-and-frequency shifts of a two-dimensional Gaussian. Similar to other time-frequency representations, the Gabor transform provides the time history of the frequency content of a non-stationary signal.

The Gabor expansion has been successfully applied in many signal processing applications such as radar signal design [175], and more extensively in image processing (image compression [50, 56], pattern recognition [128], texture analysis [128] and computer vision [114, 49, 127]). During the last thirty years, the community of perceptual and neurophysical vision research has shown special interest in the Gabor transform. The reason is that the Gaussian elementary signals fit the receptive field profiles of the simple cells in the visual cortex of mammals very well (in the sense of a least-squares fit). Indeed, the requirements of the visual nervous system (which deals with an enormous amount of information) for optimal economy lead to profiles similar to the two-dimensional Gaussian signals (which achieve the smallest possible uncertainty product). The function of these cells is analogous to the function of image processors or spatial/spatial-frequency filters. The Gabor representation provides an important mathematical tool for studying the local spatial/spatial-frequency characteristics of these cells [114, 49].

In most practical cases, a signal can be expanded in terms of only a few Gaussian signals. Here, a novel technique to represent signals using the Gabor scheme is proposed. As it will be demonstrated, the new technique has many advantages.

In the following sections, the Gabor expansion of an arbitrary signal in terms of complex Gaussian signals that form an $N \times M$ 'truncated' von Neumann lattice in the time-frequency plane is introduced. Quantitative analysis of the expansion for various values of (N, M) and various widths of the Gaussians is performed. Additionally, the stability of the Gabor expansion, which is a very desirable property, is demonstrated by examples. The potential of the method for applications in the context of optical signal processing is emphasised and practical implementation through devices that measure the Gabor coefficients ('Gabor analysers') is also discussed. The relevant algorithms are described in detail in Appendix B.

For the sake of completeness, the potential of the Bargmann analytic represen-

tation for applications in signal and image processing is explored in Section 5.6. This is another representation used in quantum theory and it can be employed as an alternative time-frequency representation.

5.2 The Gabor Expansion of a signal

Let $u(t)$ be a square-integrable real signal in time. The corresponding analytic signal (Section 3.4) is given by

$$s(t) = u(t) + jv(t). \tag{5.1}$$

We assume the analytic signal is energy-normalised:

$$\int_{-\infty}^{+\infty} |s(t)|^2 dt = 1. \tag{5.2}$$

Let us consider the basis of generalised *Gaussian* or *Gabor elementary signals* described by

$$r(t; A, \rho) = (2\rho)^{1/4} \exp[-\pi\rho t^2 + 2\pi^{1/2}(\rho A_R + jA_I)t - \rho A_R^2 - jA_R A_I], \tag{5.3}$$

where $A = A_R + jA_I$ is a complex number (representing a point in the time-frequency plane), and $\rho > 0$. The meaning of the parameter ρ is discussed in the following section. A_R and A_I are effectively the average time $\langle t \rangle$ ($\langle t \rangle = \pi^{-\frac{1}{2}} A_R$) and average frequency $\langle f \rangle$ ($\langle f \rangle = \pi^{-\frac{1}{2}} A_I$) of the signal.

All the Gaussian elementary signals are square-integrable. It is also known that the set of all these Gaussian signals with fixed ρ, and A taking all values in the complex plane, provides an *overcomplete* basis for signal analysis [76, 82, 175, 47]. More specifically, for any two elements of the basis $r(t; A, \rho)$ and $r(t; B, \rho)$ it can be proved that

$$\int_{-\infty}^{+\infty} r(t; A, \rho) r^*(t; B, \rho) dt = \exp[-\frac{1}{2}(|A|^2 + |B|^2) + AB] \tag{5.4}$$

and

$$\int\int \frac{1}{\pi} r(t; A, \rho) r^*(\tau; A, \rho) d^2A = \delta(t - \tau), \tag{5.5}$$

where the asterisk indicates the complex conjugate and the integrals are taken from $-\infty$ to $+\infty$. d^2A is used as an abbreviation for $dA_R dA_I$. Eq. (5.4) expresses the non-orthogonality of the two signals $r(t; A, \rho)$ and $r(t; B, \rho)$. The two Gaussian signals overlap and therefore they are not orthogonal; the left-hand side of Eq. (5.4) is called the *overlap integral.* Eq. (5.5) provides the so-called *resolution of the identity* which is a very important property of the Gaussian elementary signals. Even though the Gaussian basis is non-orthogonal, Eq. (5.5) enables us to expand an arbitrary complex normalised signal $s(t)$ as

$$s(t) = \int\int \frac{1}{\pi} \mathcal{S}(A, \rho) r(t; A, \rho) d^2A, \tag{5.6}$$

where

$$\mathcal{S}(A, \rho) = \int_{-\infty}^{+\infty} r^*(\tau; A, \rho) s(\tau) d\tau. \tag{5.7}$$

The resolution of identity expressed by Eq. (5.5) ensures that the Gaussian signals of Eq. (5.3) span the whole Hilbert space of square-integrable signals and can form a basis for representation of other signals.

Eq. (5.6) implies that an elementary signal $r(t; A, \rho)$ can always be expressed in terms of all the others, i.e. the signals of the Gaussian basis are not linearly independent, and consequently the basis is overcomplete. This suggests that the expansion of Eq. (5.6) is not unique. Using Eqs. (5.6) and Eq. (5.4), any element of the basis $r(t; A, \rho)$ can be expressed as

$$r(t; A, \rho) = \int\int \frac{1}{\pi} r(t; B, \rho) \exp\left[-\frac{1}{2}(|A|^2 + |B|^2) + AB\right] d^2B. \tag{5.8}$$

5.3 The Analogy Between Gabor Expansion in Signal Processing and Coherent States in Quantum Theory

The analogy between signal theory and quantum mechanics was discussed in Chapter 3. The Gabor representation with $\rho = 1$ is related to the expansion of an arbitrary quantum state in terms of the over-complete set of the *coherent states*

of a harmonic oscillator [77, 99, 111] . The generalised Gabor representation with $\rho \neq 1$ corresponds to the expansion of an arbitrary quantum state in terms of the *squeezed states*, recently of interest in quantum optics [108, 125, 164]. For a further discussion on quantum states, see Chapter 6.

The uncertainty principle in signal processing is given by Eq. 2.24 and quantifies the known statement that narrow signals in the time domain are wide in the frequency domain, and vice versa. As it was noted in Section 2.4, the Gaussian signals of Eq. 5.3 assume the smallest uncertainty product allowed by the uncertainty principle:

$$\Delta t \cdot \Delta f = \frac{1}{4\pi}; \tag{5.9}$$

the effective widths (see Chapter 2, Eqs. (2.22), (2.23)) for *normalised* signals are given by

$$\Delta t = \langle t^2 \rangle - \langle t \rangle^2, \tag{5.10}$$

$$\Delta f = \langle f^2 \rangle - \langle f \rangle^2, \tag{5.11}$$

$$\langle t^n \rangle = \frac{1}{2} \int t^n |s(t)|^2 dt; \quad n = 1, 2 \tag{5.12}$$

$$\langle f^n \rangle = \frac{1}{2} \int f^n |\tilde{s}(f)|^2 df; \quad n = 1, 2. \tag{5.13}$$

$\tilde{s}(f)$ is the Fourier transform of $s(t)$ and the brackets indicate expected values. The Gabor elementary signals corresponding to the coherent states (with $\rho = 1$) exhibit equivalent amounts of uncertainty in both time and frequency domains.

The "squeezing" parameter ρ determines the trade-off of uncertainty between time and frequency:

$$\rho = \Delta f / \Delta t. \tag{5.14}$$

It is clear that the parameter ρ allows us to improve time resolution at the expense of the frequency resolution, or vice versa. The effective widths in time and frequency domain are determined by ρ, as follows:

$$\Delta t = (4\pi\rho)^{-1/2}; \tag{5.15}$$

$$\Delta f = (4\pi)^{-1/2} \rho^{1/2}. \tag{5.16}$$

In the following sections, a technique for the numerical implementation of the Gaussian expansion will be presented. Additionally, the use of ρ in signal processing applications will be demonstrated.

5.4 The Basis of a 'Truncated' von-Neumann Lattice

The above analysis uses all Gaussian signals with fixed ρ, and A taking all values in the complex plane. The basis of all the Gaussian signals is overcomplete and there exist much smaller subsets of this basis which are also overcomplete sets. For practical applications, it is convenient to consider small discrete subsets of the whole basis.

The most well known subset is the set of the Gaussian elementary signals of Eq. (5.3) which are located on the points of the so-called *von-Neumann lattice* [119] in the time-frequency plane. In this case, A takes the discrete values

$$A = m\alpha_1 + jn\alpha_2, \tag{5.17}$$

where m, n take all integer values and α_1, α_2 are the lattice constants. It is known [119, 13, 125, 8] that when the area $\alpha_1\alpha_2$ of the elementary cell of this lattice is smaller(greater) than $\frac{1}{4\pi}$, the corresponding basis of Gaussian signals is overcomplete(undercomplete). The von-Neumann lattice can be considered as a regular sampling grid on the whole Gaussian basis[13, 77, 82, 175].

In many practical applications, even the (exactly complete) von-Neumann lattice might be offering much more information about the signal than what is actually needed. Practical signals (in digital form) are bounded in both time and frequency; assuming that frequency components above a certain frequency contribute only to noise, physical signals can be also considered to be bounded in both frequency and time. In mathematical language, this means that they can be represented in terms of a very small subspace of the total Hilbert space. In these cases, it is clear that a properly chosen finite subset of the (full) von Neumann lattice could be sufficient.

So let us consider a *truncated* version of the lattice of Eq. (5.17) where $m = 1, .., M$ and $n = 1, ..., N$, which provides a basis of NM elementary signals[159]. Eqs. (5.6) and (5.7) become

$$s(t) \approx \sum_{m,n} \frac{1}{\pi} \mathcal{S}_{mn}(\rho) r(t; m\alpha_1 + jn\alpha_2, \rho) \equiv s_{rec}(t) \tag{5.18}$$

and

$$\mathcal{S}_{mn}(\rho) = \int_{-\infty}^{+\infty} r^*(\tau; m\alpha_1 + jn\alpha_2, \rho)s(\tau)d\tau. \tag{5.19}$$

The right hand side of Eq. (5.18) is approximately equal to the original signal and we refer to it as the "reconstructed signal". The integral of Eq. (5.19) becomes a sum in the case of a sampled or discrete signal. The reconstruction is limited to a discrete finite set of Gaussian elementary signals which are suitably located in the time-frequency plane according to the time-frequency characteristics of the given signal. By neglecting the non-important elements of the (full) von Neumann lattice which lie outside the *'truncated' von-Neumann lattice*, we get a signal representation using a finite set of the expansion coefficients, which from a practical point of view is much easier to handle, and which is sufficient for an accurate reconstruction of the signal. In a different context (Chapter 6), [54] and [86] have expanded quantum mechanical wavefunctions in terms of a few coherent states in a straight line. In signal theory, this corresponds to the $1 \times N$ truncated von-Neumann lattice.

The 'truncated' von-Neumann lattice is an approximate representation and it is important to introduce quantities that provide a measure of the accuracy of the expansion. As a measure of how good the reconstruction is, the reconstruction error in the time domain is evaluated:

$$D = \int_{-\infty}^{+\infty} [u(t) - u_{rec}(t)]^2 dt, \tag{5.20}$$

where $u(t)$ is the original signal and $u_{rec}(t)$ is the reconstructed signal. Additionally, the Wigner function representation (Chapter 4) can successfully describe the difference between the original and reconstructed signals in the time-frequency domain.

In the numerical results presented in Section 5.5, these quantities are used to describe how accurately the signal can be reconstructed from a small number of coefficients. It is shown that the representation of a 'truncated' von-Neumann lattice provides a satisfactory approximation of the original signal.

An important aspect is the *robustness* of the expansion. It describes the stability of the representation against small perturbations; that is, how sensitive

is the reconstruction to small amounts of random noise.

In the numerical examples presented in Section 5.5, small amounts of random noise are added to the Gabor coefficients $\mathcal{S}_{mn}$:

$$\mathcal{S}'_{mn}(\rho) = \mathcal{S}_{mn}(\rho) + \lambda h_{mn}, \tag{5.21}$$

where λ is a constant and h_{mn} a random number in the interval $[-1, 1]$ with a flat distribution. It is shown that the reconstructed signal $s'_{rec}(t)$ from the perturbed Gabor coefficients is very close to the reconstructed signal $s_{rec}(t)$ from the unperturbed Gabor coefficients, for reasonably large values of λ. The expansion is *robust* and this makes it particularly attractive for practical applications.

5.5 Numerical Implementation of the Gabor Expansion using a Truncated von-Neumann Lattice

Various optical signals were analysed with very good results. Here, as an example, a signal obtained from the output of a powder monitor (see Appendix A) in the form of dominant wavelength as a function of time is considered (Fig. 5.1, 32 data points in time). The Gabor expansion in terms of a truncated von-Neumann lattice is implemented. A number of specialised algorithms were developed to perform the required processing (see Appendix B). Particular attention should be drawn to the reconstruction algorithm; a high degree of numerical accuracy is required because the calculation of the Gabor expansion involves very demanding exponential operations. The performance of the algorithms used in the following examples is found to be satisfactory. In the calculations, the normalised analytic form of the signal is used (as described in Sections 3.4, 5.1).

The Gaussian expansion of the given signal is calculated for different sets of coefficients in the time-frequency space for the cases $\rho = 1$ and $\rho = 0.1$. Reconstructions for the cases of $N \times M$ corresponding to 1×3, 3×3, and 1×8 are illustrated in Figs. 5.2-4. The reconstructed signals with $\rho = 1$ are indicated by a dashed line and those with $\rho = 0.1$ with a dotted line, whilst the original

signal is indicated by a solid line. The signal is reconstructed from its expansion coefficients using Eq. (5.18). The set of coefficients is a complex $N \times M$ matrix. For example, in the case 1×3 the three Gabor coefficients are: $-2.821 + j3.275$, $-1.227 + j2.806$ and $-1.397 + j2.475$.

Table 5.1 shows the reconstruction error D given by Eq. (5.20) for various cases (different sets of coefficients) with $\rho = 1$. For the specific case of the given signal, it can be seen that for the same number of coefficients $N \times M$, small N and large M give better results, i.e., in this case, when constructing the truncated von-Neumann lattice, it is better to take more points in the imaginary(frequency) axis. It is evident that it is possible to describe the signal accurately with a small number of coefficients.

The accuracy of the method can be also demonstrated by comparing and contrasting the Wigner functions for both the original and reconstructed signals. In order to describe from a different point of view the difference between the reconstructed signals and the original one, Figs. 5.5-7 show the corresponding Wigner functions for the original signal and for the cases 1×3 and 3×3 (with $\rho = 1$). Differences in the detailed structure of these signals in the time-frequency plane are clearly seen.

As we have seen from Eq. (5.14), we can use the parameter ρ to selectively reduce the uncertainty in either the time domain or the frequency domain. To point out the effect of the parameter ρ on the efficiency of the reconstruction, Table 5.2 shows the reconstruction error given by Eq. (5.20) for different values of the parameter ρ for the case of 1×4 lattice. Fig. 5.8 shows the graph of the reconstruction error D against ρ for the same case. In this specific case, small values of ρ ($\rho << 1$) produce more accurate representations. The advantage of the parameter ρ is that it enables us to optimise the reconstruction of a given signal.

Additionally, the stability of the representation has been investigated. In the given example, arbitrary small error values are added to the existing coefficients as described by Eq. (5.21) (with $\lambda = 0.35$). Figs. 5.9-11 show the outcome for the cases 1×3, 3×3 and 1×8 (with $\rho = 1$). In these graphs, the solid line indicates the original signal, the dashed line the initial reconstruction and

RECONSTRUCTION ERROR ($\rho = 1$)			
$N \times M$	α_1	α_2	D
2×2	5.00	0.5	0.4458
3×3	4.25	0.4	0.2397
4×4	3.25	0.3	0.1946
5×5	2.75	0.3	0.1693
6×6	2.50	0.2	0.1616
1×3	5.00	0.4	0.4986
1×4	5.00	0.3	0.3865
1×8	5.00	0.2	0.2752
1×16	5.00	0.1	0.0893
3×1	4.25	0.6	0.5231
4×1	3.25	0.6	0.3406
8×1	2.00	0.6	0.2268
16×1	1.25	0.6	0.2227
8×2	2.00	0.5	0.2549
2×8	5.00	0.2	0.1283
9×4	2.00	0.3	0.2114
4×9	3.25	0.2	0.1199
18×2	1.00	0.5	0.2175
2×18	5.00	0.1	0.0932

Table 5.1: Reconstruction error D, as calculated by Eq. (5.20), for various reconstructions of the original signal (shown in Fig. 5.1) using different $N \times M$ lattices with $\rho = 1$; α_1 (time domain) and α_2 (frequency domain) are given in units of ms and kHz respectively.

Reconstruction Error vs ρ	
ρ	D
0.2	0.2167
0.4	0.2755
0.6	0.3288
0.8	0.3669
1.0	0.3865
1.2	0.4134
1.4	0.4484
1.6	0.4792
1.8	0.5290
2.0	0.6036

Table 5.2: Reconstruction error D, as calculated by Eq. (5.20), for different values of the parameter ρ, for the case of 1×4 reconstruction of the original signal (shown in Fig. 5.1).

the dotted line the distorted reconstructed signal from coefficients with random noise. The difference between the two reconstructed signals as measured by the quantity $\int_{-\infty}^{+\infty} [u_{rec}(t) - u'_{rec}(t)]^2 dt$ (where $u'_{rec}(t)$ is the "noisy" reconstruction) is found to be 0.002, 0.060 and 0.095 correspondingly for each case. As it can be seen, the expansion is *robust* in the sense that random perturbations in the coefficients affect weakly the reconstruction. This is very important for practical applications.

As demonstrated, the basis of a truncated von-Neumann lattice, can be successfully used as an efficient method to represent signals. Depending on the specific application, we can select the optimum $N \times M$ combination for a satisfactory representation of the original signal and we can also optimise the parameter ρ. This results in information *compression* in time and spectral domains.

5.6 Practical Applications in Optical and Acoustical frequencies: Gabor Devices

An important application of the previous analysis is the development of '*Gabor devices*' or '*analysers*'. Processing of a signal in time and frequency can be carried out by a Gabor linear system described in the same time-frequency space [103]. This '*Gabor filter*' modifies the Gabor time-frequency representation of a signal according to the required specification. In fact, Gabor filters are a generalisation of the ordinary linear time-invariant systems. Their function can be described by the multiplication of the Gabor transform of the signal and the (time-frequency) "transfer function" of the Gabor filter.

The method can be used at all frequencies. At *optical* frequencies, the Gabor expansion of Eq. (5.18) can be implemented practically using appropriate hardware that plays the role of a Gabor analyser in an analogous way to a spectrum analyser that performs a Fourier analysis in terms of sinusoidal signals. Gabor filters (with a gaussian transfer function) can be used to perform the integrations of Eq. (5.19) and thus measure directly the Gabor coefficients. In this context, ordinary chromatic analysis can be viewed as a Gabor expansion and optical chromatic systems as Gabor devices operating at optical frequencies. Chromatic methods consider the spectral distribution (chromaticity) of light, which gives a quantitative measure of colour.

In this context, a first step toward Gabor devices are the widely used "chromatic devices" that contain 3 detectors with overlapping approximately-gaussian responsivity curves which provide the three chromaticity values (RGB: Red, Green, Blue), corresponding to the tri-stimulus colour system of human vision. Indeed, the responsivity curve for an inexpensive charge-coupled device (CCD) camera (Fig. 5.12) is approximately gaussian. These RGB devices have been used successfully for optical sensing, image processing, chromatic modulation, plasma processing etc. In the context of the previous analysis, they can be considered as Gabor devices which correspond to an 1×3 truncated von-Neumann lattice [67, 95, 134, 153, 186]. The RGB methods provide a basic approximation, as the reconstruction of an optical signal is only based on the three corresponding RGB

values. Extension of these devices into other ones with N detectors leads to generalised chromatic devices which can measure directly the coefficients of the $1 \times N$ Gabor expansion. An application of such generalised chromatic methods is found in [41], where the Gabor expansion is implemented for optical signal processing and a chromatic measurement system with detectors of Gaussian responsivity is used for monitoring high voltage switch gear. The stability of the expansion that we mentioned above is very important in such applications because it implies that implementation can be done using inexpensive hardware of modest accuracy.

Emphasis should be given to the fact that, due to the inherent overcompleteness of the Gabor expansion (overlap integral of Eq. (5.4)), the use of three (or more) a priori determined terms in a truncated von-Neumann lattice (as employed in the proposed generalised chromatic methods) is adequate. The chosen terms only need to lie reasonably within the effective time-frequency area where the signals of interest "live", but they do not need to be the dominant terms in the expansion. Compared to other methods (eg. Fourier transform) and given the robustness of the Gabor expansion, this property is highly advantageous and very important for practical applications.

Similar devices can also be built for other frequencies eg. in the acoustical domain. Gabor analysers can be successfully used for the analysis of acoustic vibration signals and improve the detection of defects in mechanical systems [135].

5.7 The Bargmann Transform in Signal Processing

5.7.1 Introduction

The *Bargmann analytic representation* [12] is another representation used in quantum mechanics. In the context of signal analysis, the Bargmann analytic representation has not been used so far, although it belongs to the family of time-frequency representations. It is known to be a powerful technique for quantum mechanics.

The Bargmann function is defined in the complex plane and belongs to the general class of the analytic representations. Images and signals can be represented by such functions which are analytic in the complex plane and the powerful theory of analytic functions could be exploited for the accurate representation of a signal in terms of a small number of parameters. Useful transforms between the Bargmann representation and other representations are also available. In the following sections, an analysis for signal/image processing applications is presented.

5.7.2 The relationship between the Bargmann transform and other representations

Let us consider a one-dimensional signal represented by the function $g(x)$; it can also be a one-dimensional image in which case $g(x)$ gives the level of grayness at the point $x(-\infty < x < \infty)$. It is assumed that the function $g(x)$ is normalised:

$$\int_{-\infty}^{+\infty} |g(x)|^2 dx = 1. \tag{5.22}$$

We call the representation of a signal by the function $g(x)$, 'x-representation'. The image can be also represented in the spatial frequency domain by the Fourier transform of the function $g(x)$:

$$\tilde{g}(f) = \int_{-\infty}^{+\infty} g(x) \exp(-jfx) dx. \tag{5.23}$$

The representation of a signal by the function $\tilde{g}(f)$ is called "f-representation". Let $\mathcal{H}$ be the Hilbert space of all the functions $g(x)$. In this Hilbert space, the *Hermitian orthonormal basis* is defined by

$$U_N(x) = \pi^{-1/4} 2^{-N/2} (N!)^{-\frac{1}{2}} H_N(x) \exp(-\frac{1}{2}x^2); \tag{5.24}$$

$$\int_{-\infty}^{+\infty} U_N(x) U_M(x) dx = 1, \tag{5.25}$$

$$\sum_{N=0}^{\infty} U_N(x) U_N(y) dx = \delta(x - y), \tag{5.26}$$

where $H_N(x)$ are the Hermitian polynomials (Section 4.1, Eq. (4.8)). The function $g(x)$ can be analysed in terms of this basis as follows:

$$g(x) = \sum_{N=0}^{\infty} g_N U_N(x); \tag{5.27}$$

$$g_N = \int_{-\infty}^{+\infty} g(x) U_N(x) dx, \tag{5.28}$$

$$\sum_{N=0}^{\infty} |g_N|^2 = 1. \tag{5.29}$$

The Bargmann representation of the signal is defined to be

$$B(z) = \sum_{N=0}^{\infty} (N!)^{-\frac{1}{2}} g_N z^N, \tag{5.30}$$

and is an analytic function in the complex plane. For a two-dimensional image the Bargmann function is a function of two variables, one for each dimension.

It is not difficult to prove that the Bargmann function can be calculated directly from the $x-$ and $f-$ representations [182]:

$$B(z) = \pi^{-1/4} e^{-z^2/2} \int_{-\infty}^{+\infty} \exp\left(2^{1/2} zx - \frac{x^2}{2}\right) g(x) dx; \tag{5.31}$$

$$B(z) = \pi^{-1/4} e^{-z^2/2} \int_{-\infty}^{+\infty} \exp\left(2^{1/2} jzf - \frac{f^2}{2}\right) \tilde{g}(f) df. \tag{5.32}$$

As an example let us consider the Gaussian function

$$g(x) = \pi^{-1/4} \exp(-\frac{1}{2}x^2 + 2^{1/2} Ax - A^2), \tag{5.33}$$

where A is a real number. In this case, we have

$$g_N = (N!)^{-1/2} A^N \exp(-\frac{1}{2}A^2), \tag{5.34}$$

$$B(z) = \exp(-\frac{1}{2}A^2 + Az). \tag{5.35}$$

The inverse relations can be easily found using the relations of Eqs. (5.31), (5.32):

$$g(x) = \pi^{-5/4} e^{-x^2/2} \int_{-\infty}^{+\infty} \int_{-\infty}^{+\infty} \exp\left(-|z|^2 - \frac{x^{*2}}{2} + 2^{1/2} xz^*\right) B(z) d^2 z; \tag{5.36}$$

$$\tilde{g}(f) = \pi^{-5/4} e^{-f^2/2} \int_{-\infty}^{+\infty} \int_{-\infty}^{+\infty} \exp\left(-|z|^2 + \frac{z^{*2}}{2} - 2^{1/2} j f z^*\right) B(z) d^2 z. \quad (5.37)$$

If z_R, z_I are the real and imaginary parts of z, we can derive the rather useful forms

$$g(z_R) = \pi^{-3/4} e^{-z_R^2/2} \int_{-\infty}^{+\infty} \exp(-z_I^2) B(2^{1/2} z) dz_I; \quad (5.38)$$

$$\tilde{g}(z_I) = \pi^{-3/4} e^{-z_I^2/2} \int_{-\infty}^{+\infty} \exp(-z_R^2) B(2^{1/2} z^*) dz_R. \quad (5.39)$$

It is evident that the inverse relation that provides the g_N from a known Bargmann function $B(z)$ is given by the transform:

$$g_N = \frac{(N!)^{\frac{1}{2}}}{2\pi j} \oint_C B(z) z^{N-1} dz. \quad (5.40)$$

5.7.3 Potential Applications of the Bargmann Transform in Optical Signal Processing

Let us consider a realistic example: a one-dimensional digitised image of a face against a roughly uniform background (Fig. 5.13). Fig. 5.14 illustrates the real part of the Bargmann function for the image of Fig. 5.13 as a function of the complex variable z. The corresponding Bargmann function is calculated using Eq. (5.31).

The analyticity of the Bargmann function makes it particularly useful for theoretical studies. Its potential in practical signal processing remains to be explored (for example, approximate reconstruction of a signal can be done using Eq. (5.38)).

Here we have investigated the relationship between the Bargmann representation and other representations and we have produced some numerical results. Further work is required to reveal its potential applications in a practical signal processing context.

5.8 Discussion

In conclusion, the original contribution of this chapter comprises the novel technique of a truncated von-Neumann lattice; the use of the important properties of stability and overcompleteness, which enable adequate reconstruction from a few pre-selected terms; the generalisation of chromatic methods using Gabor devices; and the development of dedicated software to perform the necessary analyses (Appendix B).

The full Gabor expansion of Eqs. (5.6), (5.7) provides an exact representation of a signal. However in practical applications truncated Gabor expansions are considered. A truncated $N \times M$ von-Neumann lattice of Gaussian signals is introduced in Eqs. (5.18), (5.19). A quantitative analysis of the reconstruction error shows that the truncated von-Neumann lattice provides a satisfactorily accurate representation.

Addition of small amounts of random noise to the Gabor coefficients do not affect the results drastically. The method is robust and this means that satisfactory performance can be achieved with inexpensive hardware. The effect of the relative width of the Gaussian signals (squeezing effect) can be useful in certain applications. Indeed, it has been pointed out that variation of the relative width (which depends on ρ) can be used for an improvement of the truncated Gabor approximation.

Comparing and contrasting the Gabor analysis with the Fourier analysis, they both reconstruct exactly a signal if we consider an infinite number of terms. In practical applications where truncated series are used, signals which in one expansion are well represented with only a few terms, in the other expansion may require many terms for the same degree of accuracy. A truncated expansion characterises always a family of signals which differ from each other only in the higher order terms which have been truncated. Two signals which cannot be distinguished in a truncated Fourier expansion, might be easily distinguishable in a truncated Gabor expansion, and vice versa. The Gabor transform is a time-frequency representation and is particularly suitable for the case of non-stationary signals (Chapter 2). It reveals the localised frequency distribution of a signal,

instead of the global frequency information provided by the Fourier transform.

In the case of an N-point discrete signal, the ordinary DFT requires N points in the frequency domain for a complete reconstruction. The number of points of the 'truncated' Gabor representation in the time-frequency plane is smaller and is related to the dimensions of the chosen truncated von-Neumann lattice. Of course, in the latter case, the accuracy of the approximation depends on the number of coefficients which determines the amount of information to be retained from the original signal. Compared to the Fourier representation, the Gabor transform is very flexible and enables reconstruction using fast and simple algorithms.

Additionally, the Gabor expansion reduces the amount of the data required to reconstruct the signal (data compression). Compression of information is an important aspect of the truncated expansion. Using only a few coefficients, the Gabor expansion efficiently represents the important components of the signal and is capable to retain sufficient information to reconstruct the signal with low distortion. It can be successfully used in applications in data transmission/compression and noise reduction, since for such applications strictly accurate representation is not required and a certain amount of distortion is acceptable.

Practical implementation of these ideas with devices that use Gabor analysers to measure directly the coefficients of the Gabor expansion seems to be very promising. Gabor analysers are the analogue of the spectrum analysers for the Fourier expansion. They consist of a number of Gabor filters with Gaussian transfer function. The method is suitable for practical applications in optical and acoustical frequencies. Suitable numerical algorithms can be found in Appendix B. Application of the same techniques in a different context (quantum optics) are presented in Chapter 6.

Figures

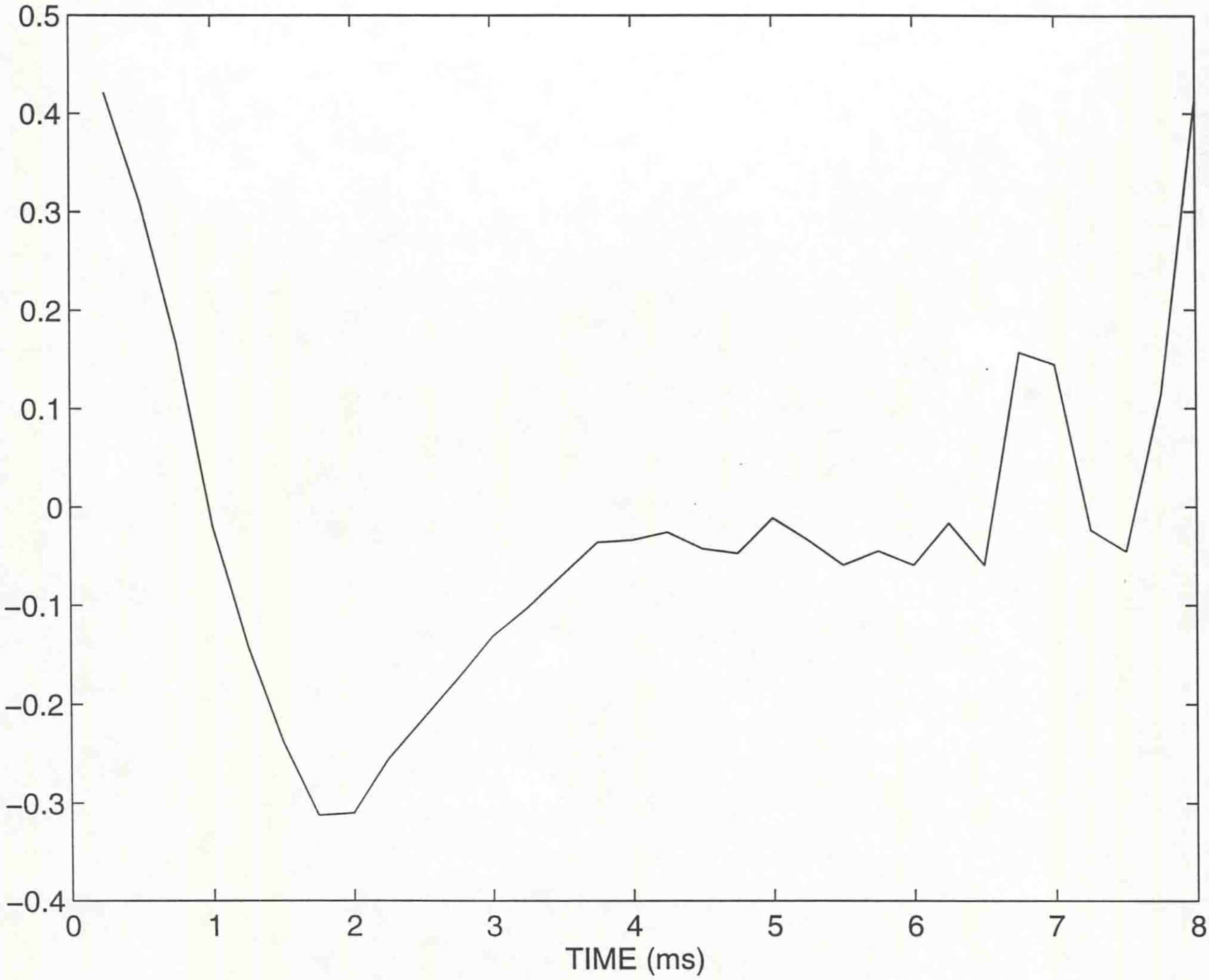

Figure 5.1: Original signal - Dominant wavelength of optical emission as a function of time.

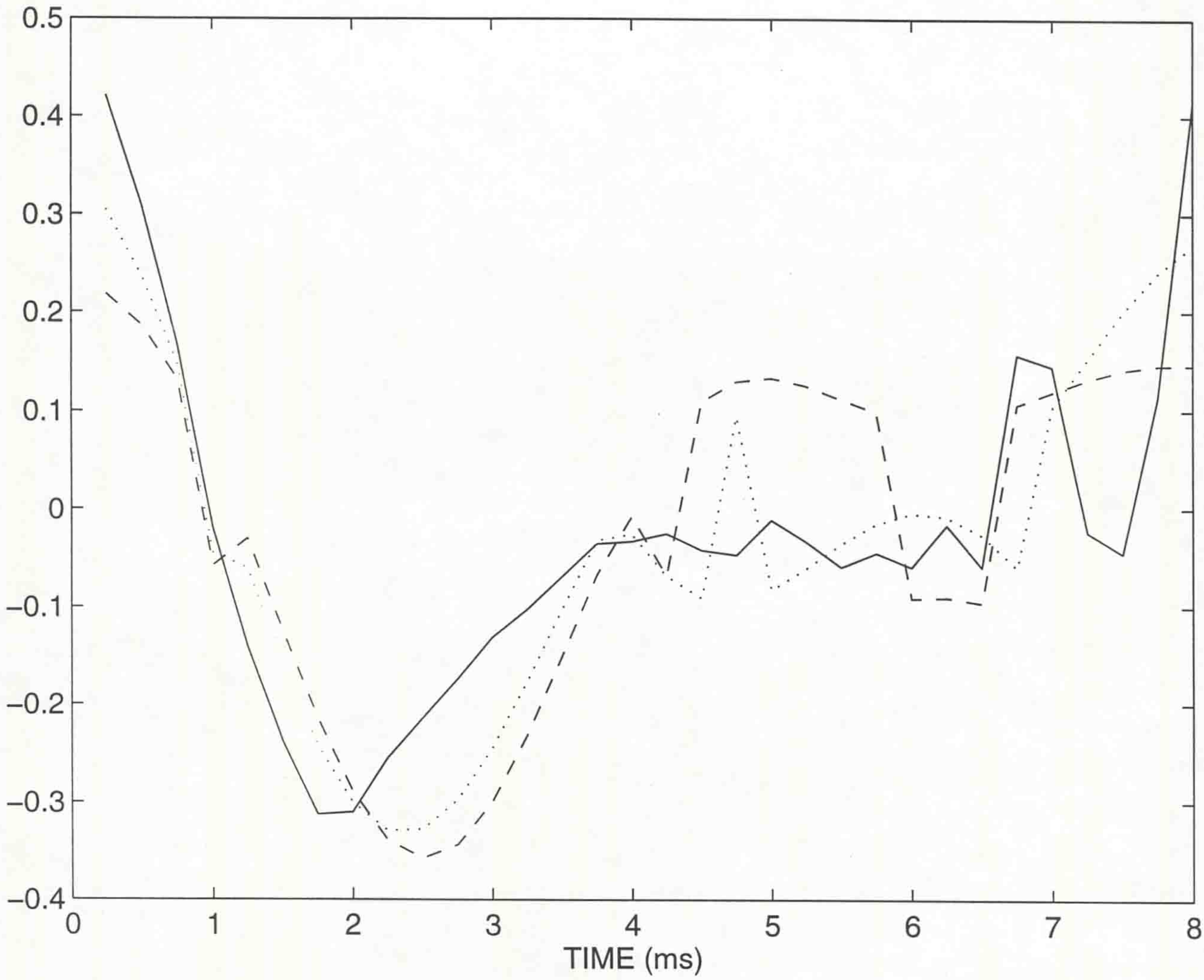

Figure 5.2: 1×3 reconstruction . Original signal (solid line), reconstructed signal with $\rho = 1.0$ (dashed line) and reconstructed signal with $\rho = 0.1$ (dotted line).

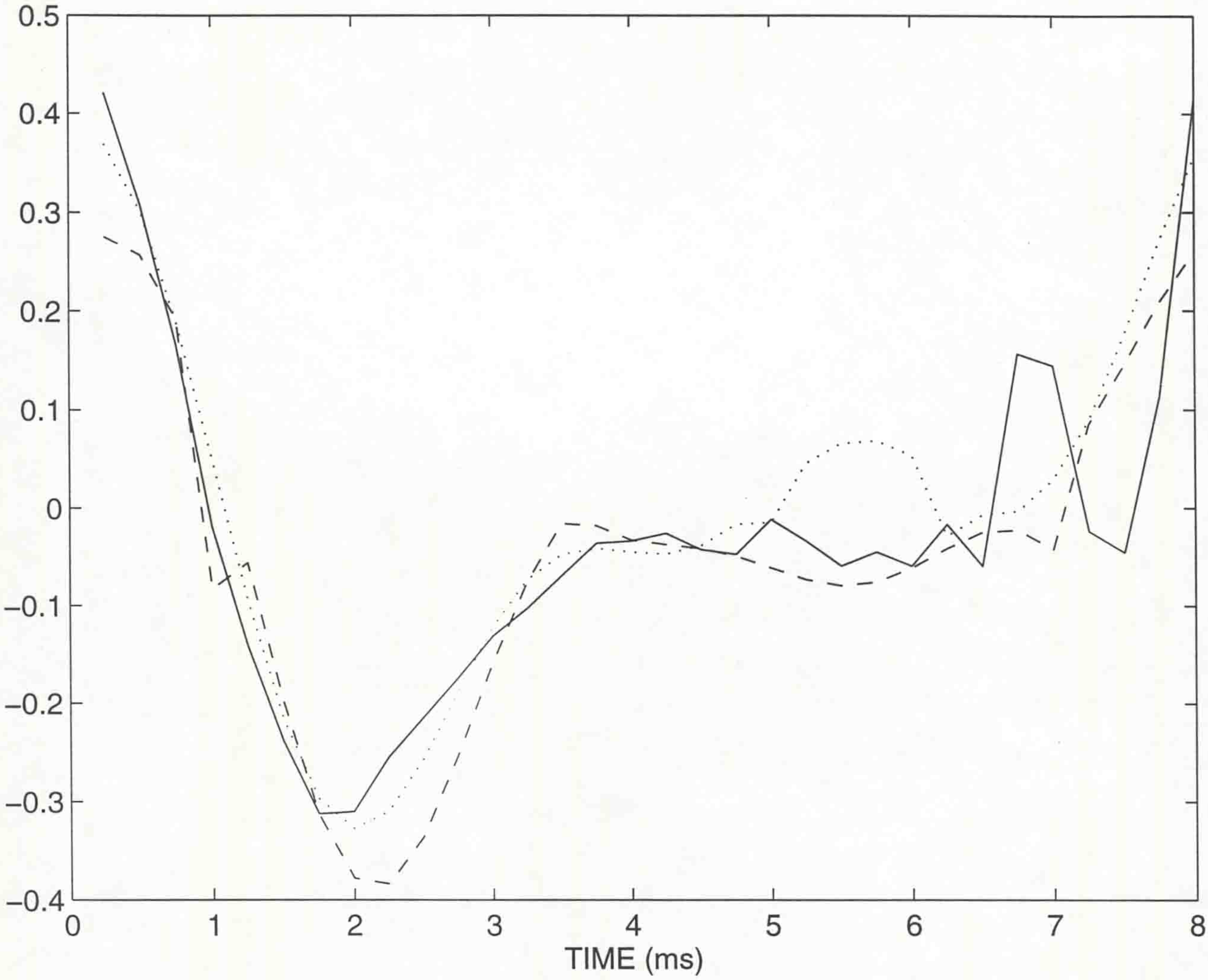

Figure 5.3: 3×3 reconstruction . Original signal (solid line), reconstructed signal with $\rho = 1.0$ (dashed line) and reconstructed signal with $\rho = 0.1$ (dotted line).

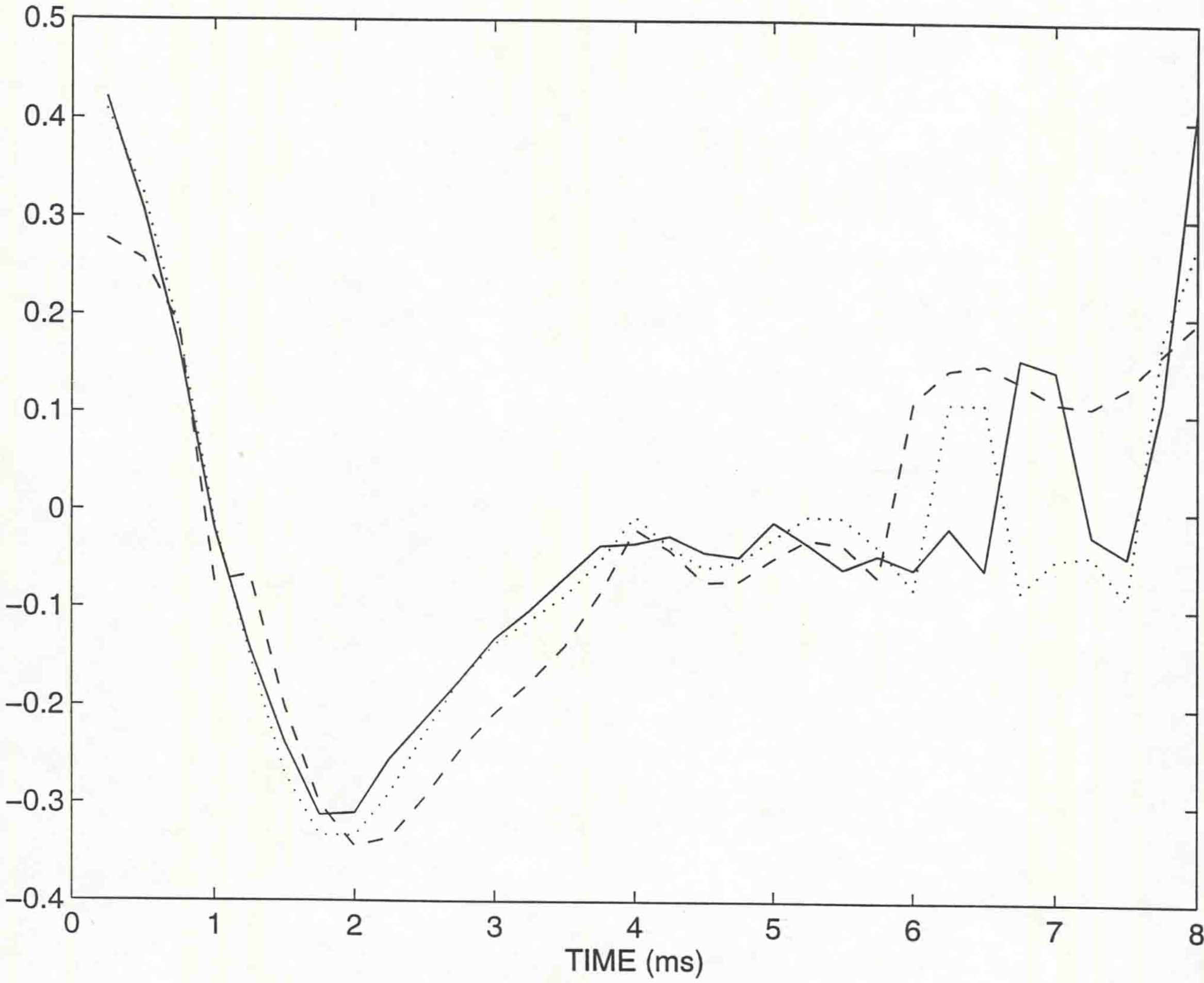

Figure 5.4: 1×8 reconstruction . Original signal (solid line), reconstructed signal with $\rho = 1.0$ (dashed line) and reconstructed signal with $\rho = 0.1$ (dotted line).

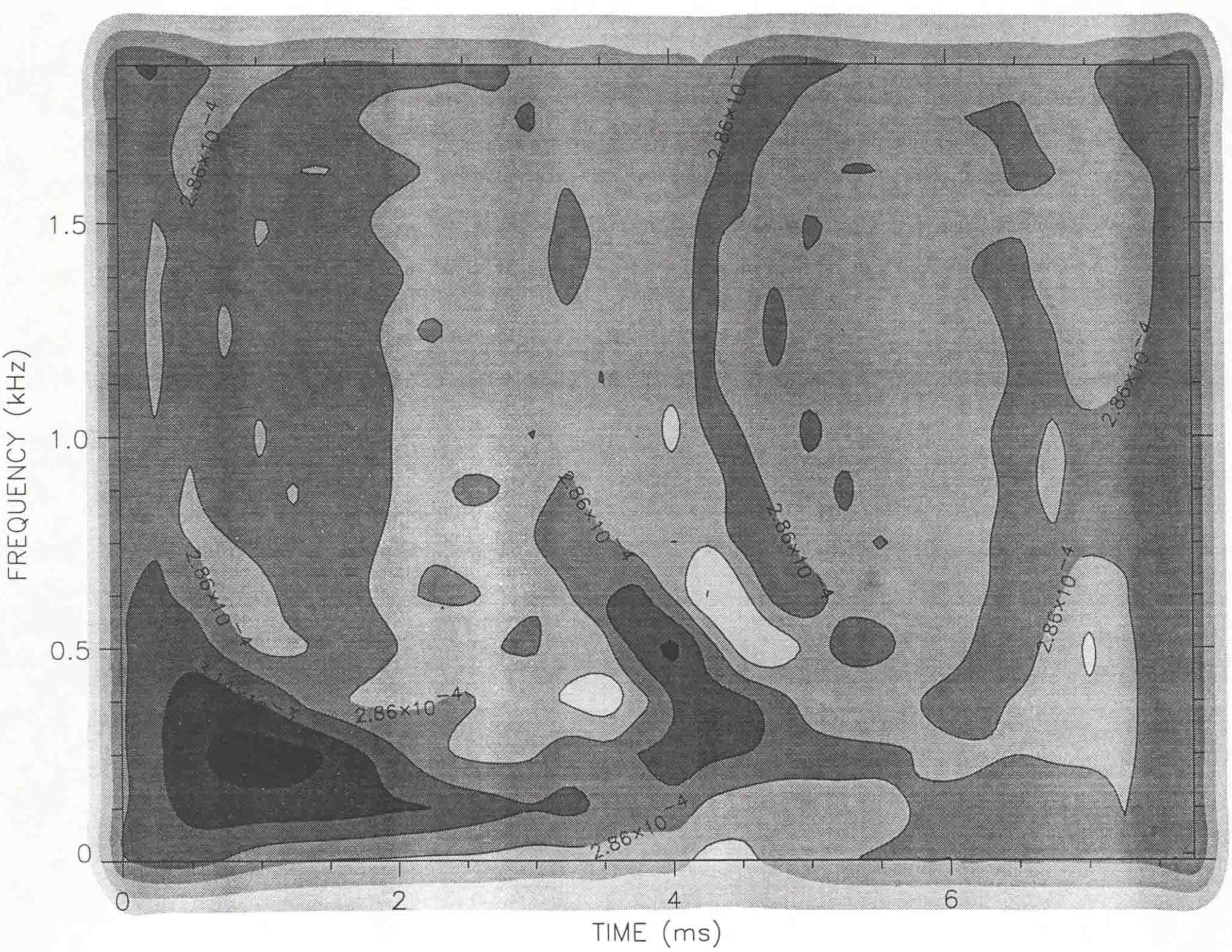

Figure 5.5: Wigner function of the original signal.

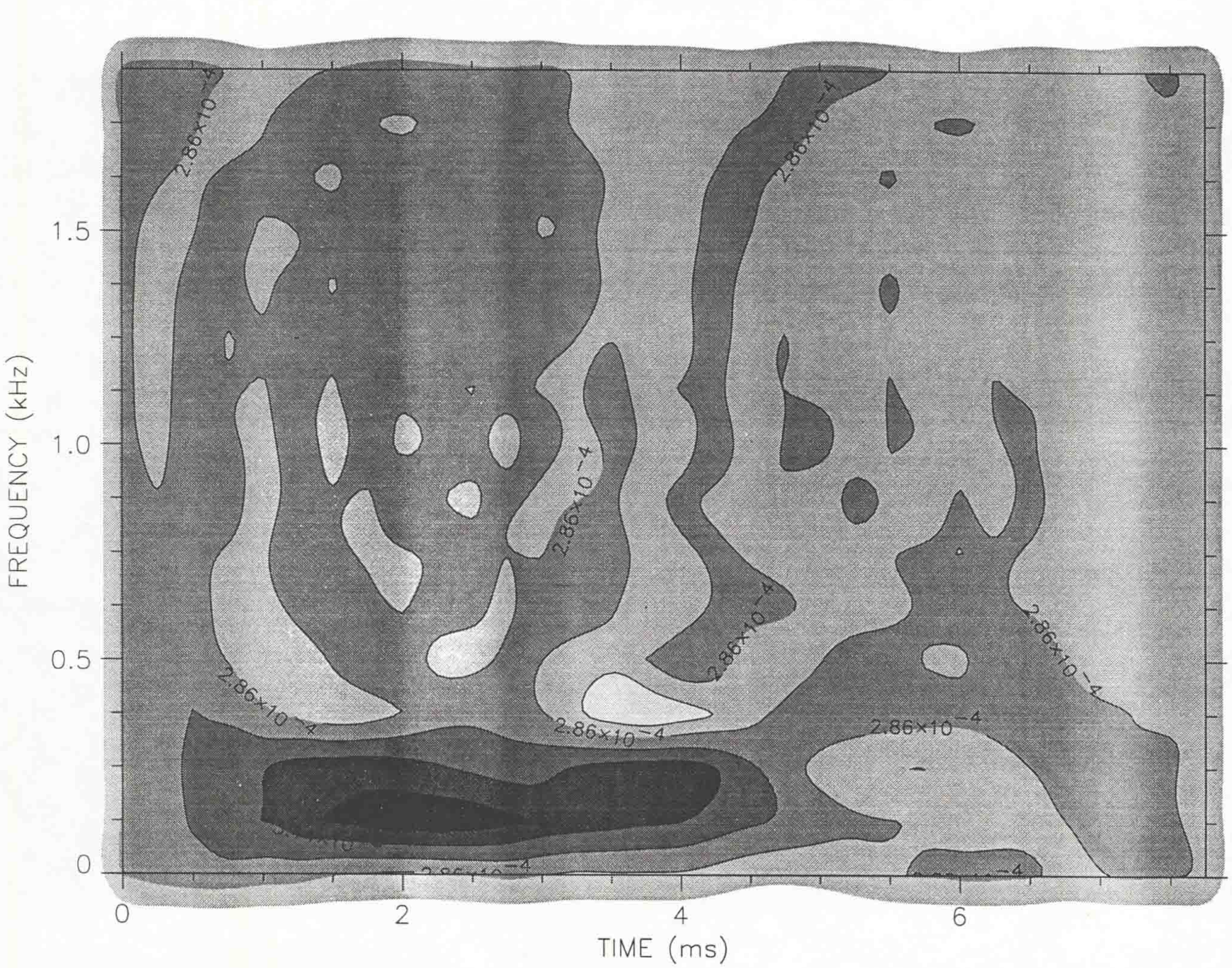

Figure 5.6: Wigner function of the reconstructed signal for the case 1×3 ($\rho = 1.0$).

Figure 5.7: Wigner function of the reconstructed signal for the case 3×3 ($\rho = 1.0$).

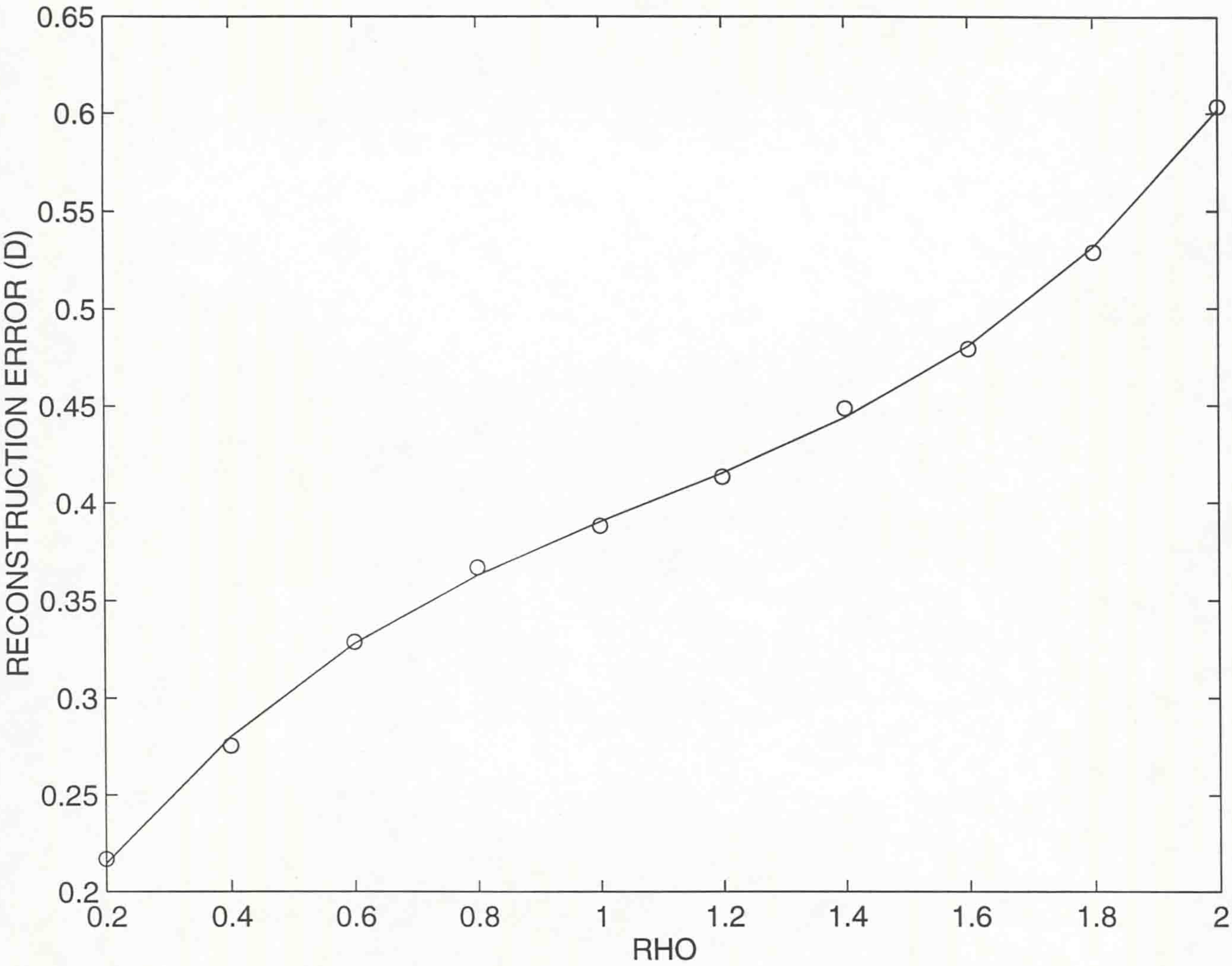

Figure 5.8: The reconstruction error as a function of ρ, for the case 1×4.

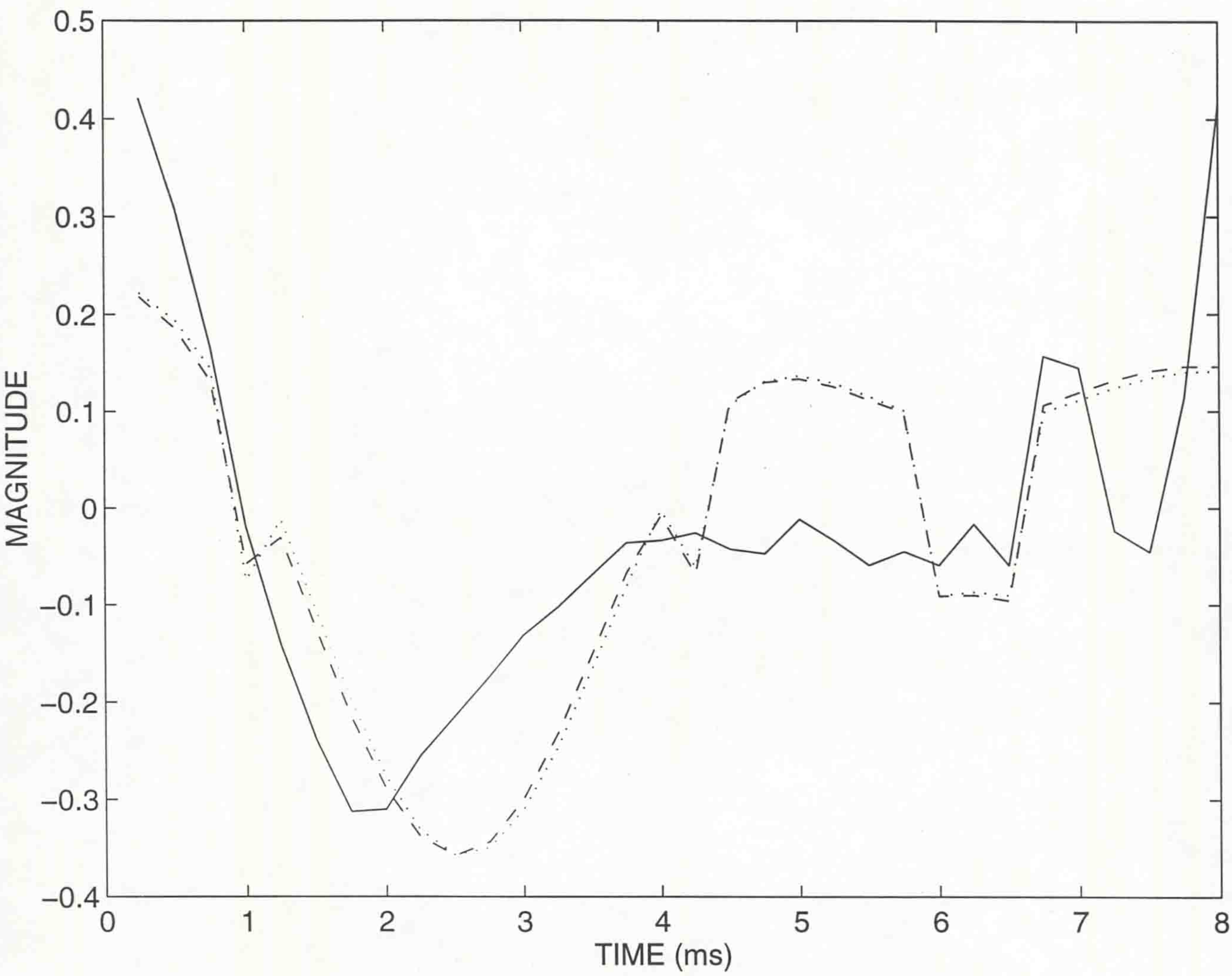

Figure 5.9: 1×3 reconstruction . Original signal (solid line), reconstructed signal with $\rho = 1.0$ (dashed line) and reconstructed signal from coefficients with random noise (dotted line)

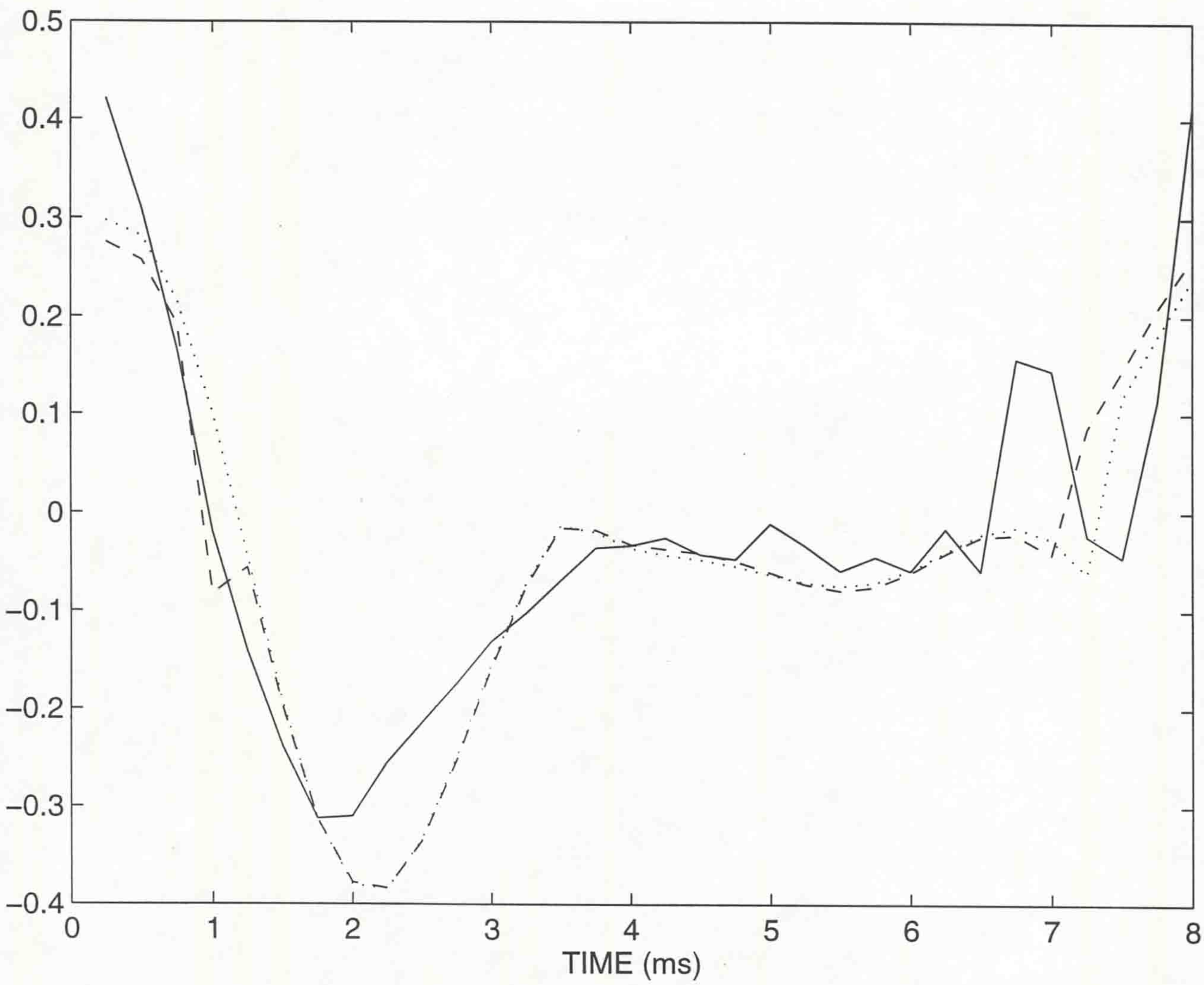

Figure 5.10: 3×3 reconstruction . Original signal (solid line), reconstructed signal with $\rho = 1.0$ (dashed line) and reconstructed signal from coefficients with random noise (dotted line).

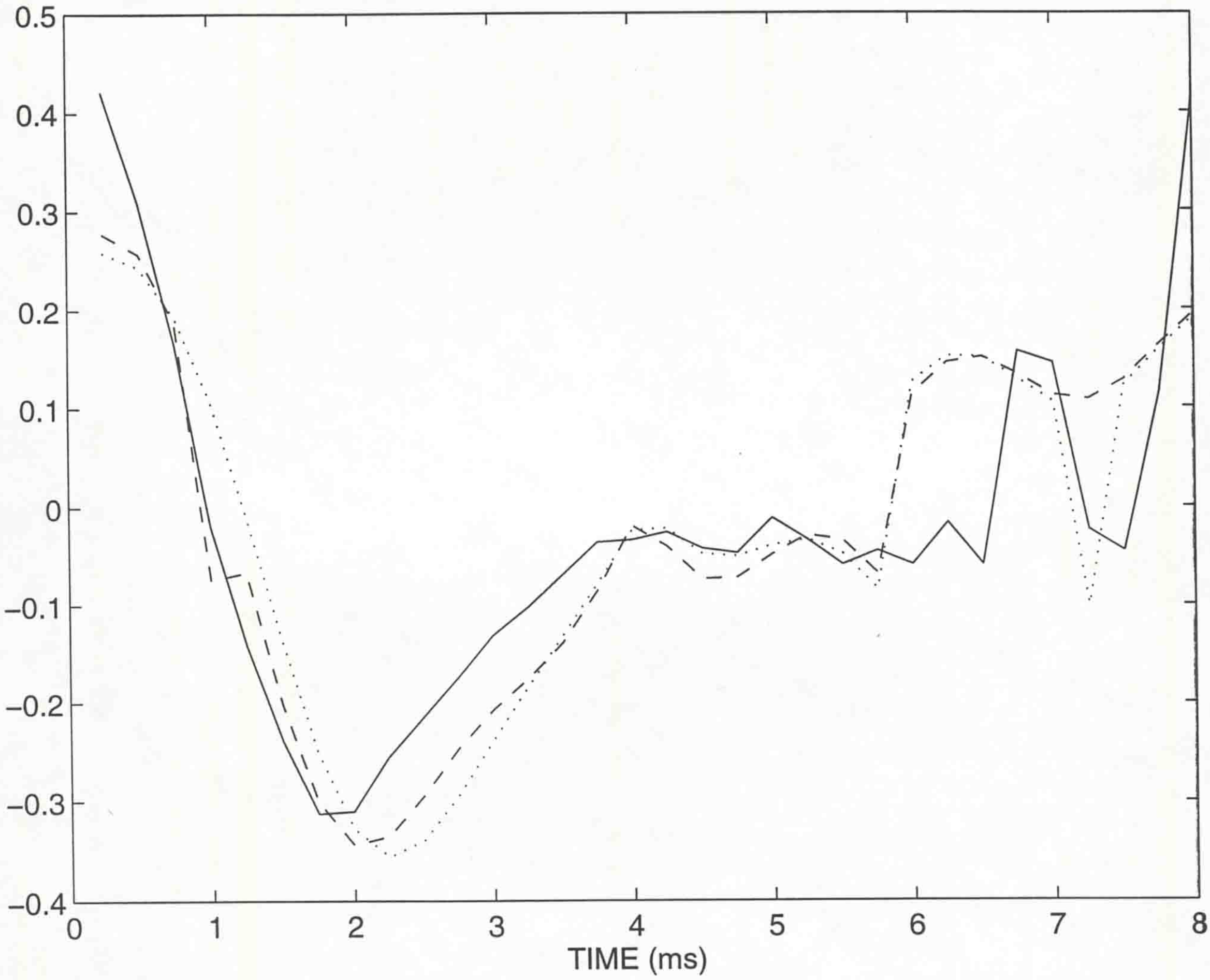

Figure 5.11: 1×8 reconstruction . Original signal (solid line), reconstructed signal with $\rho = 1.0$ (dashed line) and reconstructed signal from coefficients with random noise (dotted line).

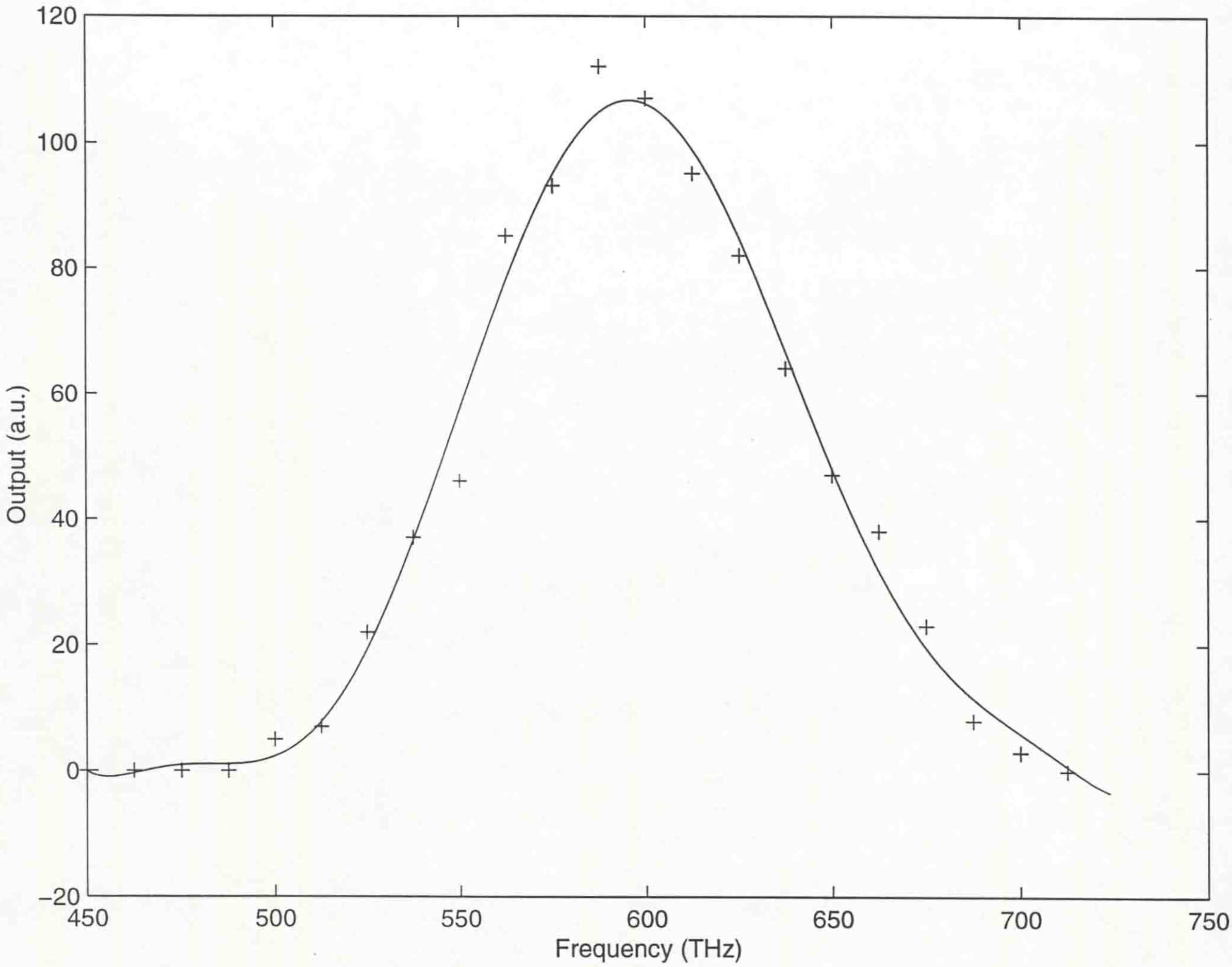

Figure 5.12: Responsivity curve for an element of an ordinary Charge-Coupled Device (CCD) camera.

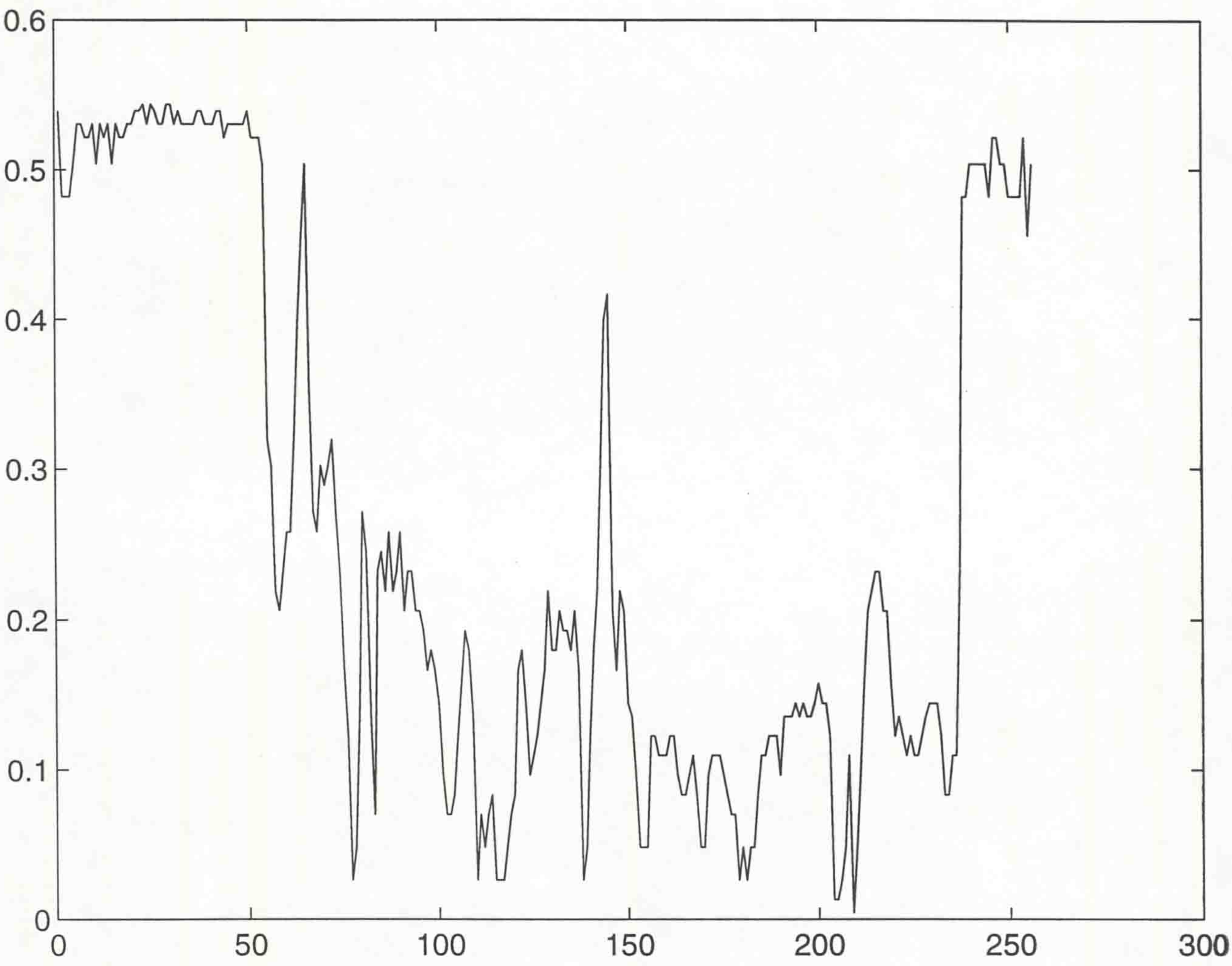

Figure 5.13: One-dimensional line from a two-dimensional digitised image of a face against a roughly uniform bright background.

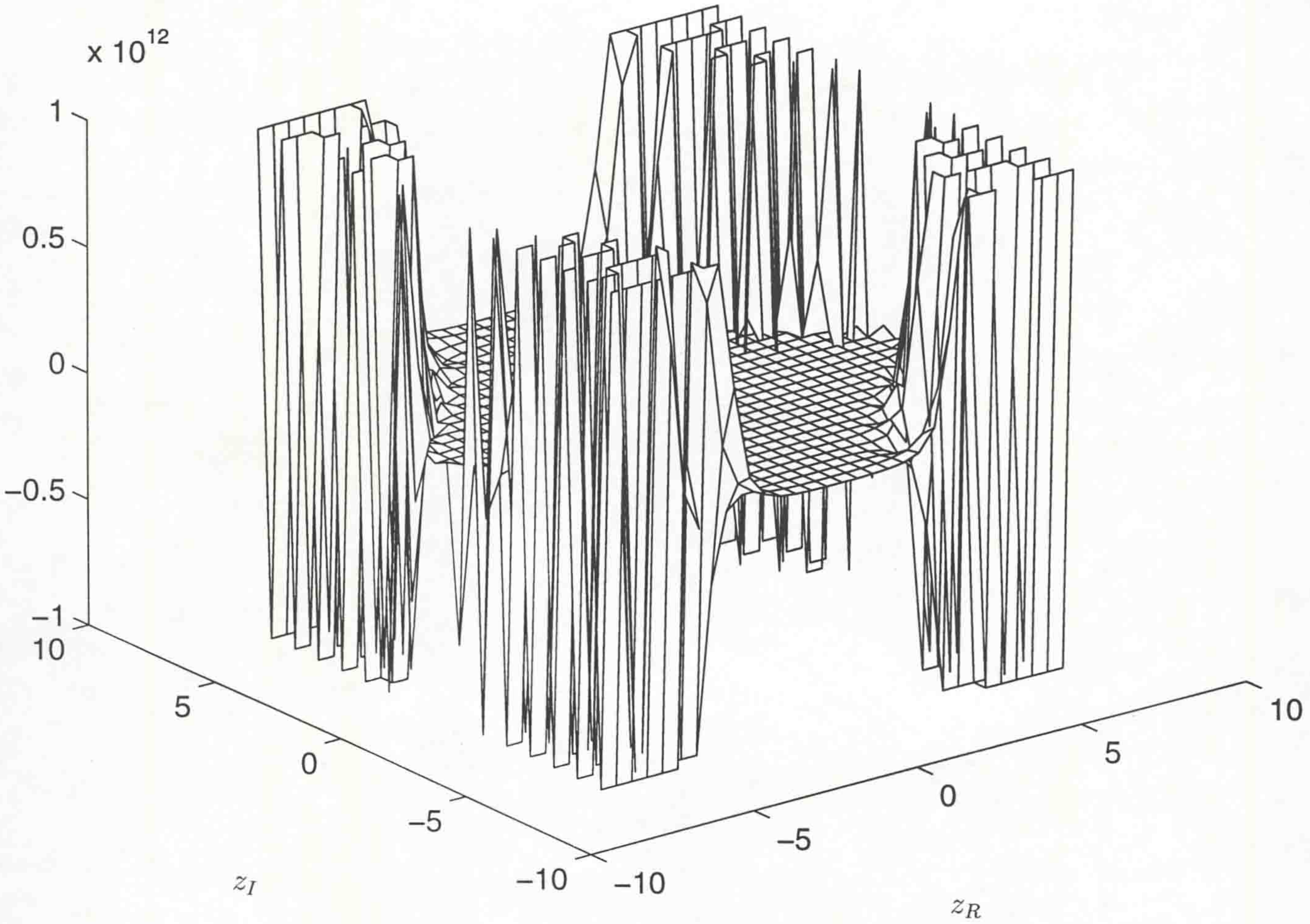

Figure 5.14: The real part of the Bargmann function (Eq. (5.31)) for the image of Fig. 5.13 and as a function of the complex variable z.

Chapter 6

Application of the Same Methods in Quantum Optics and Quantum Optical Communications

6.1 Introduction

Following the formal analogy between signal theory and quantum mechanics (Section 5.3), there exists an important application of the novel technique introduced in Chapter 5 in the modern field of quantum optics.

In quantum theory, it is well known that the *coherent states* form an overcomplete set in the Hilbert space. This basis corresponds to the Gaussian basis presented in Section 5.2 in a different context. The term "coherent state" is due to R. Glauber, who pointed out the importance of coherent states in the area of quantum optics [66, 65]. The coherent states are used in many different areas of theoretical physics [109, 185, 136, 17, 20, 179, 199, 176, 178, 125, 124, 14, 154, 196, 177, 18, 12, 181]. The von-Neumann lattice of coherent states is another well known overcomplete basis in the Hilbert space (see Section 5.4). In this chapter, a small finite subset of the von-Neumann lattice of coherent states is used to construct quantum states. This approach contributes to the existing framework of quantum state engineering [157, 156] .

Recent work in this area has shown that quantum states can be expressed as finite superpositions of coherent states [196, 176, 101, 86, 83, 84, 138, 174, 54]. Coherent states along a straight line in the complex plane have been considered [176, 86, 26, 2] and resolutions of the identity in terms of these states have been studied [180]. It is also known that number eigenstates can be constructed using superpositions of coherent states through quantum interference [101]. An up-to-date review of the subject can be found in [27]. More recently, related work has been done by J. Janszky *et al.* [85, 162] and A. Vourdas [180]. Particular attention has been paid to the experimental side of the subject. Indeed, nonclassical field states can be generated using micromaser or laser systems. Substantial progress in realising experimentally discrete superpositions of coherent states has been made in the fields of quantum optics [196, 73] and atomic physics [23, 22, 72, 74]. Engineering of quantum states is a fast growing field.

Here, it is demonstrated that non-classical states can be sufficiently approximated by superpositions of a few (properly chosen) coherent states. More specifically, a 'truncated' von-Neumann lattice is used as a discrete coherent-state basis for an approximate construction quantum states, with a good accuracy. Numerical results show that the technique is very accurate. Examples of noisy reconstruction (where additive random noise is applied to the coefficients) are used to demonstrate the robustness of the expansion, which is a very desirable property. Indeed, it is shown that the reconstruction is robust, in the sense that the constructed state is particularly insensitive to small amounts of random noise in the coefficients. Detailed comparison between original and reconstructed states as well as the associated Wigner function representations shows that the agreement in all cases is very good. The advantages of the method are presented and its ability to construct non-classical states accurately is demonstrated.

The method is general and can be applied for any family of quantum states [156]. Here, construction of squeezed states and number eigenstates is considered in a quantum optical context. For this purpose, the software developed in Chapter 5 can be used with slight modifications (Appendix B). In the following section, basic definitions for these quantum states and some properties of the coherent states are briefly introduced.

6.2 Coherent States, Squeezed States, and Number Eigenstates

6.2.1 Basic Definitions

The Hamiltonian $\hat{H}$ of a single-mode electromagnetic field is

$$\hat{H} = \hat{a}^\dagger \hat{a} + \frac{1}{2}, \tag{6.1}$$

in units where the Planck's constant $\hbar$, the velocity of light c, and the angular frequency ω are equal to 1, and $\hat{a}^\dagger$, $\hat{a}$ are the photon creation and annihilation operators, respectively:

$$\hat{a}^\dagger = \frac{\hat{x} - i\hat{p}}{\sqrt{2}}, \tag{6.2}$$

$$\hat{a} = \frac{\hat{x} + i\hat{p}}{\sqrt{2}}, \tag{6.3}$$

where $\hat{x}$ and $\hat{p}$ are the position and momentum operators respectively. The commutator of operators $\hat{a}^\dagger$, $\hat{a}$ is

$$[\hat{a}, \hat{a}^\dagger] = \hat{\mathbf{1}}. \tag{6.4}$$

The *photon number* (or *Fock*) *states* $|n\rangle$, $n = 0, 1, 2, ...$, are eigenstates of the Hamiltonian of Eq. (6.1). The number eigenstates describe states of an exact number of photons. They exhibit large fluctuations and are not minimum uncertainty states. The wavefunction $\psi_n(x)$ of the number eigenstate $|n\rangle$ is given by

$$\psi_n(x) = \pi^{-1/4} 2^{-n/2} (n!)^{-\frac{1}{2}} H_n(x) \exp(-\frac{1}{2}x^2), \tag{6.5}$$

where $H_n(x)$ are the Hermitian polynomials (Section 4.1, Eq. (4.8)). From our discussion in Section 5.7, it follows that the set of the number eigenstates $|n\rangle$, $n = 0, 1, 2, ...$, forms a *Hermitian basis* which is complete and orthonormal. The *vacuum state* $|0\rangle$ is a special member of the number eigenstates with $n = 0$ (ground state of the radiation field).

In quantum optics, the Wigner function is a *quasi-probability distribution* of great importance. It characterises uniquely the quantum state and describes

completely the quantum-mechanical system in the whole phase space. For an arbitrary quantum state $|f\rangle$, its Wigner function $W(x,p)$ is defined by

$$W(x,p) = \int_{-\infty}^{+\infty} dq \langle x + \frac{1}{2}q|f\rangle\langle f|x - \frac{1}{2}q\rangle \exp[-ipq]. \tag{6.6}$$

The Wigner function for the number eigenstate $|n\rangle$ is known to be [78]:

$$W_{(n)}(x,p) = (-1)^n e^{-(x^2+p^2)} L_n[2(x^2+p^2)], \tag{6.7}$$

where L_n is the Laguerre polynomial of order n, and it has a rotational symmetry (see Section 4.1). Eq. (6.7) implies that number eigenstates are rotationally invariant and highly nonclassical.

The *coherent states* $|A\rangle$, are defined as right eigenstates of the annihilation operator:

$$\hat{a}|A\rangle = A|A\rangle, \tag{6.8}$$

where a is a complex amplitude. They can also be regarded as displaced vacuum states:

$$|A\rangle = \hat{D}(A)|0\rangle, \tag{6.9}$$

where $\hat{D}(A)$ is the Glauber unitary displacement operator:

$$\hat{D}(A) = \exp(A\hat{a}^\dagger - A^*\hat{a}). \tag{6.10}$$

It is known that

$$\hat{D}(A)\hat{a}\hat{D}^\dagger(A) = \hat{a} - A\hat{\mathbf{1}}; \tag{6.11}$$

$$\hat{D}(A)\hat{a}^\dagger\hat{D}^\dagger(A) = \hat{a}^\dagger - A^*\hat{\mathbf{1}}. \tag{6.12}$$

Clearly, the vacuum state is a special case of a coherent state.

The wavefunction $\psi_A(x)$ of the coherent state $|A\rangle$ is a Gaussian:

$$\psi_A(x) = \langle x|A\rangle = \pi^{-1/4}\exp[-\frac{1}{2}x^2 + \sqrt{2}Ax - (\mathrm{Re}A)A]. \tag{6.13}$$

The Wigner function of a coherent state is also gaussian (Section 4.2):

$$W_A(x,p) = \left(\frac{\pi}{2}\right)^{-1/2} \exp\left\{-\left[(x-\sqrt{2}\mathrm{Re}A)^2 + (p-\sqrt{2}\mathrm{Im}A)^2\right]\right\}. \tag{6.14}$$

Coherent states are minimum uncertainty states, that is

$$\langle (\Delta x)_A^2 \rangle \langle (\Delta p)_A^2 \rangle = \frac{1}{4}, \tag{6.15}$$

where $\langle (\Delta x)_A^2 \rangle$ and $\langle (\Delta p)_A^2 \rangle$ are the variances in the "position" space and in the "momentum" space, respectively. According to Heisenberg's uncertainty principle, the uncertainty product of Eq. (6.15) expresses the minimal quantum fluctuations of physical observables (vacuum fluctuations). In coherent states, both "position" and "momentum" variables have equal dispersions. Being quantum states, coherent states are as close to classical behaviour as possible. Because they are highly localised, that is, they 'occupy' minimum area in the 'position-momentum' space, they are as close as possible to single points in classical phase space; they can be regarded as points in phase space with vacuum fluctuations (Eq. (6.9)).

The *squeezed states* $|A; r, \theta\rangle$ can be regarded as a generalisation of the coherent states $|A\rangle$:

$$|A; r, \theta\rangle = S(r, \theta)|A\rangle, \tag{6.16}$$

where $S(r, \theta)$ is the so-called unitary squeeze operator

$$S(r, \theta) = \exp[-\frac{1}{4} r e^{-i\theta} (a^\dagger)^2 + \frac{1}{4} r e^{i\theta} a^2]; \tag{6.17}$$

$re^{i\theta}$ is the complex *squeezing parameter*. The wavefunction of a squeezed state is a 'generalised' Gaussian. Like coherent states, squeezed states are also minimum uncertainty states and satisfy Eq. (6.15). However, in squeezed states, the dispersion of the "position" variable is reduced at the expense of an increase in the dispersion of the "momentum" variable. This means that fluctuations in one variable can be below the coherent-state limit. This reduction of fluctuations below the vacuum level is called *squeezing*. Squeezing is particularly desirable in a lot of practical applications, because it reduces *quantum noise*.

Not surprisingly, the Wigner function for the squeezed state is also a 'squeezed' Gaussian. The squeezed states correspond to the generalised Gaussian elementary signals of Eq. (5.3), that were studied in Chapter 5. The amplitude r of the complex squeezing parameter in Eq. (6.17) is connected to the parameter ρ (Chapter 5) by

$$r = \ln \rho. \tag{6.18}$$

Recently, the fundamental and practical aspects of squeezing have received a lot of interest [194, 184, 140, 183, 108, 164, 165, 176, 177, 96, 97]. Currently, experimental work on squeezing of light is making rapid progress. During the last decade, significant reductions in quantum noise have been achieved using various experimental configurations [152, 145, 190, 123, 126] and recently noise level below 0.25 (compared to 1.0 of the vacuum limit) has been recorded. The vacuum fluctuations of light can now be controlled and manipulated and this is very promising for a wide range of applications. The first application of squeezed light considered the reduction of quantum noise in optical communications [195, 194, 144]. Light squeezing is of great value in low-noise optical communications because it can dramatically increase the signal-to-noise ratio. Other applications of squeezed light have been considered in the areas of optical interferometry [30] and laser spectrometry [29, 198].

Squeezed states and number eigenstates are highly nonclassical states, while coherent states are the most classical of quantum states. In the following sections, it will be shown that both squeezed states and number eigenstates can be approximately expressed as a superposition of a small number of coherent states. There has been a lot of theoretical and experimental progress in the problem of how to construct superpositions of coherent states and this opens the way for the construction of an arbitrary quantum state (known as quantum state engineering).

6.2.2 Coherent states as an overcomplete basis

The coherent states form a non-orthogonal basis in the Hilbert space and, in this context, the resolution of the identity is given by

$$\int \frac{d^2A}{\pi} |A\rangle\langle A| = \mathbf{1}, \tag{6.19}$$

where d^2A is a shorthand notation for $d(\mathrm{Re}A)d(\mathrm{Im}A)$. An arbitrary (normalised) state $|f\rangle$ can be expressed as

$$|f\rangle = \int \frac{d^2A}{\pi} f(A)|A\rangle; \quad f(A) = \langle A|f\rangle \,. \tag{6.20}$$

It is well known [100, 13, 8, 111, 107, 125] that the set of all coherent states $\{|A\rangle\}$, where A takes all the values in the complex plane, is highly overcomplete and, as mentioned earlier, there are smaller subsets of coherent states which are also overcomplete. For example, the set of coherent states lying on a sequence $\{z_N\}$ which converges to some point z_o in the complex plane is overcomplete [125]; the set of coherent states lying on a one-dimensional manifold in the complex plane is therefore overcomplete set.

The *von-Neumann lattice* of coherent states is also known to form an overcomplete basis in the Hilbert space [119, 13, 125, 8] (Chapter 5). In the language of quantum theory, the von-Neumann lattice is the set of coherent states $\{|S^{1/2}M + iS^{1/2}N\rangle\}$ where M, N are integers and S is the lattice area. It is well known that this set is overcomplete if $S < \pi$; undercomplete if $S > \pi$; and exactly complete if $S = \pi$ (in analogy to the signal processing case in Chapter 5).

6.3 The 'truncated' von-Neumann lattice of coherent states

Here, a finite rectangular sublattice of the von-Neumann lattice, i.e. a 'truncated' von-Neumann lattice, of coherent states is used for an approximate construction of various quantum states. For any quantum state $|f\rangle$, many of the coherent states on a (full) von-Neumann lattice are very far in phase space and, consequently, their contribution to the expansion of $|f\rangle$ is very small. From a practical point of view, a truncated von-Neumann lattice would be much easier to handle, and could still provide an accurate reconstruction of $|f\rangle$.

A truncated von-Neumann lattice of coherent states is the set of states

$$|A_{MN}\rangle = |\alpha M + i\beta N + \gamma\rangle, \tag{6.21}$$

where α, β are lattice constants; γ is a complex number; and (M, N) is a pair of integers which takes values in a set I (which is a finite subset of $Z \times Z$). We call I' the set of the rest of the values of the pair of integers (M, N) (i.e. $I' = Z \times Z - I$). In order to have a good approximation, the set I should be chosen in such a way

that for all $(M, N) \in I'$ we have

$$\langle f|A_{MN}\rangle \ << \mathbf{1}. \tag{6.22}$$

One way of achieving this is by calculating the expectation values $\langle x\rangle$, $\langle p\rangle$, and the dispersions Δx, Δp where

$$\langle x\rangle \ = \ \langle f|\hat{x}|f\rangle, \tag{6.23}$$

$$\langle x^2\rangle \ = \ \langle f|x^2|f\rangle, \tag{6.24}$$

$$\Delta x = [\langle x^2\rangle - \langle x\rangle^2]^{1/2}, \tag{6.25}$$

and similar definitions hold for the momentum p. The set I contains all the values of M, N such that

$$\langle x\rangle - \mu(\Delta x) \ < \alpha M + \mathrm{Re}\ \gamma < \ \ \langle x\rangle + \mu(\Delta x), \tag{6.26}$$

$$\langle p\rangle - \mu'(\Delta p) \ < \beta N + \mathrm{Im}\ \gamma < \ \ \langle x\rangle + \mu'(\Delta p), \tag{6.27}$$

where μ, μ' are positive numbers. Clearly, the bigger the μ, μ' are and the bigger the size of I is, the better the approximation.

Using the truncated von-Neumann lattice, an approximate expansion of the state $|f\rangle$ is obtained:

$$|f\rangle \ \approx \sum_{M,N} f_{MN}|A_{MN}\rangle \ \equiv \ |f_1\rangle, \quad (M,N) \in I \tag{6.28}$$

$$f_{MN} = \langle A_{MN}|f\rangle \ .$$

6.4 Robustness of the expansion and measures of accuracy

An important aspect of this analysis is to demonstrate with examples, the robustness of this expansion; that is, the expansion is stable in the sense that random

noise in the coefficients affects weakly the constructed state. This is a very important property of the expansion and enhances its potential to be implemented practically. In the examples presented in Section 6.5, this is shown by evaluating the sum

$$|f_2\rangle \equiv \sum_{M,N} f'_{MN}|A_{MN}\rangle, \tag{6.29}$$

$$f'_{MN} = f_{MN} + (r^{(R)}_{MN} + ir^{(I)}_{MN}),$$

where $r^{(R)}_{MN}, r^{(I)}_{MN}$ are random numbers with a flat distribution in the interval $[-\lambda/2, \lambda/2]$. λ is the width of the noise.

In quantum state engineering, the objective is to construct accurately a known quantum state; in this case, one is able to select the optimal truncated lattice (ie the dominant terms of the Gabor expansion) for individual quantum states. The robustness of the method guarantees reasonable accuracy. In contrast, the generalised chromatic approach presented in Chapter 5 is restricted to an *a priori* determined set of terms to enable processing large numbers of similar signals.

As a measure of how close the $|f_1\rangle$ and $|f_2\rangle$ are to $|f\rangle$ the following quantities have been calculated:

$$D_i = \int |\langle x|f\rangle - \langle x|f_i\rangle|^2 \, dx, \quad i = 1, 2 \tag{6.30}$$

$$\Delta_i = \int \left| |\langle x|f\rangle|^2 - |\langle x|f_i\rangle|^2 \right| dx, \quad i = 1, 2. \tag{6.31}$$

Clearly the quantities D_1, Δ_1 refer to the noiseless case, while the D_2, Δ_2 refer to the noisy case.

In order to show that the agreement is indeed very good in the whole quantum phase space, the associated Wigner function representations were calculated according to Eq. (6.6): the Wigner function $W(x, p)$ for the state $|f\rangle$; the Wigner function $W_1(x, p)$ for the state $|f_1\rangle$ of Equation 6.28; and the Wigner function $W_2(x, p)$ for the 'noisy' state $|f_2\rangle$ of Equation 6.29. A measure of the difference between these Wigner functions can be given by the quantity

$$\Delta W_i = \int |W_i(x, p) - W(x, p)| dx dp, \tag{6.32}$$

where $i = 1, 2$. It is clear that $i = 1$ characterises the noiseless case and $i = 2$ characterises the noisy case.

is related to the integrand in Eq. (6.30), for the noiseless case; and Fig. 6.5 illustrates the difference $|\langle x|f\rangle|^2 - |\langle x|f_i\rangle|^2$, which is related to the integrand in Eq. (6.31), for the same case. It is seen that, for the case of the number state, the results are also very good.

In Table 6.1 we give the quantities D_1, D_2, Δ_1, Δ_2 that characterise the difference between the exact and the approximate result for all cases. It becomes clear that the method is *robust*. From a practical point of view, this means that equipment limitations and other factors of experimental error do not have a significant effect on the result.

case	D_1	D_2	Δ_1	Δ_2	ΔW_1	ΔW_2
A	0.01003	0.02678	0.15078	0.16655	0.39500	0.42490
B	0.00032	0.00202	0.01444	0.04997	0.05686	0.09708
C	0.02894	0.04882	0.18033	0.19776	0.36488	0.46587

Table 6.1: The quantities $D_1, D_2, \Delta_1, \Delta_2, \Delta W_1, \Delta W_2$ defined in Sections 6.4-5 by Eqs. (6.30), (6.31), and (6.32) correspondingly, for (A) squeezed states with the 3×2 lattice defined in Section 6.5:Eq. (6.33), (B) squeezed states with the 5×3 lattice defined in Section 6.5:Eq. (6.34), (C) number eigenstates with the 3×3 lattice defined in Section 6.5:Eq. (6.35); the constructed states are calculated according to Eq. (6.28). The quantities D_i, Δ_i and ΔW_i $(i = 1, 2)$ provide three different measures to quantify the accuracy of the method.

Additionally, the associated Wigner function representations were calculated using Eq. (6.6) to verify the agreement from a phase-space perspective. In Figures 6.6-8, the Wigner functions $W(x,p)$, $W_1(x,p)$ and $W_2(x,p)$ (see Section 6.4) for the given squeezed state are shown respectively (3×2 lattice). It is seen that the Wigner functions for $|f_1; s\rangle$ and $|f_2; s\rangle$ are very close to the Gaussian. This confirms that the constructed states $|f_1; s\rangle$ and $|f_2; s\rangle$ (for the 3×2 lattice) are very close to the squeezed state. Figures for the 5×3 lattice case are not presented, since in this case no deviation from a Gaussian is visible. To show the difference between $W(x,p)$ and $W_1(x,p)$ (noiseless case, 3×2 lattice) in detail, the quantity $W_1(x,p) - W(x,p)$ (related to the integrand in Eq. (6.32)) is plotted

6.5 Examples

As an example, let us consider the squeezed state (Eq. (6.16)) with $A = 6.2(1+i)$, $r = 0.5$, $\theta = 0$. Two different truncated von-Neumann lattices are used. The first one is a 3×2 truncated lattice:

$$A_{MN} = (4.8 + 1.4M) + i(5.5 + 1.4N) \quad M = 0, 1, 2 \; ; \; N = 0, 1 \tag{6.33}$$

and the second one is a 5×3 truncated lattice:

$$A_{MN} = (4.6 + 0.8M) + i(5 + 1.2N), \quad M = 0, 1, 2, 3, 4 \; ; \; N = 0, 1, 2 \; . \tag{6.34}$$

The noise added in these two cases had width $\lambda = 1$ (see Eq. (6.29)) .

Let us also consider the number eigenstate $|n = 2\rangle$. In this case, the use of a 3×3 truncated lattice seems more suitable:

$$A_{MN} = (-1.25 + 1.25M) + i(-1.25 + 1.25N) \quad M = 0, 1, 2 \; ; \; N = 0, 1, 2 \; . \tag{6.35}$$

The noise added in this case had width $\lambda = 3$. We shall denote $|f_1; s\rangle$ and $|f_1; n\rangle$ the state of Eq. 6.28 corresponding to the squeezed state of Eq. 6.16 and to the number eigenstate $|2\rangle$, correspondingly. Similarly we shall denote $|f_2; s\rangle$ and $|f_2; n\rangle$ the "noisy" state of Eq. 6.29 corresponding to the squeezed state of Eq. 6.16 and to the number eigenstate $|2\rangle$, correspondingly.

Fig. 6.1 shows $P(x) = |\langle x|f\rangle|^2$ for the squeezed state (3 cases). It is seen that the agreement in all cases is very good. In particular, with the 5×3 lattice for the squeezed state case, the agreement is excellent even in the noisy case. Correspondingly, Fig. 6.2 shows $P(x)$ for the number state (3 cases). Additionally, Fig. 6.3 shows the wavefunction $\psi(x) = \langle x|f\rangle$ for the three cases. According to Eq. (6.5), the wavefunction $\psi(x)$ of the second-order number eigenstate is given by

$$\psi(x) \equiv \psi_2(x) = (\pi)^{-1/4} 2^{-3/2} H_2(x) \exp(-\frac{1}{2}x^2), \tag{6.36}$$

where

$$H_2(x) = 4x^2 - 2 \tag{6.37}$$

is the hermite polynomial of the second order. In order to have a better understanding of the results, Fig. 6.4 illustrates the difference $\langle x|f\rangle - \langle x|f_i\rangle$, which

in Fig. 6.9.

According to Eq. (6.7), the Wigner function for the number eigenstate $|2\rangle$ is

$$W(x,p) = e^{-(x^2+p^2)} L_2[2(x^2+p^2)], \tag{6.38}$$

where L_2 is the second-order Laguerre polynomial. In Figures 6.10-12, the Wigner functions $W(x,p)$, $W_1(x,p)$ and $W_2(x,p)$ for the given number state ($|2\rangle$) are presented. It can be seen that the Wigner functions for $|f_1;n\rangle$ and $|f_2;n\rangle$ are very close to the exact result. For example, they have the rotational symmetry with a very good approximation. The difference $W_1(x,p) - W(x,p)$ for the noiseless case is plotted in Fig 6.13. The quantities ΔW_1 and ΔW_2 that characterise the difference between the approximate and the exact result are also given in Table 6.1 for all cases.

6.6 Discussion

The work presented in this chapter uses the expansion described earlier (Chapter 5) and is a contribution to the current framework of quantum state engineering. The concept of the truncated von-Neumann lattice of coherent states has been introduced in Equations (6.21)-(6.27) and discrete superpositions of coherent states on this lattice have been used to build quantum states. It has been shown that the method can be used to construct accurately non-classical states (squeezed states and number eigenstates). An important result is the fact that the expansion is *robust*, in the sense that small random noise in the coefficients does not affect significantly the results. An original aspect of the method is its robustness which makes it particularly attractive for practical applications. Synthesis of quantum states extends further our ability to manipulate light. Particularly, engineering of squeezed states is of great importance due to its noise reduction properties. Several applications in quantum optical telecommunications and experimental quantum optics can be envisaged. The method also promises potential benefits in many other areas.

Figures

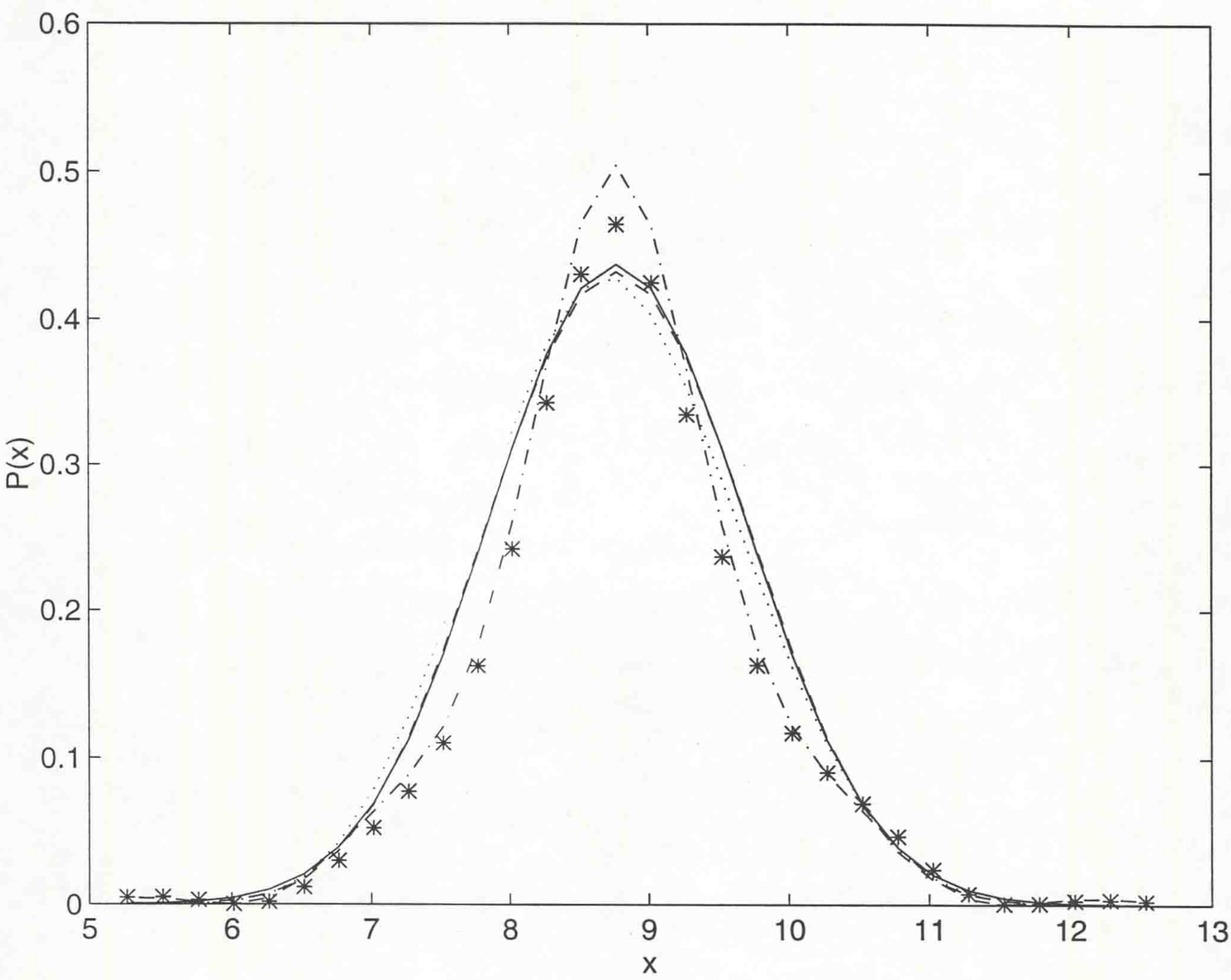

Figure 6.1: Probability distribution $P(x)$ for the squeezed state $|A; r, \theta\rangle$ with $A = 6.2(1+i)$, $r = 0.5$, $\theta = 0$ (solid line); the constructed state $|f_1; s\rangle$ with the 3×2 lattice (dash-dot line); the 'noisy' constructed state $|f_2; s\rangle$ with the 3×2 lattice (star line); and correspondingly, the state $|f_1; s\rangle$ with the 5×3 lattice (dashed line); the state $|f_2; s\rangle$ with the 5×3 lattice (dotted line).

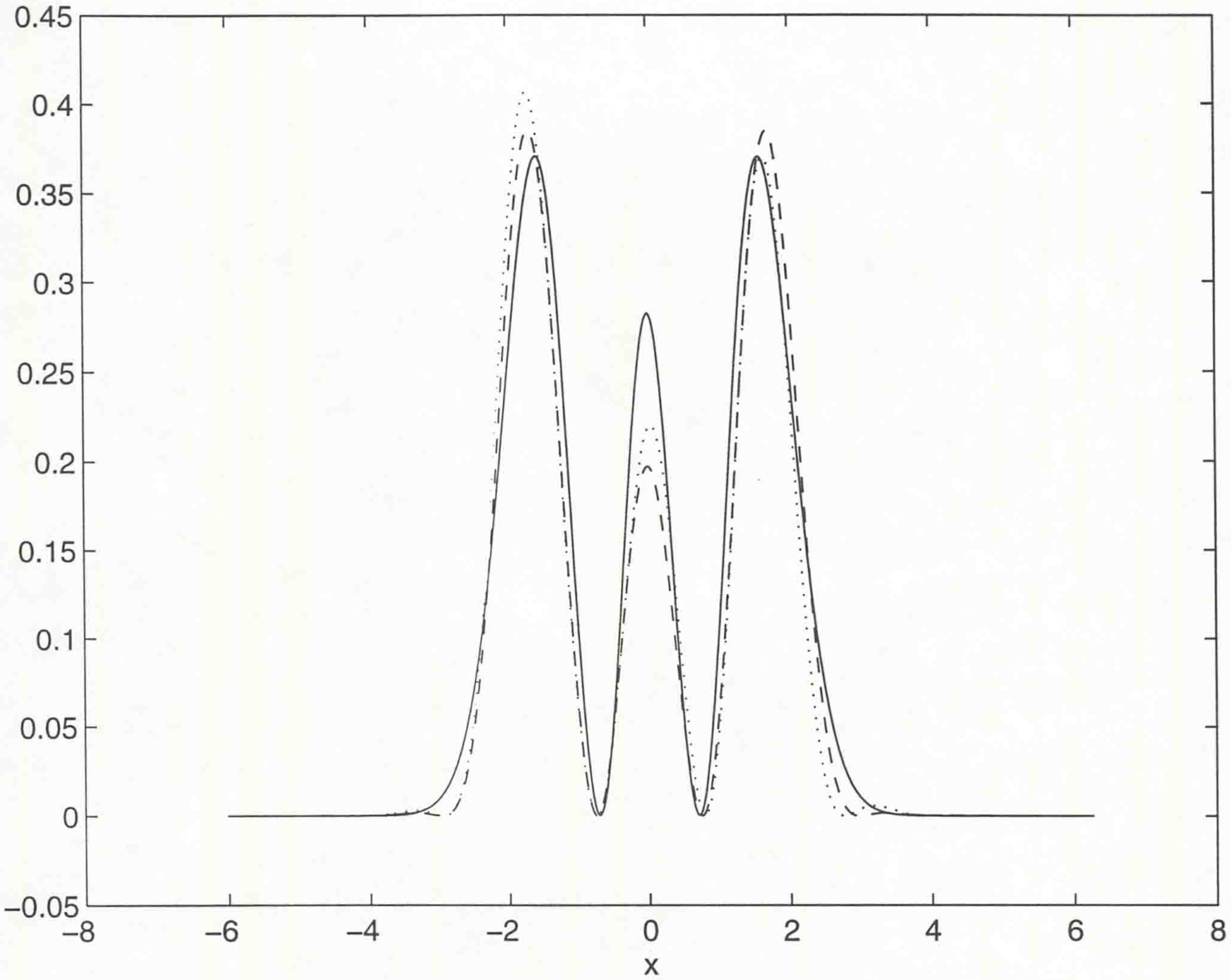

Figure 6.2: Probability distribution $P(x)$ for the number eigenstate $|2\rangle$ (solid line); the state $|f_1; n\rangle$ with the 3×3 lattice (dashed line); the state $|f_2; n\rangle$ with the 3×3 lattice (dotted line).

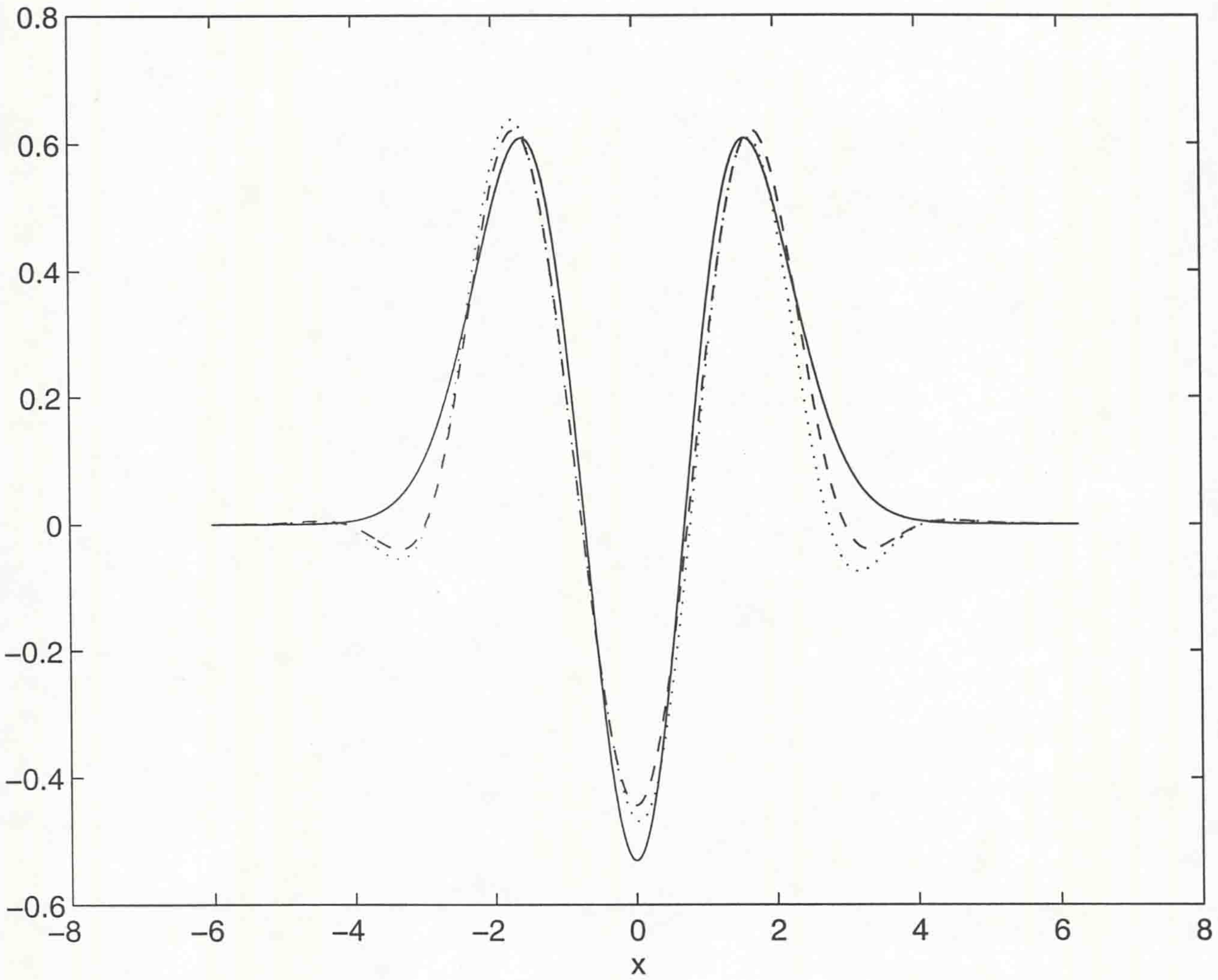

Figure 6.3: Wavefunction $\psi(x)$ for the number eigenstate $|2\rangle$ (solid line); the state $|f_1; n\rangle$ with the 3×3 lattice (dashed line); the state $|f_2; n\rangle$ with the 3×3 lattice (dotted line).

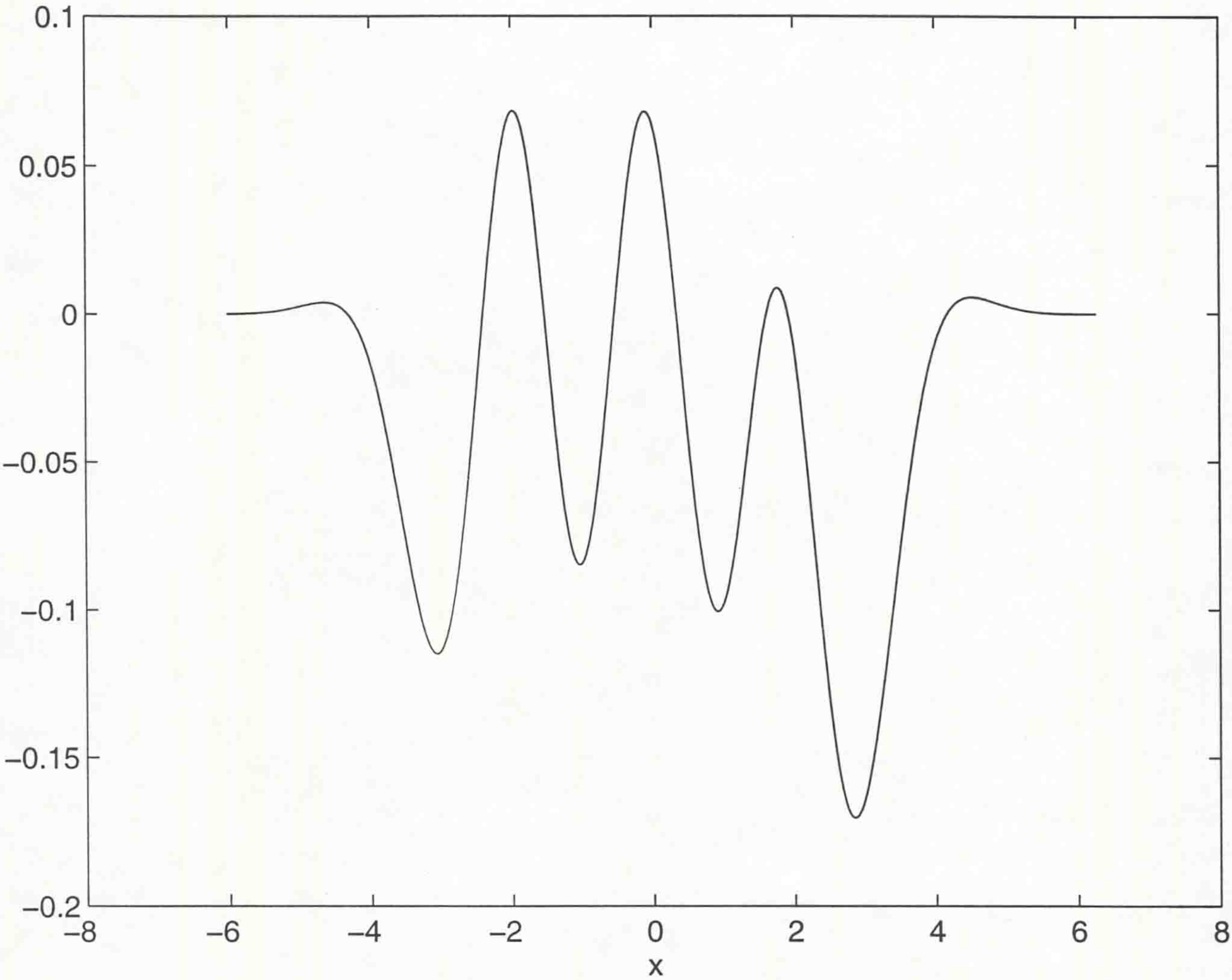

Figure 6.4: The difference ($\langle x|f\rangle - \langle x|f_i\rangle$) for the number eigenstate (noiseless case).

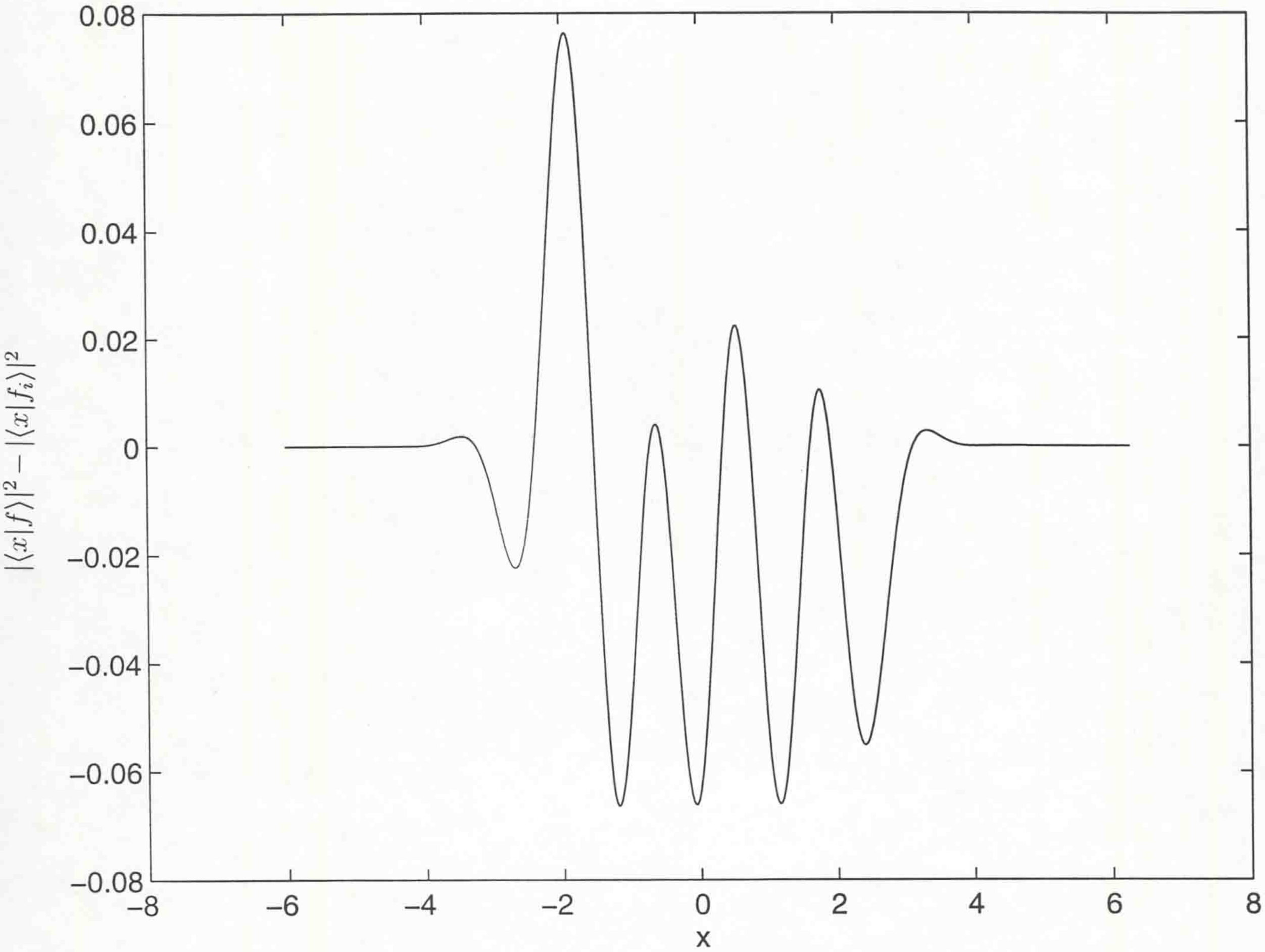

Figure 6.5: The difference $|\langle x|f\rangle|^2 - |\langle x|f_i\rangle|^2$ for the number eigenstate (noiseless case).

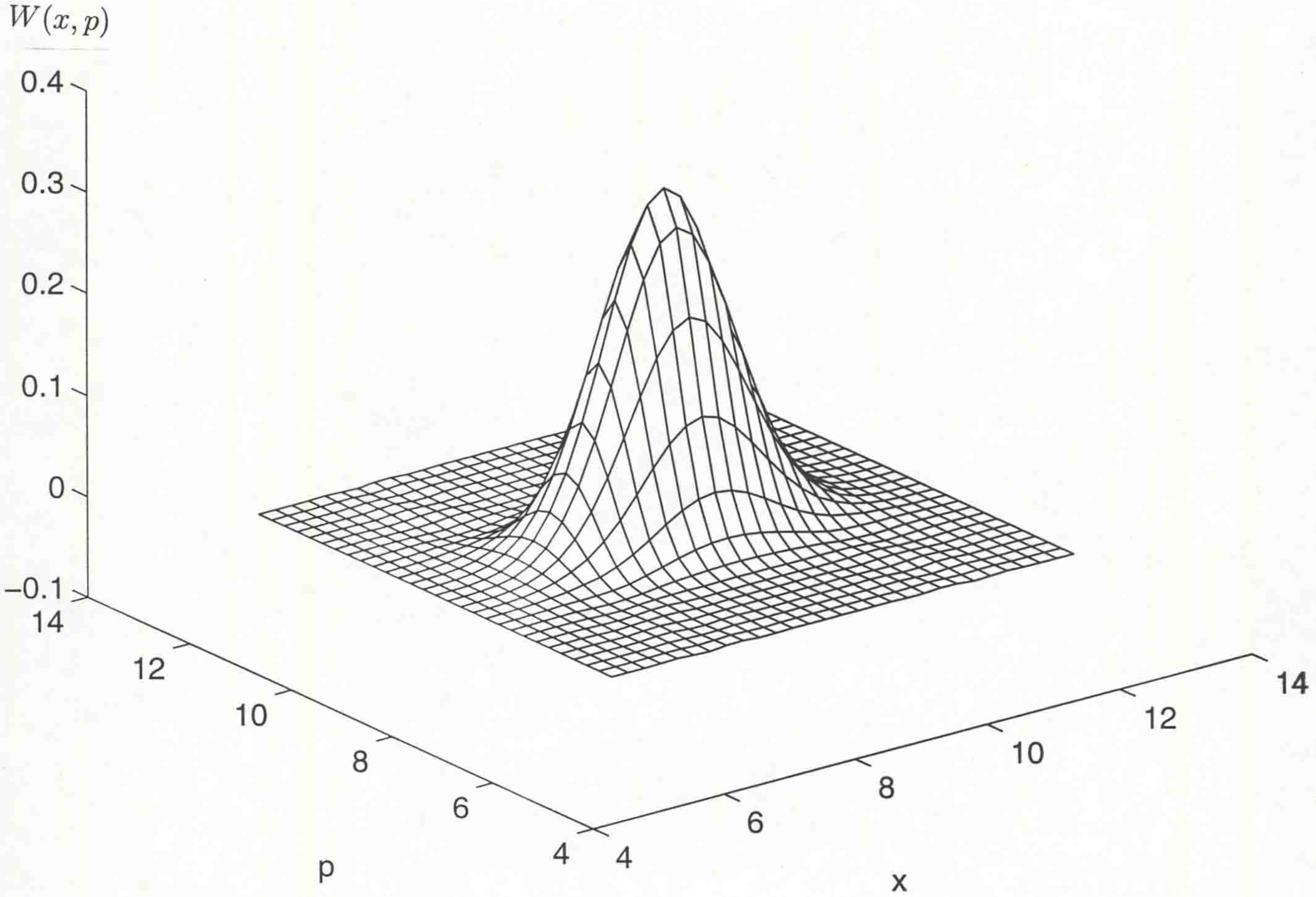

Figure 6.6: The Wigner function for the squeezed state $|A; r, \theta\rangle$ with $A = 6.2(1 + i)$, $r = 0.5$.

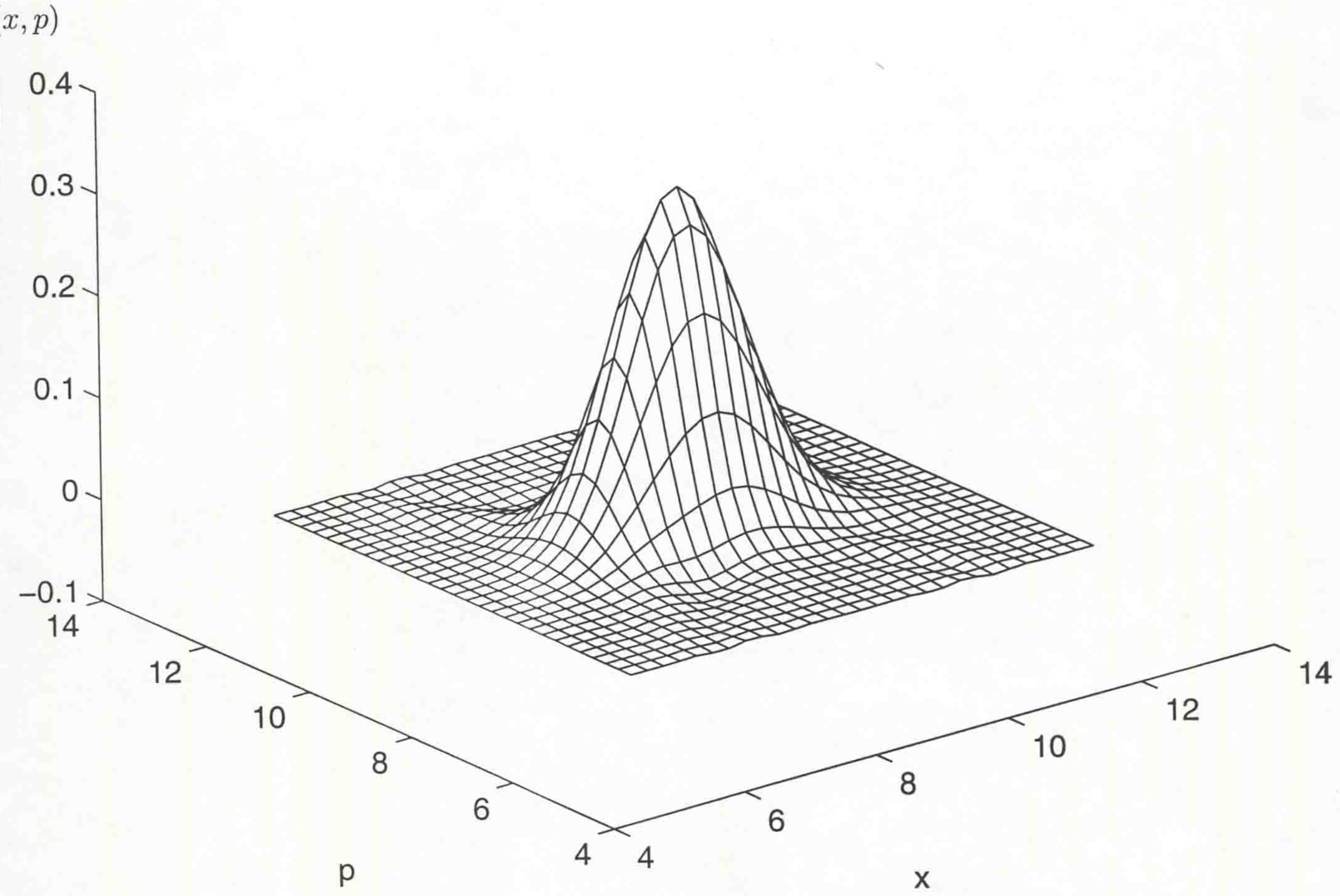

Figure 6.7: The Wigner function for the constructed squeezed state $|f_1; s\rangle$ with the 3×2 lattice.

$V_2(x,p)$

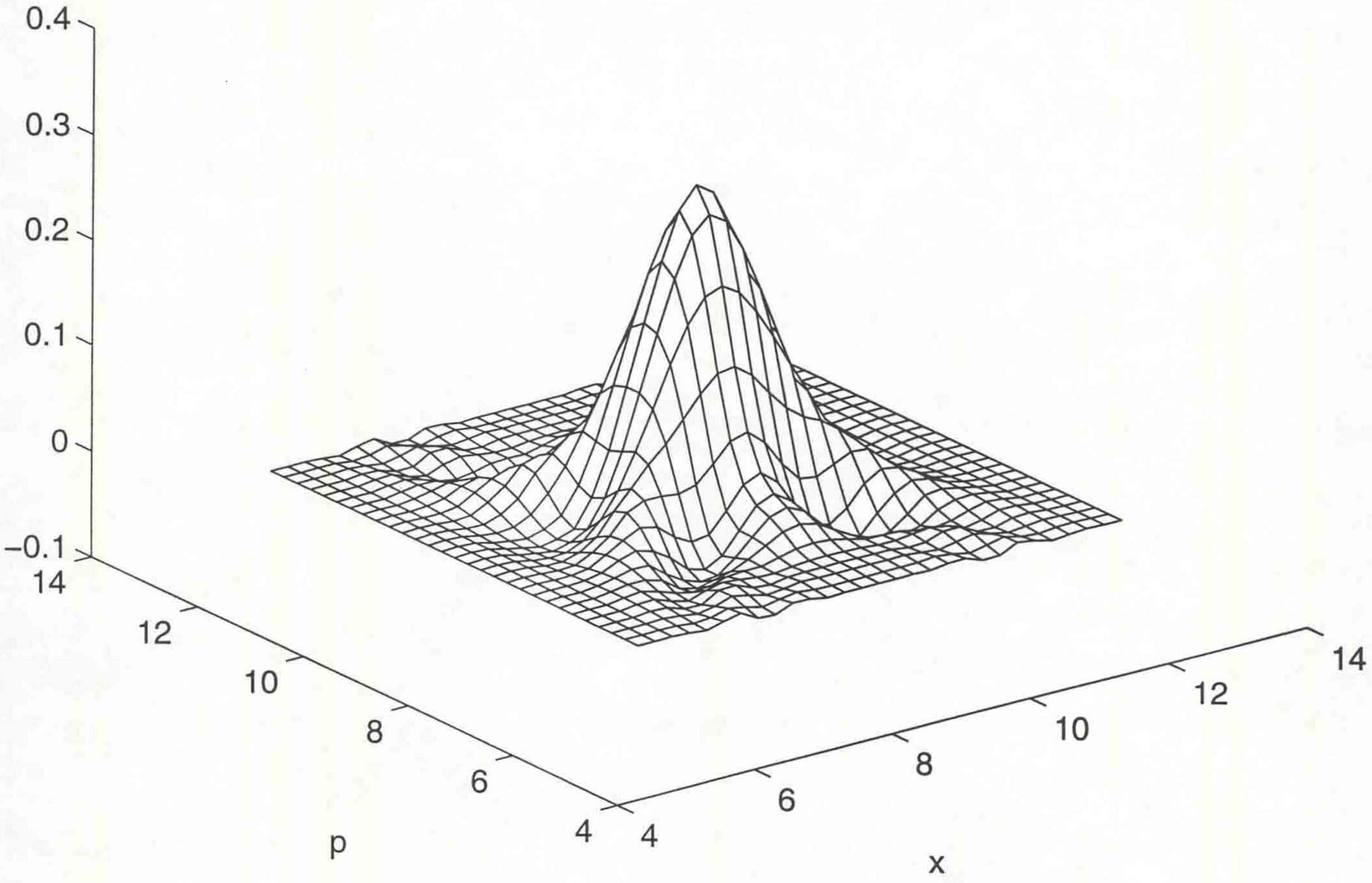

Figure 6.8: The Wigner function for the 'noisy' constructed squeezed state $|f_2; s\rangle$ with the 3×2 lattice.

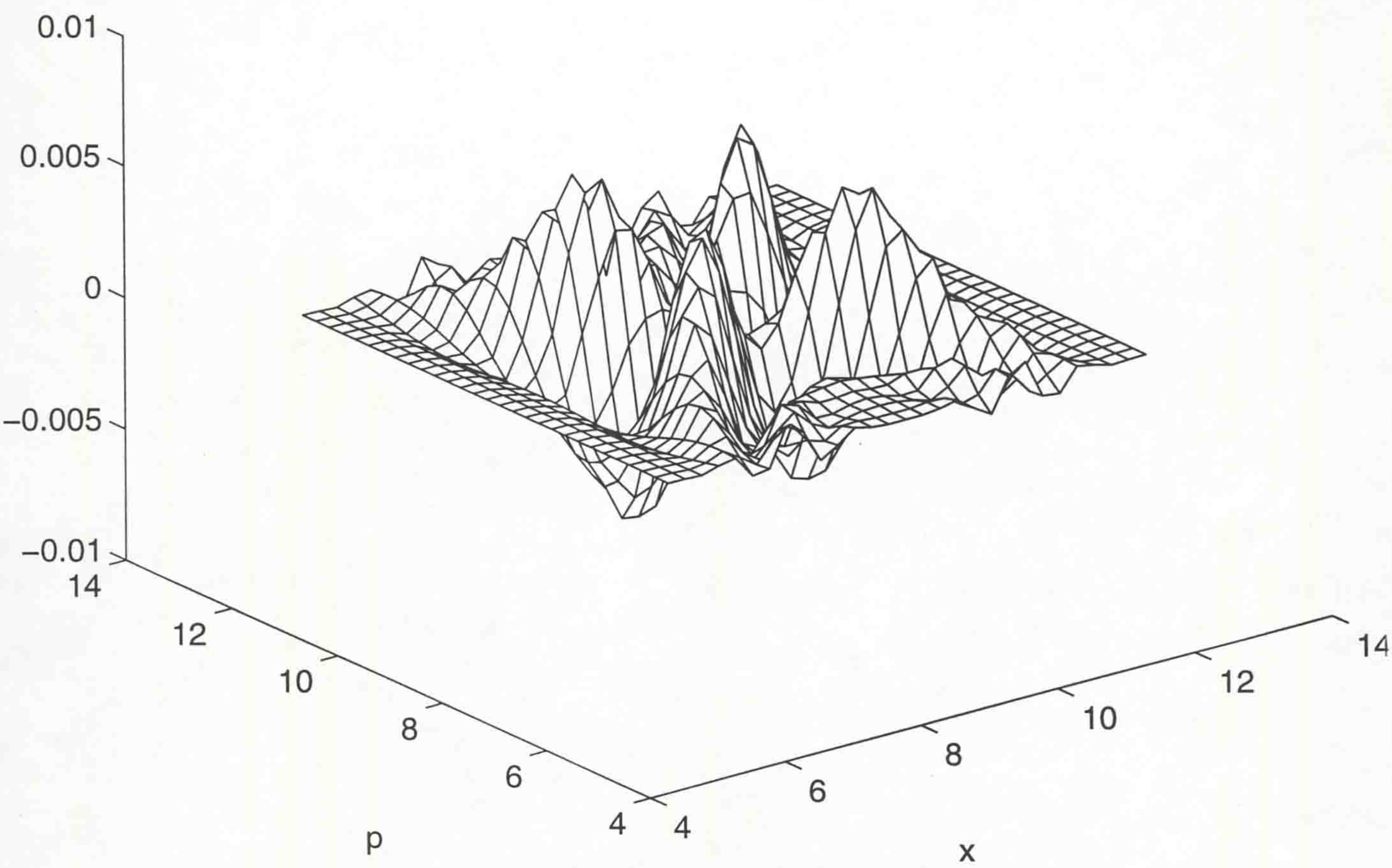

Figure 6.9: The difference $(W_1(x,p) - W(x,p))$ between the Wigner functions of the exact and the constructed squeezed states (noiseless case, 3×2 lattice)

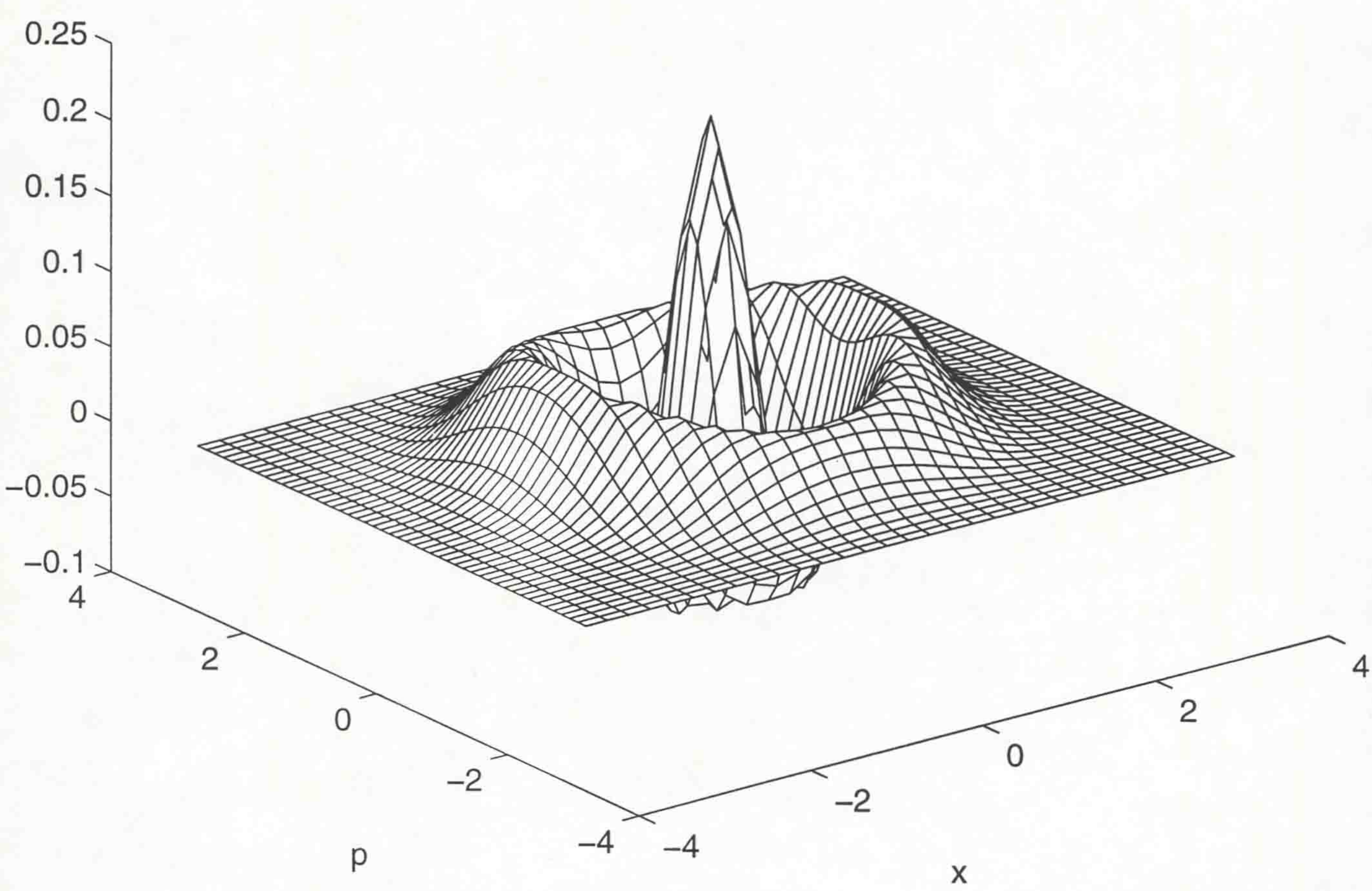

Figure 6.10: The Wigner function for the number state $|2\rangle$.

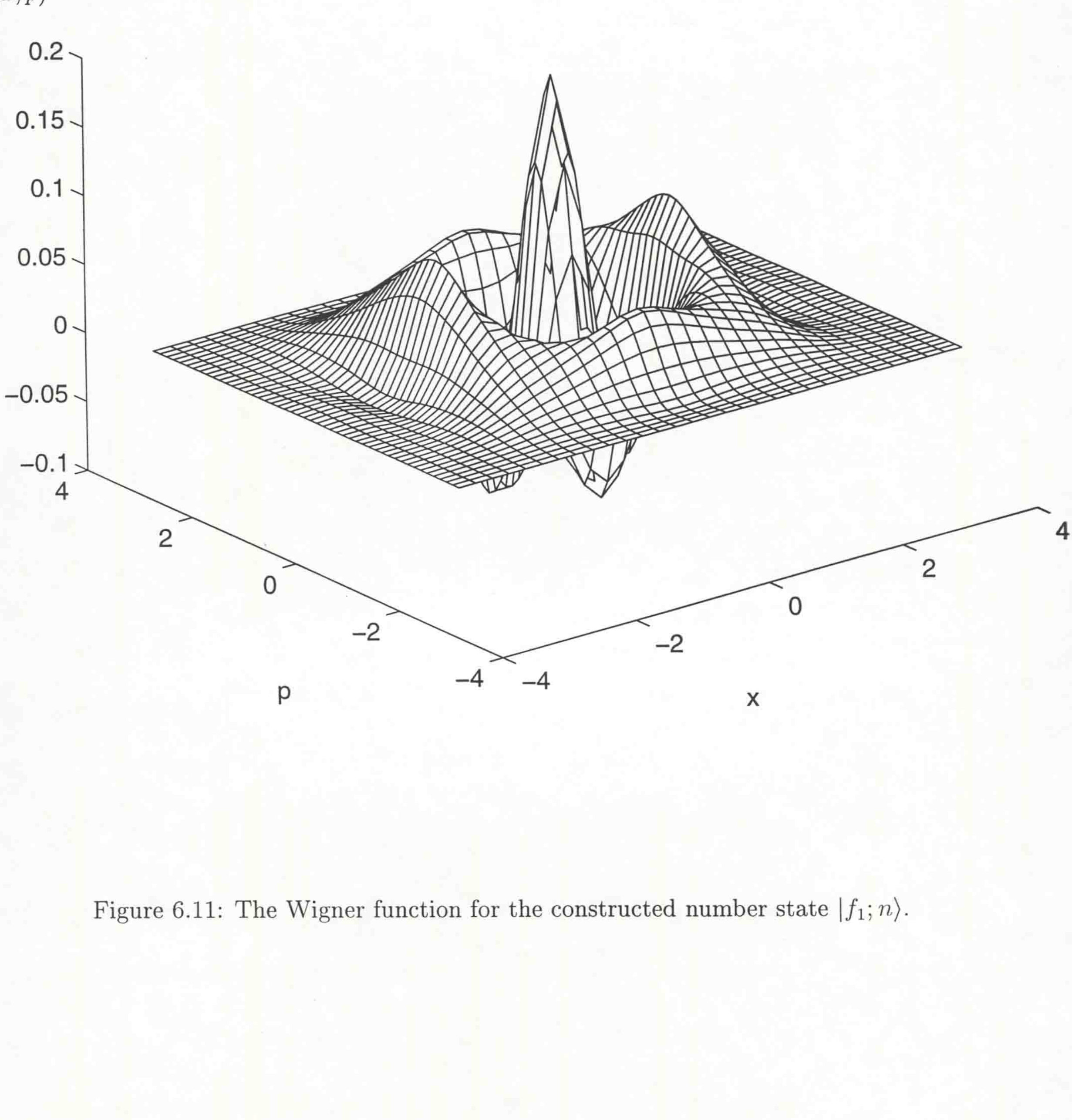

Figure 6.11: The Wigner function for the constructed number state $|f_1; n\rangle$.

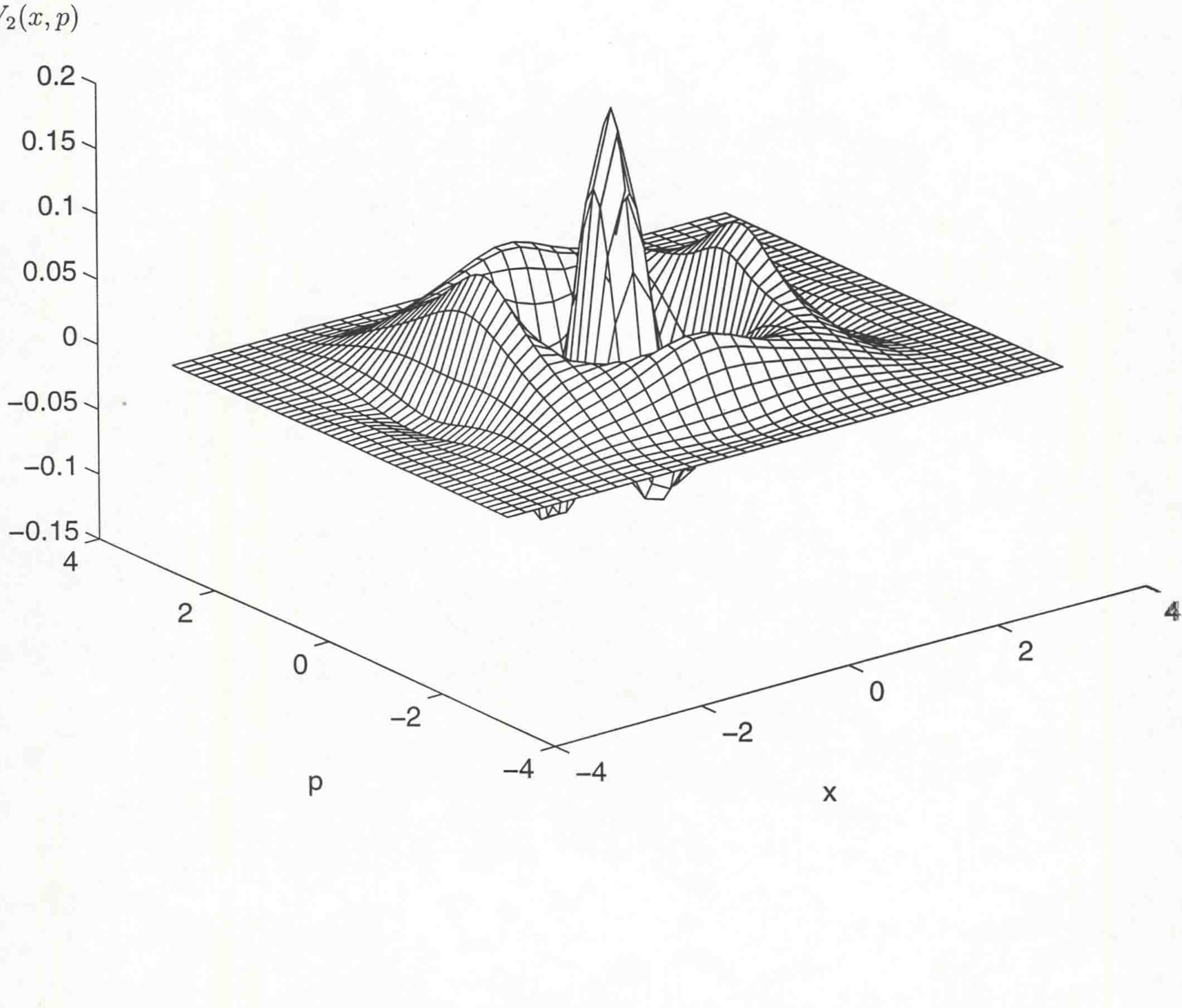

Figure 6.12: The Wigner function for the 'noisy' constructed number state $|f_2; n\rangle$.

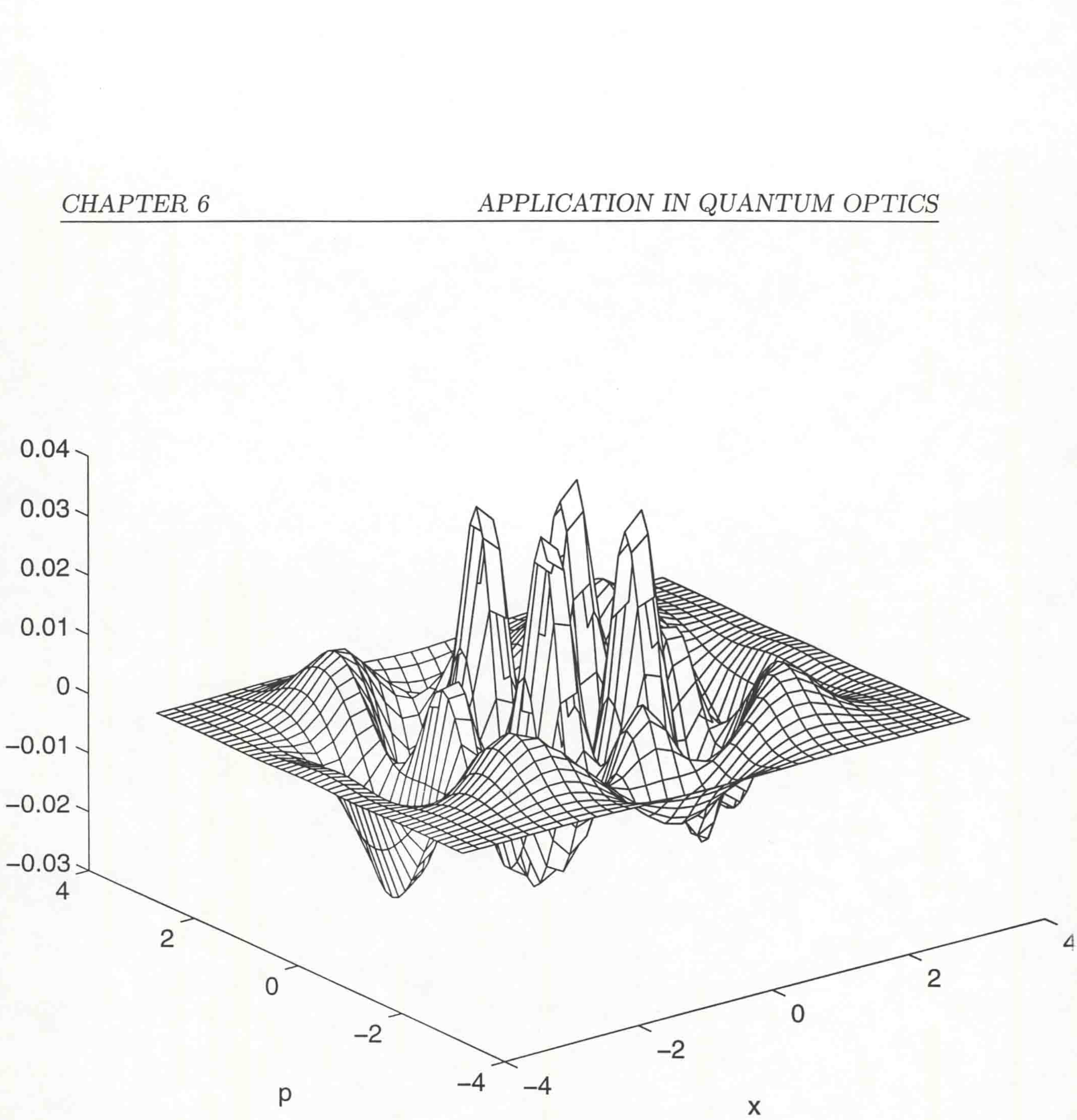

Figure 6.13: The difference $(W_1(x,p) - W(x,p))$ between the Wigner functions of the exact and the constructed number states (noiseless case)

Part II

ENTROPIC METHODS IN OPTICAL SIGNAL PROCESSING

Chapter 7

Speckle Noise Analysis Using Entropic Methods

7.1 Introduction

In many practical situations, optical measurement of a physical or chemical parameter is desirable. For example, optical sensing can be applied efficiently in environments with high magnetic or electrical fields. Due to their attractive properties, optical fibres have been used widely for sensing and monitoring applications. Intrinsic fibre sensors rely upon an optical signal propagating through the fibre being influenced by the parameter to be measured. One class of such intrinsic fibre sensors utilises interference between the various propagation modes in a multimode fibre to produce changes in the spatial distribution of the intensity of light (speckle pattern) at the fibre output in response to, for instance, acoustical vibrations [42, 135]. Noise however limits the use of the detailed shape of this distribution for the development of highly sensitive sensors. This type of noise, known as *speckle noise*, is caused by surface roughness, fibre defects, small vibrations, and other factors [44, 59, 155].

In this chapter, the spatial variation of the speckle pattern as captured by a charge-coupled device (CCD) camera (in the form of digital data) is examined and entropic methods are employed for reducing the noise content of the observed

image. The speckle pattern provides very detailed information, a part of which is merely undesirable noise. Assuming that the useful information is in the lowest moments of the intensity distribution and that the higher moments are influenced mainly by noise, a new 'improved' distribution can be obtained which has the same lowest moments as the observed one. As it will be explained in the following section, the unbiased way to do this is to maximise the entropy of the distribution under the constraint of having fixed lower moments [87, 141, 90, 106].

From a mathematical point of view, this leads to a treatment of the problem of moments with the maximum entropy method for the case of a discrete variable that takes a finite number of values. Much of the work presented in the literature on similar problems considers the moments of distributions of a continuous variable [116, 55, 34, 163, 102]. In contrast, here, the variable position represented by the pixel number is *discrete* and it takes a finite number of values. The mathematical details in these two cases are different. For example, in the case of a thermodynamic system, the maximum entropy approach leads to the Bose-Einstein distribution when the Hilbert space of the system is infinite dimensional, and to the uniform distribution ($p_N = 1/N$) when the Hilbert space is N-dimensional. The statistics in these two cases are different and therefore a separate study of these two cases is required. Similarly, the study of distributions of a discrete variable that takes a finite number of values is different from the continuous case.

Here, these ideas are applied in the context of noise analysis of the output image in an optical fibre. A local dependence of the speckle noise is assumed, as described in existing work on speckle noise analysis [153, 44]. The well known maximum entropy method is used to provide the most 'likely' spatial distribution consistent with the available noisy data.

More specifically, the optical images at the exit of a fibre are captured in digital form by a CCD camera and partitioned into many small regions within each of which the first two moments of the intensity distribution in the various pixels are calculated. An 'improved' image is then constructed which has the same first two moments in each region and maximum entropy. Noise reduction is, thus, associated with the elimination of the detailed information in the higher moments

of the original image. The reconstructed image is improved in the sense that it contains the same information as the original one in the lowest moments which are assumed to contain the desirable information, whilst it loses the content of the higher moments which are assumed to be due to noise. There are several solutions corresponding to various extrema of the entropy (local minima, local maxima, saddle points). All these solutions are investigated and the global maximum is found. Dependence of the result on the size of the regions is also studied.

The technique is a contribution to the general area of digital image processing. It can be used for suppression of the speckle noise in an optical fibre system and, consequently, play an important role in increasing the sensitivity of these systems. The following section introduces briefly the maximum entropy method.

7.2 The Maximum Entropy Method in Image Processing

7.2.1 The Maximum Entropy Principle

The concept of entropy was first introduced by Clausius (1865) in the context of thermodynamics (second Law of Thermodynamics). In 1948, Shannon [141, 143] introduced a mathematically similar concept, which von Neumann named *information-theoretic entropy.*

Let $P = (p_1, p_2, ..., p_n)$ be a probability distribution, where $p_1, p_2, ..., p_n$ are the probabilities of n outcomes, satisfying the normalisation condition of probability theory [191]:

$$\sum_{i=1}^{n} p_i = 1, \quad p_i \geq 0, \tag{7.1}$$

where $i = 1, 2, ..., n$. Then the Shannon-von-Neumann entropy of the distribution P provides a measure of the uncertainty (or a measure of the missing information) of P and is defined by

$$S(p_1, p_2, ..., p_n) = -\sum_{i=1}^{n} p_i \ln p_i. \tag{7.2}$$

In this definition, the entropy is given in *nats* (natural units). In information

theory, the quantity $I = S_{max} - S$ is called *information* of the probability distribution.

The entropy function of Eq. (7.2) has a lot of interesting properties, the most important of which are given below:

I It takes its maximum value when $p_1 = p_2 = ... = p_n = \frac{1}{n}$.

II It is minimum when one of the probabilities is equal to 1 and all the others are zero.

III Its minimum value is zero.

IV Its maximum value increases with n.

The introduction of the concept of entropy in information theory led to a new formalism of statistical inference called the *maximum entropy method.*

A common problem in physical sciences is to find the corresponding probability distribution $(p_1, p_2, ..., p_n)$ from incomplete and noisy data, given some constraints. If only partial and distorted information about the probabilities is available, the *maximum entropy principle* states that the probability distribution which maximises the uncertainty about the missing information (i.e. which has maximum entropy) should be chosen; or in Jaynes' words, "when we make inferences based on incomplete information we should draw them from that probability distribution that has the maximum entropy permitted by the information we do have" [90]. The maximum entropy principle provides the least biased estimate possible on the given information. Since entropy describes the randomness in the distribution, the maximum entropy principle chooses the most random distribution that satisfies the given constraints.

The mathematical framework for the maximisation of the entropy was first given by Gibbs [64, 139] in the context of statistical mechanics. It was shown later by Jaynes [87, 88] that statistical mechanics can be regarded as a form of statistical inference and can be derived from the maximum entropy principle [166, 169].

Let us consider N trials of a random experiment with n possible outcomes at each trial. The probabilities p_i, $(i = 1, 2, ..., n)$ can now be represented by

the frequencies (or proportions) N_i/N, where N_i is the sample number for the i-th outcome, and Eq. (7.1) is still satisfied [191, 133, 92, 168, 43]. Then the expression for entropy given in Eq. (7.2) can be used in many different contexts:

- *Probability Theory*: An ideal die with n faces is tossed N times.
- *Communication Theory*: A message of length N is received, using an alphabet of n symbols.
- *Statistical Mechanics*: A system of N molecules which can be in n different quantum states.
- *Time Series*: N realisations of a time series are generated, when n different series are possible.
- *Image Processing*: N elements of luminance are distributed over n pixels to form an image.

In the case of a continuous variable x with a probability density $P(x)$, the entropy functional is defined as

$$S(P) = -\int P(x) \ln P(x)\, dx. \tag{7.3}$$

The theory and rationale of the maximum entropy method have been studied in depth [149, 148, 91, 90]. The principle of maximum entropy can be rigorously derived from four consistency axioms [146, 93]: (i) *Uniqueness*, (ii) *Permutation Invariance*, (iii) *System Independence*, and (iv) *Subset Independence*, which must be satisfied by any estimate consistent with the given constraints.

The maximum entropy method has proved to be a valuable estimation tool in the case of noisy and incomplete data and has been used in a wide variety of applications [3, 150, 9, 147, 105, 104, 115]. Applications in statistical mechanics are straightforward [87, 89, 167, 51]. It has also been applied in areas like statistics [68], image analysis [61, 70, 24, 53, 60], analysis of scattering data [4], spectral analysis [25], astrophysics [70], and crystallography [106]. The consequences of maximum entropy formalism in quantum theory were also pointed out very early [88, 17].

The constraints for the maximisation of the entropy are usually expressed as certain expectation values or bounds on these values. A trivial constraint is obviously imposed by the normalisation condition of Eq. (7.1). In the case that no constraints are applied, then the result is the uniform distribution (see properties above). Maximisation of the entropy is achieved by requiring its first derivative to be equal to zero. This leads to several solutions corresponding to the various extrema.

7.2.2 Entropy of an Image

In the case that the intensity of an image is additive and takes always positive values, the maximum entropy method can be applied straightforwardly. Indeed, the maximum entropy method has been shown to be the only consistent extremum principle for the problem of reconstructing a positive image from incomplete and noisy data [146, 150]. Various approaches have been suggested for optimal reconstruction of noisy images [70, 45, 24, 53, 60, 61, 71, 62].

In the case of optical images, which are both positive and additive, the so-called *configurational entropy* [150, 67, 71] can be defined as follows:

Let I_i be the intensity of light at the i-th pixel of a one-dimensional image of n pixels ($i = 1, 2, ..., n$). The normalised intensities f_i are given by

$$f_i = \frac{I_i}{\sum_{i=1}^{n} I_i}, \tag{7.4}$$

$$\sum_{i=1}^{n} f_i = 1, \tag{7.5}$$

$$0 \leq f_i \leq 1.$$

The f_i satisfy the Kolmogorov axioms of probability theory (positivity, additivity and the normalisation condition) and can be treated as probabilities. The configurational entropy of the image is expressed as

$$S(f_1, f_2, ..., f_n) = -\sum_{i=1}^{n} f_i \ln f_i. \tag{7.6}$$

In the case that prior information is known, the maximisation of the entropy is subject to the given constraints, which define the set of "feasible" images. The

general expression for a constraint is

$$C(f_1, f_2, ..., f_n) \geq C_0. \tag{7.7}$$

For maximisation under constraints, we can use the method of Lagrange multipliers. In the case of one constraint, the function to be maximised becomes

$$Q(f_i, \lambda) = -\sum_{i=1}^{n} f_i \ln f_i - \lambda C(f_i). \tag{7.8}$$

It is seen that, in the case of optical noisy images, the maximum entropy theory can be easily applied. The reconstructed image is the one which has maximum entropy and is consistent with the given constraints. In the general case, Eq. (7.8) is implicit and nonlinear in respect to the Lagrange's multipliers. Extension of these ideas to the two-dimensional case is trivial.

In the following sections, an example of specialised application of the maximum entropy method is presented [158, 160]; the undetermined moment problem for the case of digital images is considered and optimal reconstruction of speckle noise images is carried out.

7.3 The Method of Moments for the Discrete Case

7.3.1 Introduction

The classical problem of moments consists of determining the distribution of a variable from the knowledge of its moments. In the case that all moments are known, the distribution is defined uniquely. But in the case that only the first K moments are given, there are many solutions which have the given moments and which differ from each other with respect to the unknown moments. The maximum entropy method chooses among them the one with maximum entropy.

Earlier studies on similar problems consider the moments of distributions of a continuous variable [55, 34, 163, 102] and maximise a functional of the form of Eq. (7.3). Applications of the moment method in various areas (eg. quantum

physics [17, 116]) have been also considered. Here, the case of a discrete variable that takes a finite number of values is considered. An initial study of the general N-moment problem is presented and an explicit solution of the two-moment problem is given in section 7.3.2. For completeness, we have also considered the simple case where the first moment only is used as a constraint (section 7.3.1).

Let us consider a two-dimensional optical image and divide it into M square regions, each of which contains L pixels. Let I_{ij} be the intensity and f_{ij} be the normalised intensity of the j pixel in the i region:

$$f_{ij} = \frac{I_{ij}}{\sum\limits_{i,j} I_{ij}}, \tag{7.9}$$

$$\sum_{i,j} f_{ij} = 1, \tag{7.10}$$

$$0 \leq f_{ij} \leq 1,$$

where $i = 1, 2, ..., M, j = 1, 2, ..., L$. The moments within each region are calculated from the formulae:

$$m_i^{(1)} = \frac{1}{L} \sum_{j=1}^{L} f_{ij}, \tag{7.11}$$

$$\sum_{i=1}^{M} m_i^{(1)} = \frac{1}{N},$$

and

$$m_i^{(N)} = \frac{1}{L} \sum_{j=1}^{L} \left(f_{ij} - m_i^{(1)} \right)^N. \tag{7.12}$$

The entropy of the image is given by

$$S = -\sum_{i,j} f_{ij} \ln f_{ij}. \tag{7.13}$$

The expression to be maximised, in this case, is

$$Q\left(f_{ij}, \lambda_i^{(N)}\right) = -\sum_{i,j} f_{ij} \ln f_{ij} - \sum_{i,N} \lambda_i^{(N)} \left\{ \frac{1}{L} \sum_{j=1}^{L} \left(f_{ij} - m_i^{(1)}\right)^N - m_i^{(N)} \right\}, \tag{7.14}$$

where $\lambda_i^{(N)}$ are the Lagrange multipliers corresponding to the N-th moment. The distribution of the new values of f_{ij} will have maximum entropy and at the same time it will also have the original moments $m_i^{(N)}$ $(N = 1, 2, ..., K)$.

7.3.2 The case of the first moment

In this case, the single constraint corresponds to fixed mean value in each region, which is here denoted as $\mu_i \left(= m_i^{(1)}\right)$. The expression to be maximised, in this case, is:

$$Q(f_{ij}, \lambda_i) = -\sum_{i,j} f_{ij} \ln f_{ij} - \sum_i \lambda_i \left(\sum_j f_{ij} - L\mu_i \right), \tag{7.15}$$

where λ_i are the undetermined Lagrange multipliers referring to the i region. Maximisation with respect to f_{ij} gives

$$\ln f_{ij} + 1 + \lambda_i = 0, \tag{7.16}$$

which leads to the result $f_{ij} = \mu_i$, that is, of substituting all intensities within a region with their average. This rather trivial and intuitively clear result is derived here through the maximum entropy method.

7.3.3 The case of the first two moments

In this case, the constraints correspond to preservation of the mean value and the standard deviation in each region which here we denote as $\mu_i \left(= m_i^{(1)}\right)$ and $\sigma_i \left(= \left(m_i^{(2)}\right)^{1/2}\right)$, correspondingly.

The expression to be maximised, in this case, is:

$$Q(f_{ij}, \lambda_i, \tau_i) = -\sum_{i,j} f_{ij} \ln f_{ij} - \sum_i \lambda_i \left(\sum_j f_{ij} - L\mu_i \right) - \sum_i \tau_i \left(\sum_j (f_{ij} - \mu_i)^2 - L\sigma_i^2 \right), \tag{7.17}$$

where λ_i is the undetermined Lagrange multiplier for the first moment term and τ_i is the Lagrange multiplier for the second moment term, referring to the i region $(i = 1, 2, ..., M)$. Taking the first derivative of Q with respect to f_{ij} to be equal to zero, we obtain:

$$\frac{\partial Q}{\partial f_{ij}} = 0 \longrightarrow f_{ij} = \frac{L\mu_i \exp(-2\tau_i f_{ij})}{\sum_j \exp(-2\tau_i f_{ij})}. \tag{7.18}$$

The relations in Eqs. (7.11), (7.12), and (7.18), with $N = 2$, are considered for every region and they form a nonlinear system of $M(L + 2)$ equations with

$M(L+2)$ unknowns (ML intensity values and $2M$ Lagrange multipliers). This system of equations provides the solution. From relation (7.18), one can easily derive that

$$\ln f_{ij} - \ln f_{ik} = -2\tau_i(f_{ij} - f_{ik}). \tag{7.19}$$

The last equation can be satisfied for all pixels within a region only if the normalised intensities within that region take one of two possible values: $f_{ij} = A_i$ or B_i. If we assume that in the i region there are x_i pixels with normalised intensity A_i and y_i pixels with normalised intensity B_i, then we have:

$$x_i + y_i = L, \tag{7.20}$$

$$x_i A_i + y_i B_i = \mu_i L = \sum_j f_{ij}, \tag{7.21}$$

and

$$x_i(A_i - \mu_i)^2 + y_i(B_i - \mu_i)^2 = L\sigma_i^2. \tag{7.22}$$

Equations (7.20), (7.21), and (7.22) give the solution:

$$A_i = \mu_i \mp \sigma_i \left(\frac{L - x_i}{x_i}\right)^{\frac{1}{2}}, \tag{7.23}$$

and

$$B_i = \mu_i \pm \sigma_i \left(\frac{x_i}{L - x_i}\right)^{\frac{1}{2}}. \tag{7.24}$$

x_i can take all values between 1 and $L-1$, but only the ones that lead to non-negative A_i, B_i are acceptable. All these solutions represent local extrema of the entropy function. An investigation of all these local extrema is needed in order to find the global maximum. The method does not define which of the pixels have normalised intensity A_i and which have B_i, because the entropy remains the same if we scramble the pixels within a certain region (permutation invariance).

7.4 Practical Implementation for Maximum Entropy Analysis of Speckle Noise

The speckle images used for this application were experimentally produced at the Optics Laboratory in the Department of Electrical Engineering and Electronics (see [153]). The software developed for this analysis is presented in Appendix B.

The images represent speckle patterns which are produced at the output of a step index multimode optical fibre with a core diameter of $50\mu m$, and captured by a colour CCD camera. A monochromatic source is used to excite modes within the fibre. The CCD array views the exit plane of the optical fibre and provides the far-field intensity distribution. The images captured and digitised by the CCD camera are square arrays of 496×496 pixels.

The speckle pattern is a result of modal interference and is affected by noise due to surface roughness and other imperfections in the fibre, stability of the laser source and small displacements of the fibre caused by vibration. Existing analysis [153, 44, 59] stresses the local statistical properties of speckle noise. In this context, the speckle image can be divided in small regions and the method of moments presented in Section 7.3 can be applied for each region.

Since the CCD camera provides RGB data (see Section 5.6), we used the data corresponding to the blue optical band which had the highest overall intensity. Fig. 7.1 shows a 496×496 256-level digital image of the speckle pattern as captured by a CCD camera. The random nature of the speckle pattern can be seen. The 'improved' versions of this image with $L = 4, 16, 64$ for the case of one moment are given in Figs. 7.2-4.

It should be emphasized at this point that the term 'improved image' is used here in the context of the previous rationale on maximum entropy and the given requirements. The new version of the image is 'improved' in the sense that the higher moments have been removed (based on the assumption that they are associated with noise), and provides a simpler and 'cleaner' dataset which is easier to handle, process or transmit. It should be clear that in a different context, where a detailed study of the noise is required (eg. speckle interferometry), this approach would be inappropriate.

For the two-moment case, Figs. 7.5-7 show the 'improved' images with $L = 4, 16, 64$ respectively. In each of these three cases we have investigated all possible values of x_i that lead to non-negative A_i, B_i and which correspond to local extrema. Table 7.1 gives the entropies of all these extrema and the images corresponding to the global maxima are plotted in Figs. 7.5-7.

In order to see in detail the effect of the maximum entropy method, Figs. 7.8

Region size	x_i	Entropy (in nats)	
$L = 4$	3	10.587677	*
$L = 16$	15	10.617421	
$L = 16$	14	10.617425	*
$L = 64$	63	10.708898	
$L = 64$	62	10.708955	
$L = 64$	61	10.708997	*
$L = 64$	60	10.708917	

Table 7.1: *Method of Two Moments*: The local extrema of the entropy (given in *nats*) for all possible values of the integer x_i, which represents the number of pixels with normalised intensity A_i as given by Eq. (7.23), for various region sizes. The asterisk indicates the maximum of all the extrema which is the maximum entropy image.

and 7.9 show a line-scan of the original state of the image, together with the 'improved' versions with $L = 4, 16, 64, 256$, for the cases of one moment and two moments, correspondingly. It can be seen that the method produces a smoother image and suppresses the effects of noise (eg. narrow peaks or wells).

ENTROPY OF MAXIMUM ENTROPY IMAGES (in nats)		
Region size	First moment	Two moments
original image	10.584326	10.584326
$L = 4$	10.606380	10.587677
$L = 16$	10.644367	10.617425
$L = 64$	10.736984	10.708997

Table 7.2: Entropies of the 'improved' images as reconstructed with the method of one moment and two moments for various region sizes (given in *nats*).

In Table 7.2 we present the entropies of the new images as reconstructed with the method of one moment and two moments. As expected the entropy is an increasing function of the region size and a decreasing function of the number of

moments that are used as a constraint.

7.5 Discussion

The maximum entropy method has been used for the reduction of noise in images at the output of an optical fibre. The original aspects of this work include the theoretical result of explicitly solving the discrete problem of moments and a processing method for cleaning speckle images (algorithms are presented in Appendix B). Assuming that the useful information is in the lowest moments and that the higher moments are affected by noise, a new 'clean' image is produced that has the same first two moments as the original ones and maximum entropy. A detailed investigation of all local extrema has been performed in order to find the solution corresponding to the global maximum of the entropy. The method can be used to reduce the effect of speckle noise in optical fibres and thus, improve the sensitivity of optical sensing systems operating under noisy conditions. It can be seen that the method is general and can be easily applied in other areas of digital signal and image processing.

Figures

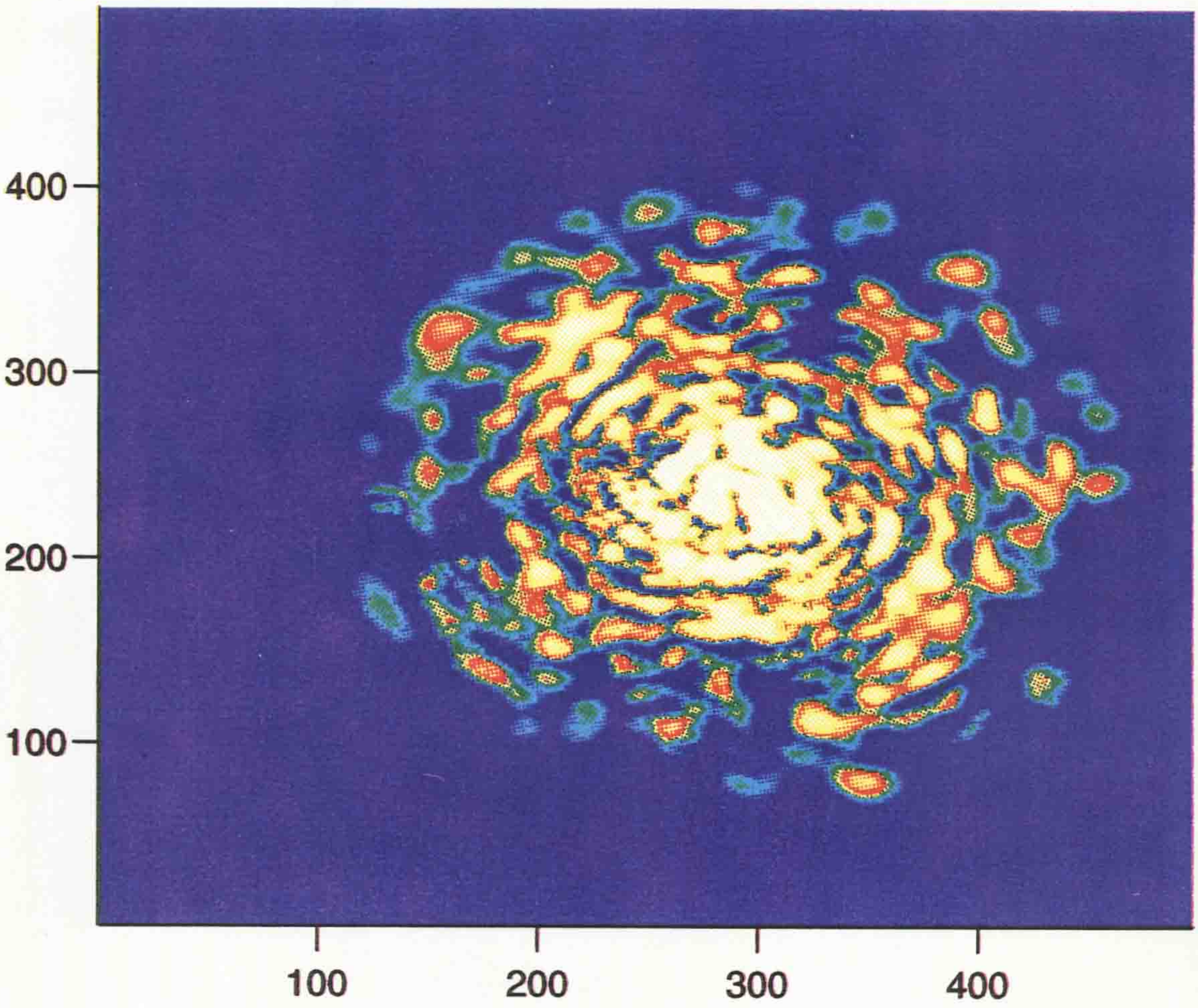

Figure 7.1: Original image, which represents a speckle pattern produced at the output of a step index multimode optical fibre. In the plot, colour indicates intensity, which increases from the blue areas (zero intensity) to the bright white ones.

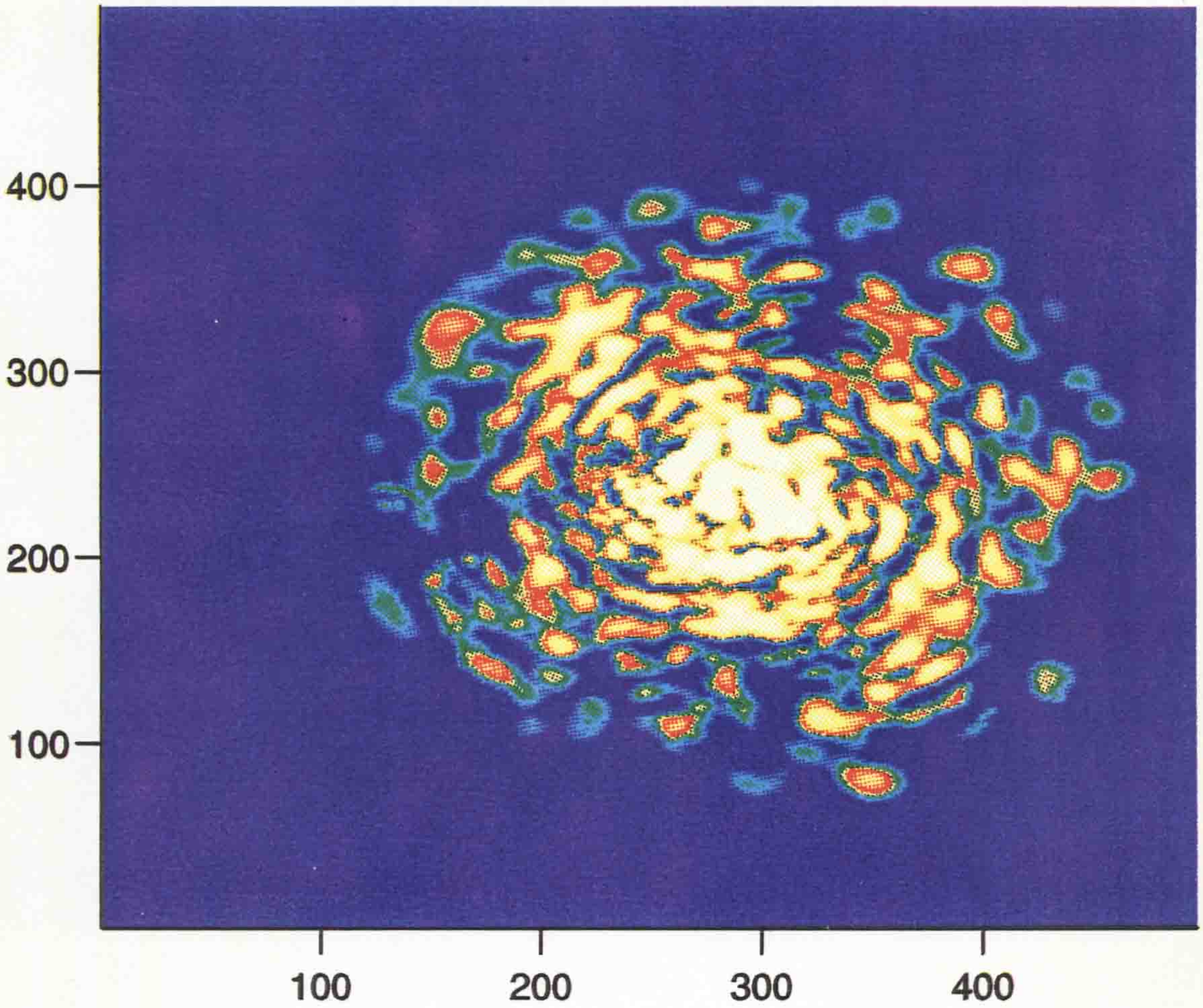

Figure 7.2: Improved image with region size $L = 4$ for the method of one moment. In the plot, colour indicates intensity, which increases from the blue areas (zero intensity) to the bright white ones.

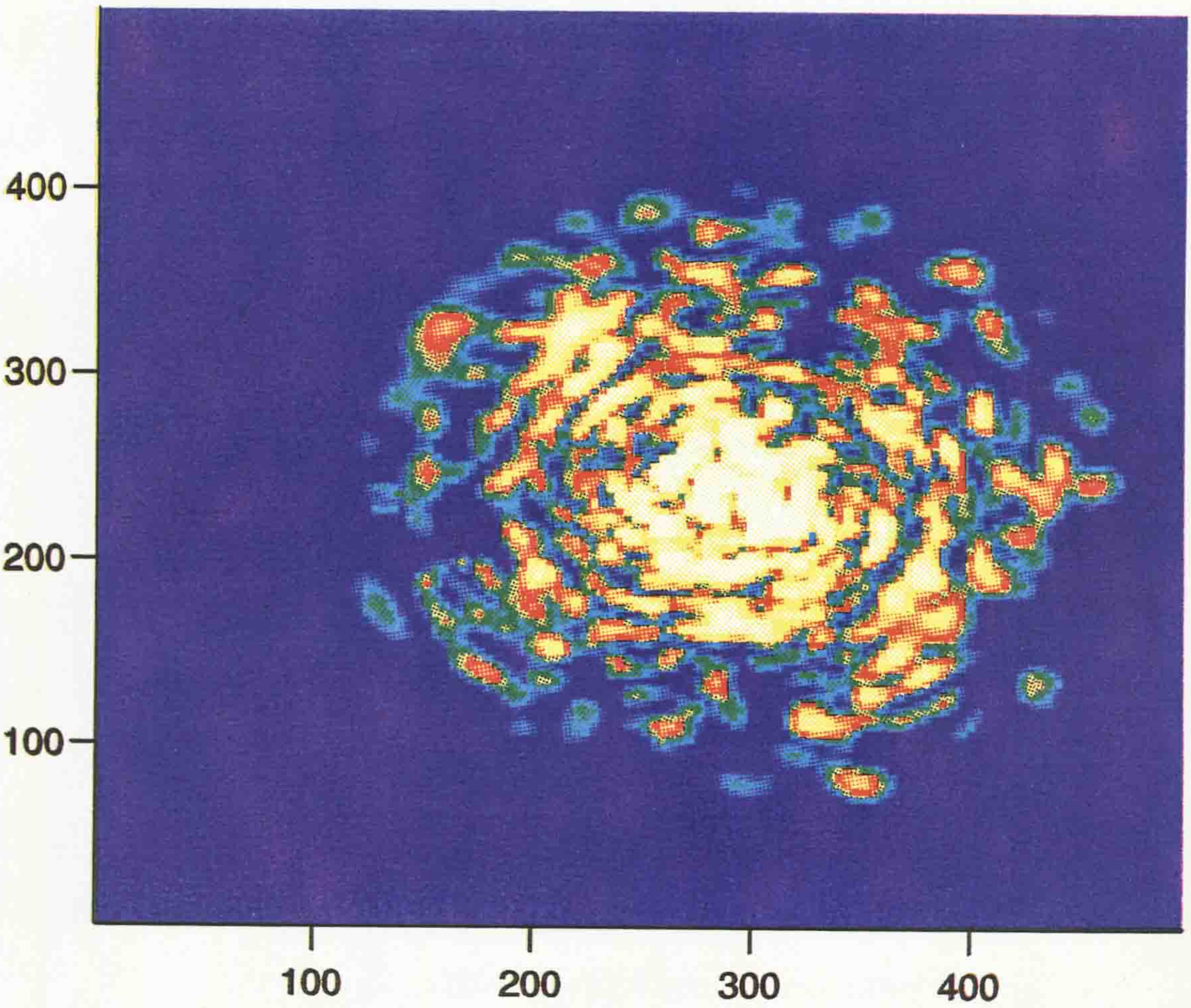

Figure 7.3: Improved image with region size $L = 16$ for the method of one moment. In the plot, colour indicates intensity, which increases from the blue areas (zero intensity) to the bright white ones.

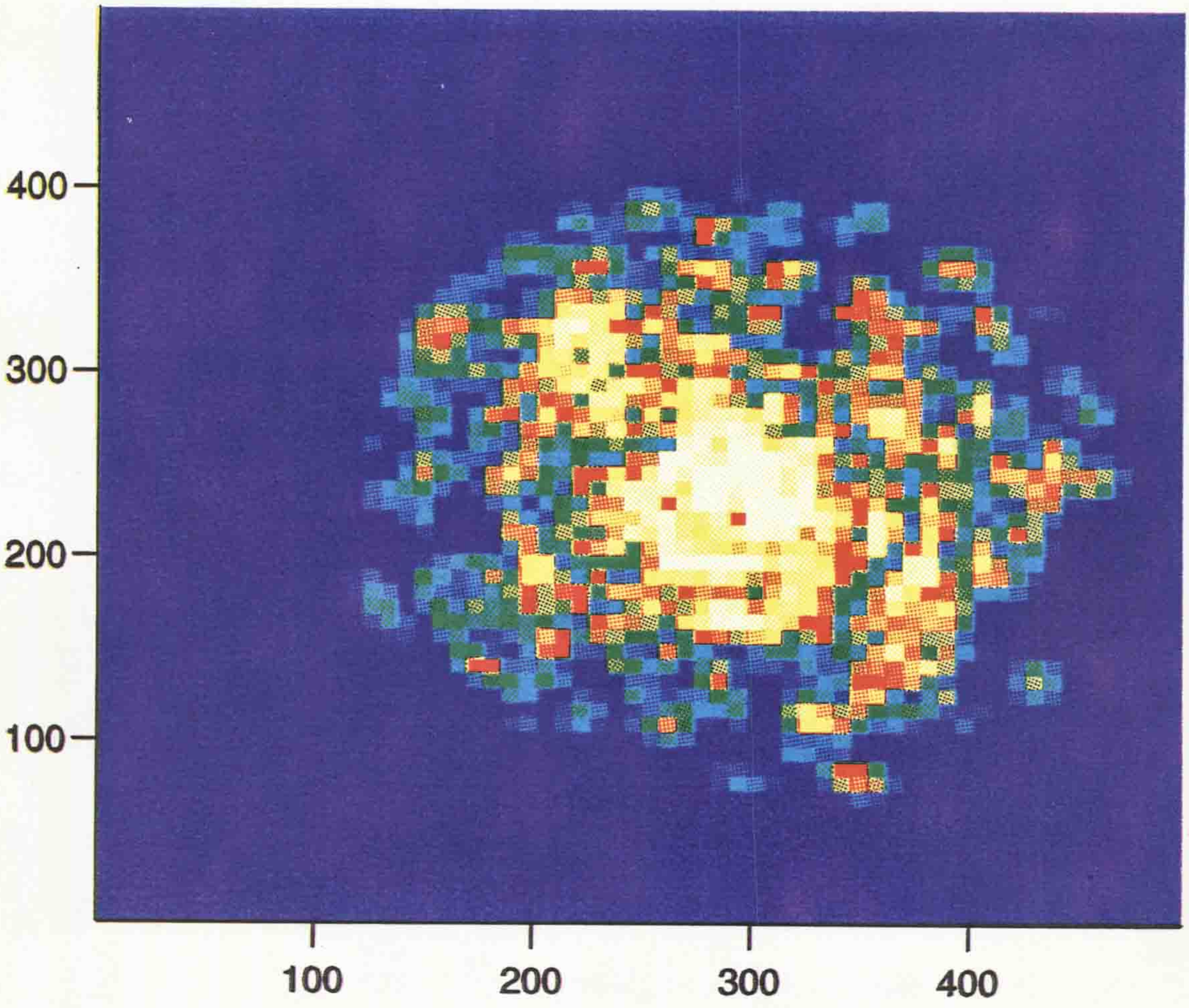

Figure 7.4: Improved image with region size $L = 64$ for the method of one moment. In the plot, colour indicates intensity, which increases from the blue areas (zero intensity) to the bright white ones.

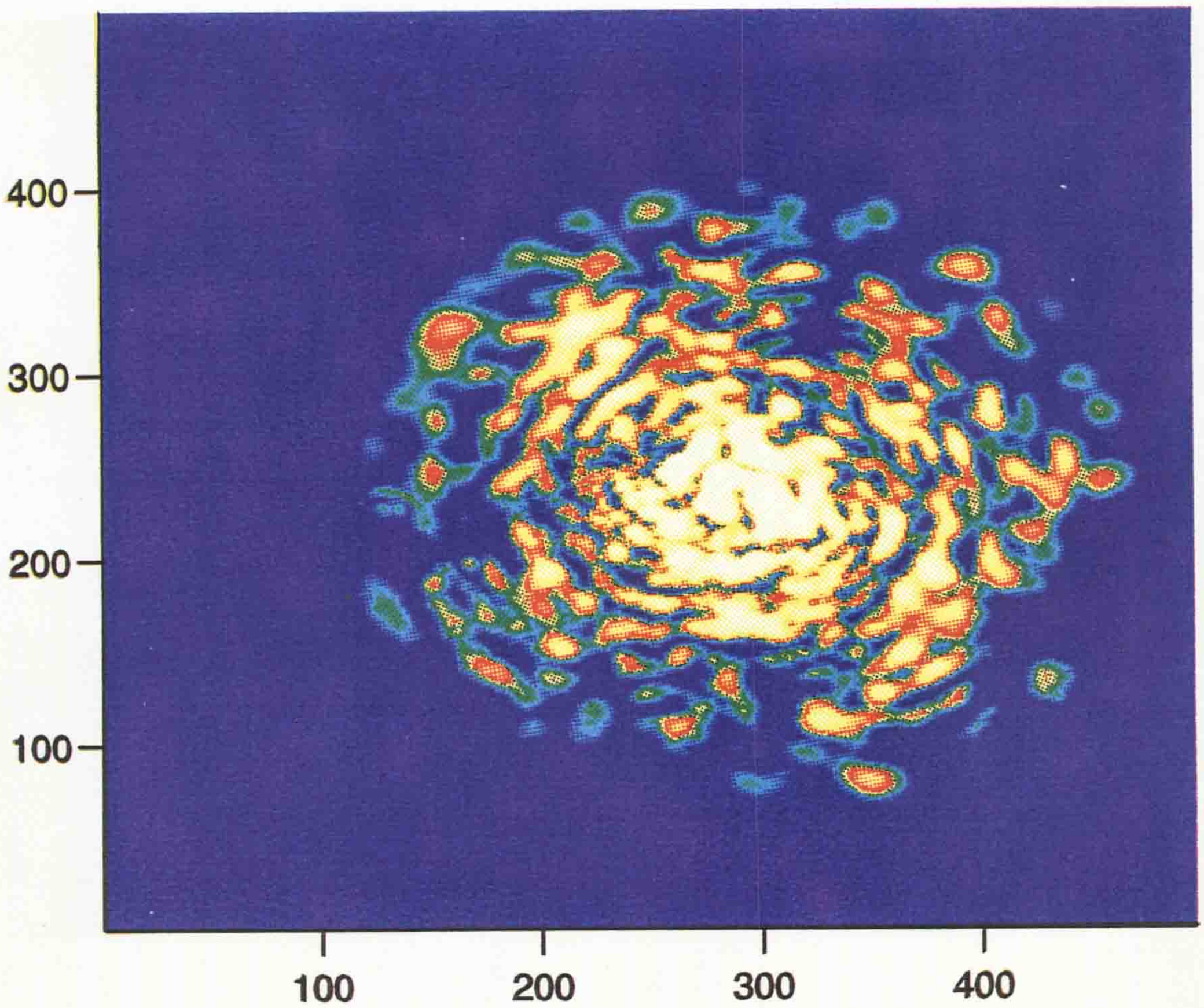

Figure 7.5: Improved image with region size $L = 4$ for the method of two moments. In the plot, colour indicates intensity, which increases from the blue areas (zero intensity) to the bright white ones.

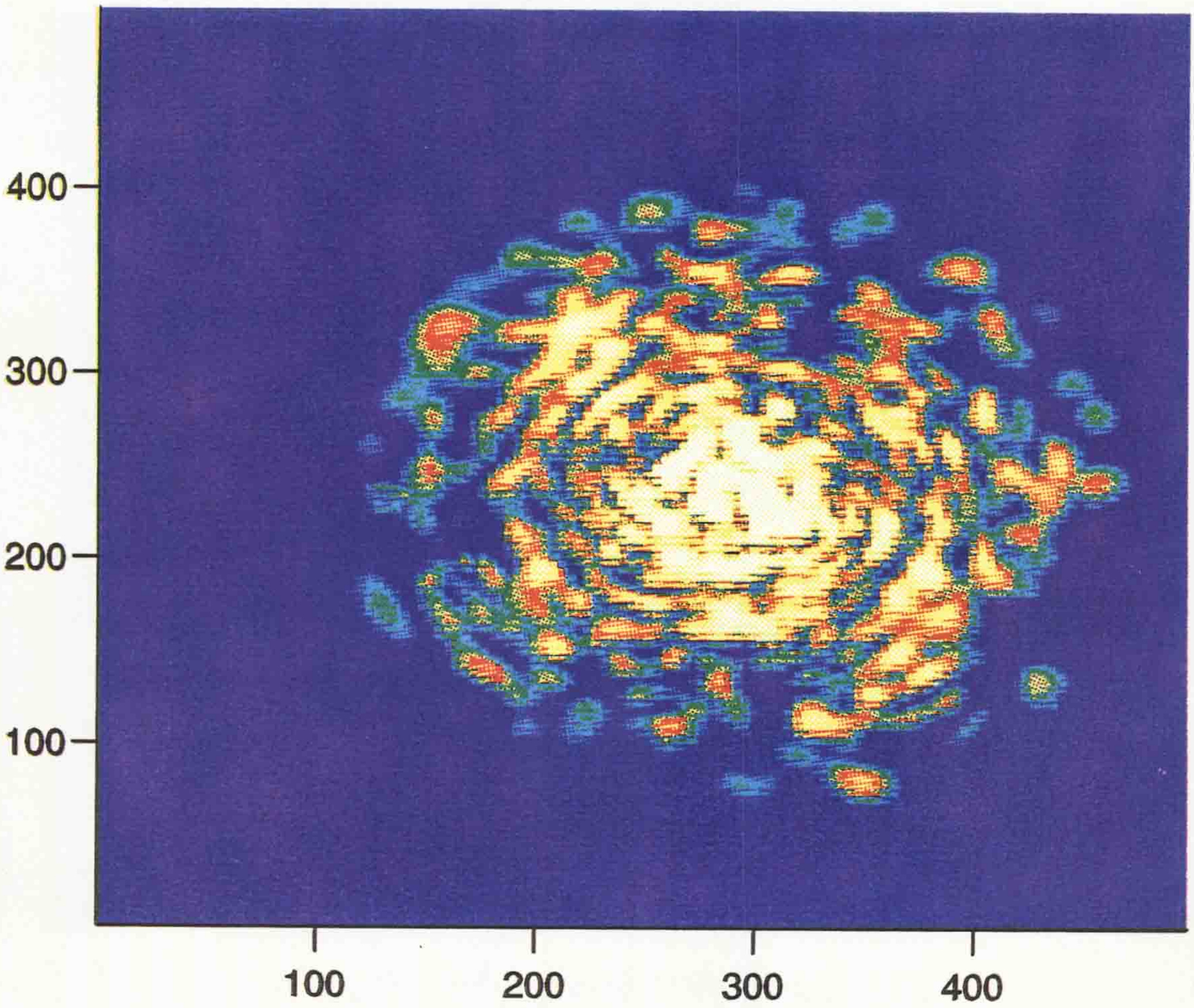

Figure 7.6: Improved image with region size $L = 16$ for the method of two moments. In the plot, colour indicates intensity, which increases from the blue areas (zero intensity) to the bright white ones.

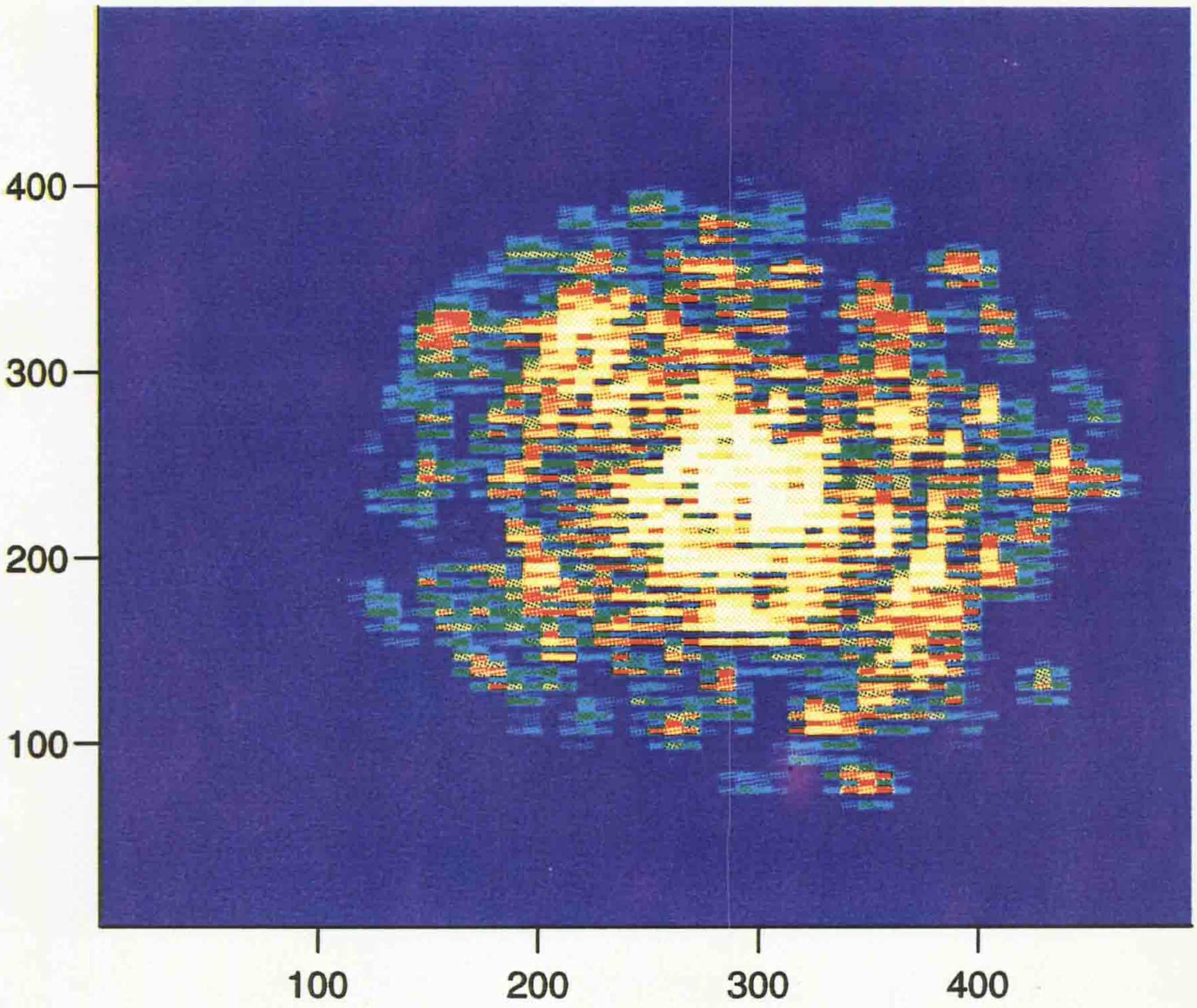

Figure 7.7: Improved image with region size $L = 64$ for the method of two moments. In the plot, colour indicates intensity, which increases from the blue areas (zero intensity) to the bright white ones.

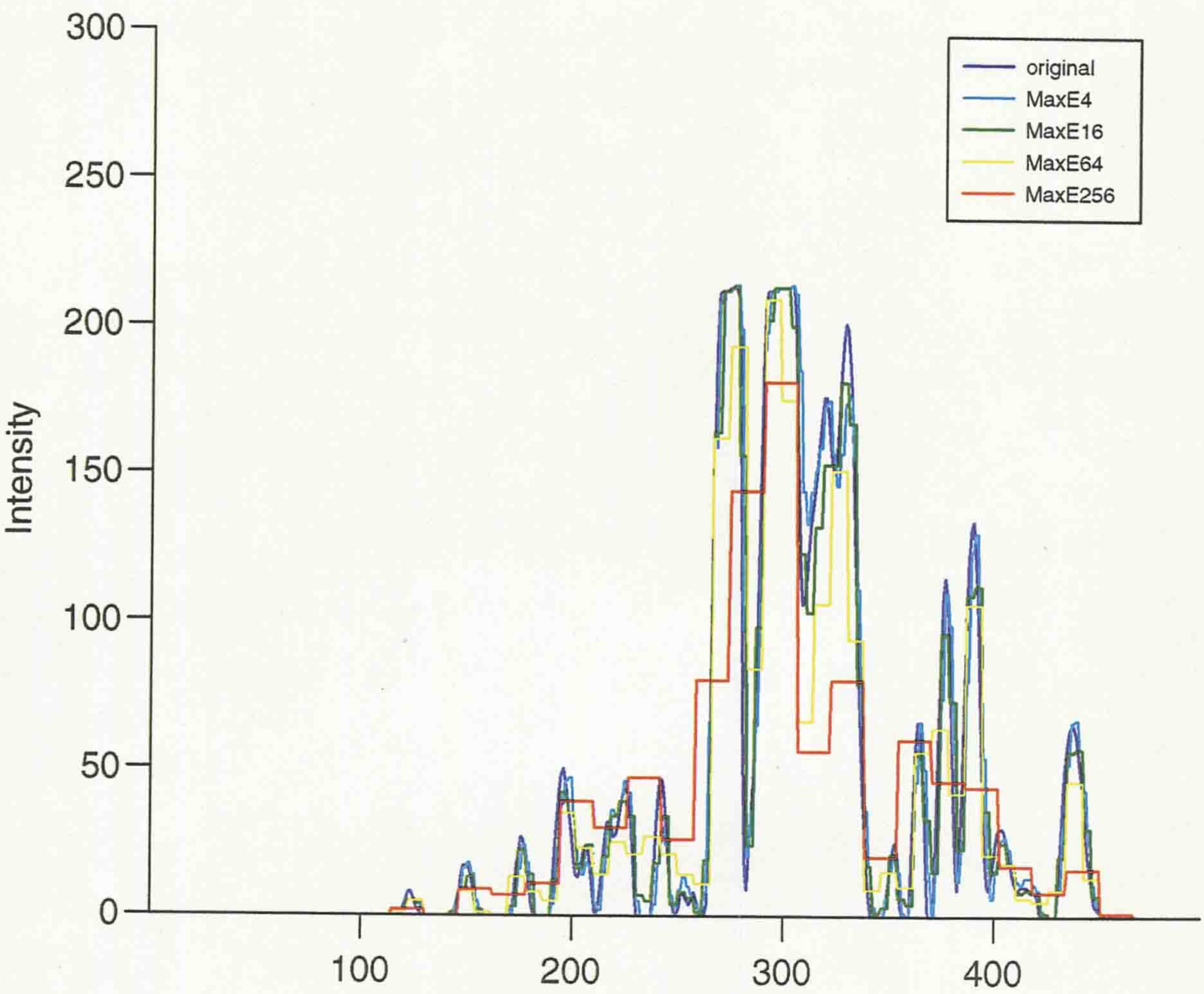

Figure 7.8: Line-scans of the original image and the improved versions with $L = 4, 16, 64, 256$, for the method of one moment.

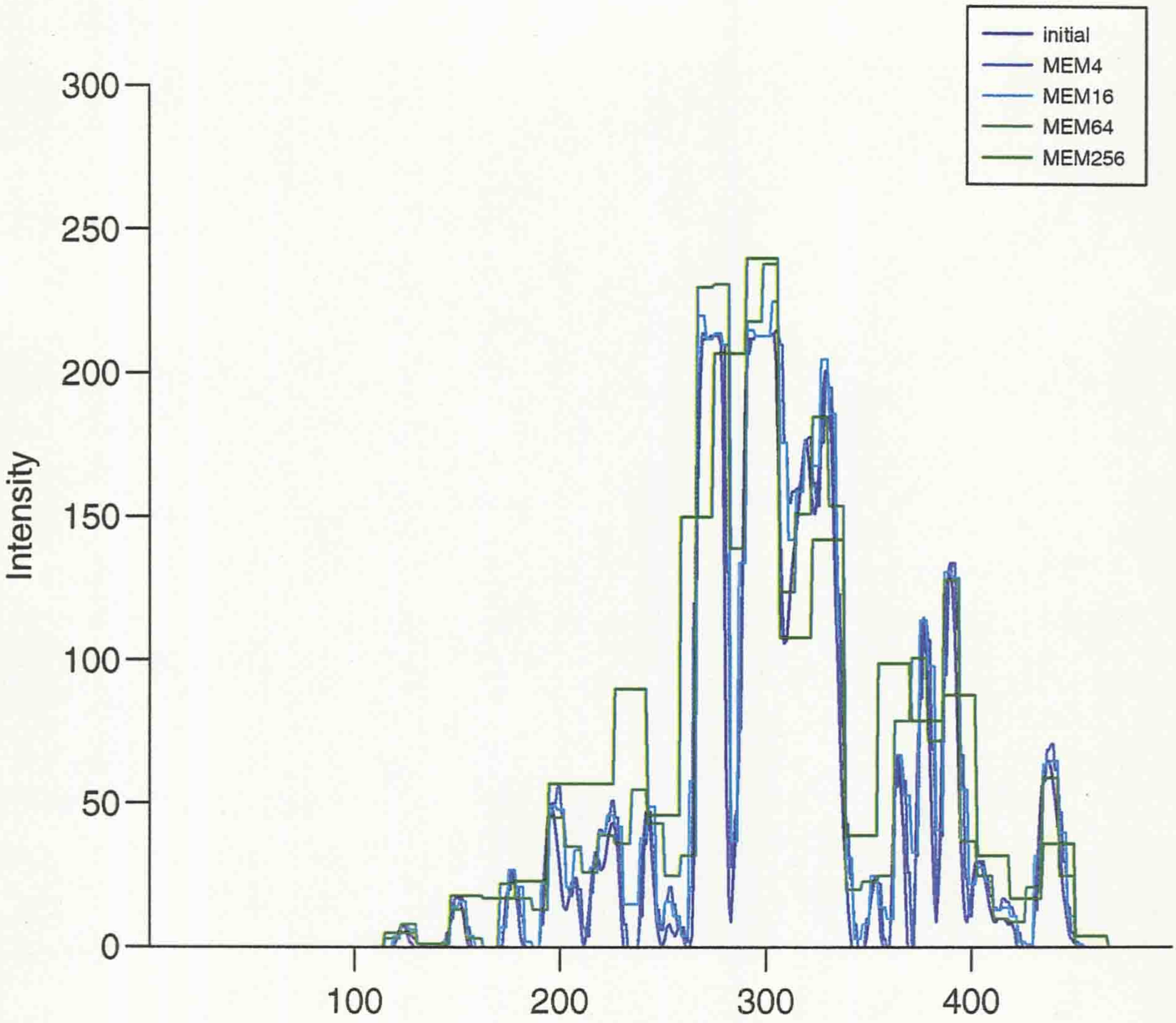

Figure 7.9: Line-scans of the original image and the improved versions with $L = 4, 16, 64, 256$, for the method of two moments.

Chapter 8

Conclusion

8.1 Summary of Main Conclusions

The main subject of this thesis is time-frequency signal analysis. Time-frequency representations have been studied and their potential for signal processing has been demonstrated. It was shown that they can be used as powerful tools for the analysis of time-varying signals.

In this work, results from quantum theory have been used in the context of signal processing and communication. It was pointed out that the powerful techniques of quantum mechanics can be of considerable benefit to applied signal analysis.

New ideas have been introduced and the practical value of the developed techniques was demonstrated by examples, mainly borrowed from the area of optical signal processing. The main conclusions of this work are:

8.1.1 Wigner Representation of Signals

The Wigner function has very attractive properties and offers a powerful method for time-frequency analysis. Implementation of the method in optical signal processing has been considered. Its capabilities for signal synthesis and for extracting the important time-frequency characteristics of a signal has been demonstrated.

Finally its potential for applications of arc plasma processing and condition monitoring of power electronic devices was demonstrated with examples of practical importance and its use as a diagnostic tool was pointed out. Extension of the method for the case of two-dimensional images opens a challenging field.

8.1.2 Gabor Expansion Using a Few Coefficients: Gabor Analysers

A truncated $N \times M$ von-Neumann lattice of Gaussian signals has been introduced and used as a basis for signal representation. Numerical implementation for the case of optical signals is demonstrated with various examples of practical importance. A quantitative analysis of the reconstruction error showed that expansion in terms of this discrete basis provides an accurate representation. The effect of the relative width of the Gaussian signals (squeezing) has also been studied and it was shown that variation of the width can be used to improve accuracy.

Compared and contrasted to the Fourier representation, the Gaussian expansion is shown to have a lot of relative advantages. In the case of nonstationary signals, the method can achieve significant improvements over the traditional Fourier approach. Its use for applications in transmission, data compression and noise reduction has been also pointed out.

The expansion has been shown to be stable, that is, addition of small amounts of random noise to the Gabor coefficients affects weakly the reconstruction. This is an attractive property in the sense that it enables practical implementation using inexpensive equipment.

The method seems to be very promising for practical applications in the areas of optical and acoustical signal processing. Gabor analysers, that measure directly the coefficients of the Gabor expansion, can be be used for practical signal analysis. Gabor analysis leads to a generalisation of the well-known chromatic methods, which can extract useful information from signals and be of significant benefit for processing applications in the optical and acoustical frequencies.

The Bargmann representation of quantum mechanics has been also considered

in the context of signal analysis. Relations between the Bargmann transform and other well-known representations have been studied and its potential for applications in image processing has been investigated.

8.1.3 Quantum State Engineering

Applications of the truncated Gaussian expansion in the context of quantum optics have been also considered. The concept of the truncated von-Neumann lattice of coherent states has been introduced and used as a tool for engineering quantum states. Superpositions of a few coherent states on a truncated von-Neumann lattice can be used to construct quantum states in an efficient way. Indeed, numerical results show that it can be used to construct highly non-classical states, such as squeezed states and number eigenstates, with very good accuracy.

It is emphasised that the expansion is robust in the sense that random noise in the coefficients does not affect significantly the generated state; this implies convenient implementation of the method for applications in quantum state engineering, particularly in quantum optical telecommunications.

8.1.4 Maximum Entropy Image of a Speckle Pattern

The final section of this thesis was dedicated to the maximum entropy method and its potential application to optical signal processing. An analytic solution for the problem of two moments has been given, and the technique was then applied to speckle pattern images for noise reduction in optical fibre systems.

More specifically, the maximum entropy method has been used to 'clean' speckle images at the output of an optical fibre. Using as a constraint the first two moments, a new maximum-entropy image can be constructed. It has been shown that in this improved image the intensities within each region are distributed in only two distinct levels. A detailed investigation of all local extrema has been carried out in order to find the solution corresponding to the global maximum of the entropy. The method can be of substantial benefit in optical sensing, improving the sensitivity of systems operating under noisy conditions; considering

that its formulation is general and application-independent, it might also be useful in many cases where the available discrete data are noisy or incomplete.

8.2 Epilogue

In conclusion, some novel ideas have been introduced in the context of practical signal processing. These techniques have yielded satisfactory results and their efficiency has been demonstrated. Of course, there are still a lot of problems requiring further investigation. The techniques presented here can be easily adapted for use in other areas.

Appendix A

Optical Fibre Particle Concentration Monitor

High power circuit breaker arcs trigger the production of suspending particles due to the decomposition of sulphur hexafluoride into a wide range of products. These particles take time to settle out of the gas and their concentration can provide a measure of the post-arc dielectric strength.

An optical fibre particle concentration monitor (or simply a powder monitor) can be used to indicate the time needed for the particles to settle out of the gas; this is useful in order to identify component wear and system failures. A prototype optical fibre particle concentration monitor was designed at the the Optics Laboratory in the Department of Electrical Engineering and Electronics, the University of Liverpool, and was used for circuit breaker tests. The electric arc signals analysed in Chapters 4-5 were obtained from this series of tests.

The prototype powder monitor uses a "LIBIDO" distimulus chromatic monitoring system. Broadband white light from the LIBIDO source (transmitted through a fibre) is collimated by a ball lens ($10mm$ diameter) and then travels through a particle-containing region of the gas (a gap of $10mm$ length) before being refocused by a second lens into a receiving fibre and complete its journey at the end of the LIBIDO detector. The light is modulated due to its passing through the suspending particles in the gap and this modulation is determined by the concentration of the particles.

It is well known that light scattering is wavelength dependent (Rayleigh and Mie scattering). The LIBIDO system measures the dominant wavelength λ_D of the modulated signal which, in the case of distimulus systems (like LIBIDO), is equivalent to the chromaticity value. Distimulus systems provide only one chromatic variable output (ie dominant wavelength). The dominant wavelength λ_D is related to the particle size N and radius r, ie $\lambda_D = f(N, r)$. Thus, for this system, particle size and concentration can be estimated using the change of the dominant wavelength of broadband white light.

The optical fibre particle concentration monitor was used to monitor the concentrations of particles within a circuit breaker tank, produced by the decomposition of arced sulphur hexafluoride. The signals shown in Figures 4.5,4.9-15 and 5.1 are taken from a series of relatively low fault current tests (up to $15kA$ maximum) using a short time scale (not more than $30ms$ recording time). The given signals (see Chapter 4) correspond to fault currents ranging from $1.9kA$ to $14.9kA$, which provide a steady and controllable production of particles.

From Figures 4.9-15, it is clear that the arc radiation reduces the dominant wavelength of light during the lifetime of the arc. This is the result of the superposition of the source light (tungsten halogen lamp of the LIBIDO system, dominant wavelength of $820nm$) and the arc radiation, which has a lower dominant wavelength ($690 - 730nm$).

Appendix B

Algorithms

The work presented in this thesis involved a substantial amount of computer programming. In this appendix, the basic routines are included.

A short description of the algorithms is presented using pseudo-code, ie the algorithms are described in terms of successive steps. In the following sections, the main steps for each routine are shown (which, of course, comprise smaller steps). These basic routines were used, sometimes with modifications, throughout this project. The algorithms were realised using FORTRAN programming language and high-precision arithmetic was used for optimum accuracy.

Additionally, a lot of auxiliary routines were written to address smaller tasks (eg. for data handling and conversion, normalisation, numerical calculation of various quantities, evaluation of special functions like squeezed and number wave-functions, etc.).

B.1 Analytic Signal: *anal-sig.f*

This routine calculates the analytic form of a real signal (Chapters 3-5).

INPUT: A file containing the points of a discrete-time real signal.

OUTPUT: A file containing the points of the imaginary part of the analytic

form.

PSEUDO-CODE

1. Initialise main parameters.
2. Read signal datafile.
3. Calculate FFT of real signal (Chapter 2: Eq. (2.21)).
4. Set negative frequencies to zero.
5. Calculate Inverse FFT of the modified spectrum (Hilbert Transform of real signal, see Chapter 3: Eq. (3.5-8)).
6. Write result (imaginary part) into the output file.

B.2 WDF analysis: *wdf-anal.f*

This routine calculates the Wigner distribution function of a real signal (Chapters 4-6).

INPUT: A file containing the points of a discrete-time real signal.

OUTPUT: A file containing the points of the two-dimensional Wigner function.

PSEUDO-CODE

1. Initialise main parameters.
2. Read signal datafile.
3. Calculate analytic signal (anal-sig.f).
4. Normalise the energy of the analytic signal (Chapter 4: Eq. (4.2)).
5. Calculate the instantaneous autocorrelation function (Chapter 4: Eq. (4.5)).

6. Calculate one-dimensional FFTs of the instantaneous autocorrelation function, keeping the t-variable fixed; thus obtaining one FT for each point in time (Chapter 4: Eq. (4.6)).

7. Create the 2-D Wigner function.

8. Write the DWDF into the output file.

B.3 WDF synthesis: *wdf-syn.f*

This routine reconstructs a signal from its WDF representation or modifies it using a filtering WDF (Chapter 4).

INPUT: A file containing the points of the 2-D Wigner function.

OUTPUT: A file containing the points of the analytic form of signal's new version.

PSEUDO-CODE

1. Initialise main parameters.

2. Read WDF datafile.

3. Read time-frequency filter datafile ($H[n, \theta]$, see Section 4.4).

4. Calculate new WDF: $H[n, \theta]W[n, \theta]$ (Section 4.4).

5. Integrate the modified WDF over frequency for each point in time and obtain the modulus of the modified analytic form.

6. Write the new version of the analytic signal into the output file.

B.4 Gabor expansion: *gab-exp.f*

This routine calculates the Gabor coefficients of a real signal (Chapters 5,6).

INPUT: A file containing the points of a discrete-time real signal.

OUTPUT: A file containing the coefficients of the Gabor expansion on a truncated von-Neumann lattice.

PSEUDO-CODE

1. Initialise parameters.
2. Read signal datafile
3. Calculate analytic signal (anal-sig.f).
4. Normalise the energy of the analytic signal (Chapter 5: Eq. (5.2)).
5. Create the truncated von-Neumann lattice (Chapter 5: Eq. (5.17)).
6. Calculate the generalised Gaussian signals at each lattice point (Chapter 5: Eq. (5.3)).
7. Evaluate the integral of Eq. (5.19) for each lattice point.
8. Produce the Gabor coefficients.
9. Write the coefficients into the output file.

B.5 Gabor reconstruction: *gab-rec.f*

This routine reconstructs a signal from its Gabor coefficients (Chapters 5,6).

INPUT: A file containing the the coefficients of the Gabor expansion on a truncated von-Neumann lattice.

OUTPUT: A file containing the points of the signal in time.

PSEUDO-CODE

1. Initialise parameters.
2. Read coefficient datafile.
3. Create the truncated von-Neumann lattice (Chapter 5: Eq. (5.17)).

4. Calculate the generalised Gaussian signals at each lattice point (Chapter 5: Eq. (5.3)).

5. Calculate the sum of Eq. (5.18) for each point in time (reconstruction).

6. Write the real part of the resulting signal into the output file.

B.6 Entropy Maximisation: *max-ent.f*

This routine processes a two-dimensional image and returns an 'improved' image with maximum entropy and the same first moments (Chapter 7).

INPUT: A file containing the points of a discrete 2-D image.

OUTPUT: A file containing the points of the 'improved' version of the image.

PSEUDO-CODE

1. Initialise parameters.

2. Read 2-D image file.

3. Normalise image (Chapter 7: Eq. (7.10).

4. Calculate entropy of original image (Chapter 7: Eq. (7.13).

5. Create partitions of size L of the original image.

6. Calculate the first moment for each region.

7. Calculate the second moment for each region.

8. Replace the pixels of the partitions with the results of Equations 7.16,23-24.

9. Compose 'improved' image.

10. Calculate entropy of 'improved' image.

11. Output 'improved' image and the entropies of the original and 'improved' versions.

Bibliography

[1] M. Abramowitz and I.A. Stegun. *Handbook of Mathematical Functions.* Dover, New York, 1972.

[2] P. Adam, J. Janszky, and A.V. Vinogradov. Gaussian coherent state expansion of the squeezed states. *Optics Communications*, 80:155, 1990.

[3] N. Agmon, Y. Alhassid, and R.D. Levine. An algorithm for finding the distribution of maximal entropy. *Journal of Computational Physics*, 30:250–258, 1979.

[4] Y. Alhassid and R.D. Levine. Connection between the maximal entropy and the scattering theoretic analyses of collision processes. *Physical Review A*, 18:89–116, 1978.

[5] J.F. Allard, J.C. Valiere, and R. Bourdier. Broadband signal analysis with the smooth pseudo-Wigner distribution. *Journal of the Acoustical Society of America*, 83:1041–1044, 1988.

[6] F. Auger and P. Flandrin. Improving the readability of time-frequency and time-scale representations by the reassignment method. *IEEE Transactions on Signal Processing*, 43:1068–1089, 1995.

[7] L. Auslander and R. Tolimieri. Characterizing the radar ambiguity functions. *IEEE Transactions on Information Theory*, 30:832–836, 1984.

[8] H. Bacry, A. Grossmann, and J. Zak. Proof of completeness of lattice states in the kq representation. *Physical Review B*, 12:1118, 1975.

[9] J. Baker-Jarvis. Solution to boundary value problems using the method of maximum entropy. *Journal of Mathematical Physics*, 30:302–306, 1989.

[10] N.L. Balazs and B.K. Jennings. Wigner's function and other distribution functions in mock phase spaces. *Physics Reports*, 104:347, 1984.

[11] R. Bamler and H. Glünder. The Wigner distribution function of two dimensional signals: Coherent-optical generation and display. *Optica Acta*, 30:1789–1803, 1983.

[12] V. Bargmann. On a Hilbert space of analytic functions and an associated integral transform. *Communications in Pure and Applied Mathematics*, 14:187–214, 1961.

[13] V. Bargmann, P. Butera, L. Girardello, and J.R. Klauder. On the completeness of the coherent states. *Reports on Mathematical Physics*, 2:221, 1971.

[14] A.O. Barut and L. Girardello. New "coherent states" associated with non-compact groups. *Communications in Mathematical Physics*, 21:41–55, 1971.

[15] M.J. Bastiaans. Wigner distribution function and its application to first-order optics. *Journal of the Optical Society of America*, 69:1710–1716, 1980.

[16] M.J. Bastiaans. Gabor's expansion of a signal into gaussian elementary signals. *Optical Engineering*, 20:594–598, 1981.

[17] C. Bendjaballah. *Introduction to Photon Communication*. Springer, Berlin, 1995.

[18] F.A. Berezin. General concept of quantization. *Communications in Mathematical Physics*, 40:153–174, 1975.

[19] G.J.A. Bird. *Radar Precision and Resolution*. Pentech Press, London, 1974.

[20] R.F. Bishop and A. Vourdas. Generalised coherent states and Bogoliubov transformations. *Journal of Physics A*, 19:2525–2536, 1986.

[21] G.F. Boudraux-Bartels and T.W. Parks. Time-varying filtering and signal estimation using Wigner distribution synthesis techniques. *IEEE Transactions on Acoustics, Speech, and Signal Processing*, 34:442–451, 1986.

[22] M. Brune, S. Haroche, J.M. Raimond, L. Davidovich, and N. Zagury. Manipulation of photons in a cavity by dispersive atom-field coupling: Quantum-nondemolition measurements and generation of 'Schrödinger cat' states. *Physical Review A*, 45:5193, 1992.

[23] M. Brune, S. Haroche, J.M. Raimond, and N. Zagury. Quantum nondemolition measurement of small photon numbers by Rydberg-atom phase-sensitive detection. *Physical Review Letters*, 65:976, 1990.

[24] R.K. Bryan and J. Skilling. Maximum entropy image reconstruction from phaseless Fourier data. *Optica Acta*, 33:287–299, 1986.

[25] J.P. Burg. The relationship between maximum entropy spectra and maximum likelihood spectra. *Geophysics*, 37:375–376, 1972.

[26] V. Bužek and P.L. Knight. The origin of squeezing in a superposition of coherent states. *Optics Communications*, 81:331, 1991.

[27] V. Bužek and P.L. Knight. Quantum interference, superposition states of light, and nonclassical effects. *Progress in Optics*, 34:1, 1995.

[28] K.E. Cahill. Coherent-state representation for the photon density operator. *Physical Review*, 138:B1566–1576, 1965.

[29] H.J. Carmichael, A.S. Lane, and D.F. Walls. Resonance fluorescence in a squeezed vacuum. *Journal of Modern Optics*, 34:821–840, 1987.

[30] C.M. Caves. Quantum mechanical noise in an interferometer. *Physical Review D*, 23:1693, 1981.

[31] H.I. Choi and W.J. Williams. Improved time-frequency representation of multicomponent signals using exponential kernels. *IEEE Transactions on Acoustics, Speech, and Signal Processing*, pages 862–871, 1989.

[32] C.K. Chui. *An Introduction to Wavelets.* Academic Press, San Diego, 1992.

[33] C.K. Chui, editor. *Wavelets: A Tutorial in Theory and Applications.* Academic Press, San Diego, 1992.

[34] S. Ciulli, M. Mounsif, N. Gorman, and T.D. Spearman. On the application of maximum entropy to the moments problem. *Journal of Mathematical Physics*, 32:1717–1719, 1991.

[35] T.A.C.M. Claasen and W.F.G. Mecklenbräuker. The Wigner distribution: a tool for time-frequency signal analysis (parts i-iii). *Philips Journal of Research*, 35:217–250, 276–300, 372–389, 1980.

[36] T.A.C.M. Claasen and W.F.G. Mecklenbräuker. The aliasing problem in discrete-time Wigner distributions. *IEEE Transactions on Acoustics, Speech, and Signal Processing*, 31:1067–1072, 1983.

[37] L. Cohen. Generalised phase-space distribution functions. *Journal of Mathematical Physics*, 7:781–786, 1966.

[38] L. Cohen. Time-frequency distributions - a review. *Proceedings of the IEEE*, 77:941–981, 1989.

[39] J.M. Combes, A. Grossmann, and Ph. Tchamitchian, editors. *Wavelets, Time-Frequency Methods and Phase Space.* Springer-Verlag, Berlin-Heidelberg, 1989.

[40] J.W. Cooley and J.W. Tukey. An algorithm for the machine calculation of complex Fourier series. *Mathematics of Computation*, 19:297–301, 1965.

[41] J.A. Cosgrave, A. Vourdas, P.C. Russell, and L.K. Stergioulas. Generalised chromatic systems based on Gabor transforms. preprint, University of Liverpool, 1996.

[42] J.A. Cosgrave, A. Vourdas, J.W. Spencer, G.R. Jones, M.M. Murphy, and A. Wilson. Acoustic monitoring of partial discharges in gas insulated substations using optical sensors. *IEE Proceedings*, 140:369–374, 1993.

[43] R.T. Cox. *The Algebra of Probable Inference.* John Hopkins University Press, Baltimore, 1961.

[44] J.C. Dainty, editor. *Laser Speckle and Related Phenomena*, Berlin, 1984. Springer.

[45] G.J. Daniell and S.F. Gull. Maximum entropy algorithm applied to image enhancement. *Proceedings of the IEE*, 127E:170–172, 1980.

[46] I. Daubechies. Orthonormal bases of compactly supported wavelets. *Communications in Pure and Applied Mathematics*, XLI:909–96, 1988.

[47] I. Daubechies. The wavelet transform, time-frequency localization and signal analysis. *IEEE Transactions on Information Theory*, 36:961–1005, 1990.

[48] I. Daubechies, S. Mallat, and A.S. (eds.) Willsky. Wavelet transforms and multiresolution signal analysis. *Special Issue of IEEE Transactions on Information Theory*, 38, 1992.

[49] J. Daugman. Uncertainty relation for resolution in space, spatial frequency, and orientation optimized by two-dimensional visual cortical filters. *Journal of the Optical Society of America*, 2:1160–1169, 1985.

[50] J. Daugman. Complete discrete 2-d Gabor transforms by neural networks for image analysis and compression. *IEEE Transactions on Acoustics, Speech and Signal Processing*, 36:1169–1179, 1988.

[51] O.C. de Bauregard and M. Tribus. Information theory and thermodynamics. *Helvetica Physica Acta*, 47:238–247, 1974.

[52] G.W. Deley. Waveform design. In M.I. Skolnik, editor, *Radar Handbook*, chapter 3, pages 3.1–3.47. McGraw-Hill, New York, 1970.

[53] A.M. Djafari. Maximum d'entropie et problémes inverse en imagerie. *Traitement du Signal*, 11:87–116, 1994.

[54] P. Domokos, P. Adam, and J. Janszky. One-dimensional coherent-state representation on a circle in phase space. *Physical Review A*, 50:4293–4297, 1994.

[55] D.C. Dowson and A. Wragg. Maximum entropy distributions having prescribed first and second moments. *IEEE Transactions on Information Theory*, 19:689–693, 1973.

[56] T. Ebrahimi and M. Kunt. Image compression by Gabor expansion. *Optical Engineering*, 30:873–880, 1991.

[57] H.G. Feichtinger and O. Christensen. Group theoretical approach to Gabor analysis. *Optical Engineering*, 34:1697–1704, 1995.

[58] P. Flandrin and B. Escudie. Time and frequency representation of finite energy signal: A physical property as a result of an Hilbertian condition. *Signal Processing*, 2:93–100, 1980.

[59] M. Francon. *Laser Speckle and Applications to Optics.* Academic Press, New York, 1979.

[60] B.R. Frieden. Restoring with maximum likelihood and maximum entropy. *Journal of the Optical Society of America*, 62:511–518, 1972.

[61] B.R. Frieden and J.J. Burke. Restoring with maximum entropy. II: Superresolution of photographs of diffraction-blurred impulses. *Journal of the Optical Society of America*, 62:1202–1210, 1972.

[62] B.R. Frieden and D.C. Wells. Restoring with maximum entropy. III: Poisson sources and background. *Journal of the Optical Society of America*, 68:93–103, 1978.

[63] D. Gabor. Theory of communication. *Journal of the IEE*, 93:429–457, 1946.

[64] J.W. Gibbs. *Elementary Principles in Statistical Mechanics.* Longman Green and Company, New York, 1928.

[65] R.J. Glauber. Coherent and incoherent states of the radiation field. *Physical Review*, 131:2766–2788, 1963.

[66] R.J. Glauber. The quantum theory of coherence. *Physical Review*, 130:2529–2539, 1963.

[67] R.C. Gonzalez and R.E. Woods. *Digital Image Processing.* Addison-Wesley, New York, 1993.

[68] I.J. Good. Maximum entropy for hypothesis formulation, especially for multidimensional contigency tables. *Annals Math. Stat.*, 34:911–934, 1963.

[69] P. Goupillaud, A. Grossmann, and J. Morlet. Cycle-octave and related transforms in seismic signal analysis. *Geoexploration*, 23:85–102, 1984.

[70] S.F. Gull and G.J. Daniell. Image reconstruction from incomplete and noisy data. *Nature*, 272:686–690, 1978.

[71] S.F. Gull and J. Skilling. The entropy of an image. In C. Ray Smith and Jr. W.T. Grandy, editors, *Maximum-Entropy and Bayesian Methods in Inverse Problems*, Fundamental Theories of Physics, pages 287–301, Dordrecht, The Netherlands, 1985. D. Reidel Publishing Company.

[72] S. Haroche. Cavity quantum electrodynamics. In J. Dalibard, J.M. Raimond, and J. Zinn Justin, editors, *Systemes fondamentaux en Optique Quantique.* Elsevier Science Publishers, Amsterdam, 1992. Les Houches session LIII.

[73] S. Haroche, M. Brune, and J.M. Raimond. Manipulation of optical fields by atomic interferometry: Quantum variations on a theme by Young. *Applied Physics B*, 54:355–365, 1992.

[74] S. Haroche and J.M. Raimond. Manipulation of non classical field states by atom interferometry. In Berman, editor, *Cavity Quantum Electrodynamics*, Advances in Atomic and Molecular Physics. Academic Press, 1994. supplement.

[75] S.B. Hearon and M.G. Amin. Minimum-variance time-frequency distribution kernels. *IEEE Transactions on Signal Processing*, 43:1258–1262, 1995.

[76] C.W. Helstrom. An expansion of a signal in Gaussian elementary signals. *IEEE Transactions on Information Theory*, 12:81–82, 1966.

[77] C.W. Helstrom. *Quantum Detection and Estimation Theory.* Academic Press, New York, 1976.

[78] M. Hillery, R.F. O'Connell, M.O. Scully, and E.P. Wigner. Distribution functions in physics: Fundamentals. *Physics Reports*, 106:121, 1984.

[79] F. Hlawatsch. Interference terms in the Wigner distribution. In V. Capellini and A.G. Constantinidis, editors, *Digital Signal Processing 84.* Elsevier (North Holland), Amsterdam, The Netherlands, 1984.

[80] F. Hlawatsch, T.G. Manickam, R.L. Urbanke, and W. Jones. Smoothed pseudo-Wigner distribution, Choi-Williams distribution, and cone-kernel representation: Ambiguity-domain analysis and experimental comparison. *Signal Processing*, 43:149–168, 1995.

[81] L.D. Jacobson and H. Wechsler. Joint spatial/spatial-frequency representation. *Signal Processing*, 14:37–68, 1988.

[82] A. Janssen. Gabor representations of generalised functions. *Journal of Mathematical Analysis and Applications*, 83:377–394, 1981.

[83] J. Janszky, P. Adam, and A.V. Vinogradov. Superposition of coherent states and squeezing. *Physical Review Letters*, 68:3816, 1992.

[84] J. Janszky, P. Domokos, and P. Adam. Coherent states on a circle and quantum interference. *Physical Review A*, 48:2213, 1993.

[85] J. Janszky, P. Domokos, S. Szabo, and P. Adam. Quantum state engineering via discrete coherent-state superpositions. *Physical Review A*, 51:4191, 1995.

[86] J. Janszky and A.V. Vinogradov. Squeezing via one-dimensional distribution of coherent states. *Physical Review Letters*, 64:2771–2774, 1990.

[87] E.T. Jaynes. Information Theory and Statistical Mechanics. *Physical Review*, 106:620–630, 1957.

[88] E.T. Jaynes. Information Theory and Statistical Mechanics II. *Physical Review*, 108:171–190, 1957.

[89] E.T. Jaynes. Information Theory and Statistical Mechanics. In K.W. Ford, editor, *Statistical Physics*, volume 3 of *Brandeis Lectures*, pages 182–218. Benjamin, New York, 1963.

[90] E.T. Jaynes. On the rationale of maximum-entropy methods. *Proceedings of the IEEE*, 70:939–952, 1982.

[91] E.T. Jaynes. Where do we go from here? In C. Ray Smith and Jr. W.T. Grandy, editors, *Maximum-Entropy and Bayesian Methods in Inverse Problems*, Fundamental Theories of Physics, pages 21–58, Dordrecht, The Netherlands, 1985. D. Reidel Publishing Company.

[92] H. Jeffreys. *Theory of Probability*. Oxford University Press, 1939.

[93] R.W Johnson and J.E. Shore. Comments on and correction to "Axiomatic derivation of the principle of maximum entropy and the principle of minimum cross-entropy". *IEEE Transactions on Information Theory*, 29:942–943, 1983.

[94] G.R. Jones, P. Russell, and I. Khandaker. Chromatic interferometry for an intelligent plasma processing system. *Meas. Sci. Technol.*, 5:639–647, 1994.

[95] G.R. Jones and P.C. Russell. Chromatic modulation based metrology. *Pure and Applied Optics*, 2:87–110, 1993.

[96] H.J. Kimble. Quantum fluctuations in quantum optics: Squeezing and related phenomena. In J. Dalibard, J.M. Raimond, and J. Zinn Justin, editors, *Systemes fondamentaux en Optique Quantique*. Elsevier Science Publishers, Amsterdam, 1992. Les Houches session LIII.

[97] H.J. Kimble and G.-L. Oppo. Quantum fluctuations and applications of squeezed light. In G.-L. Oppo, S.M. Barnett, E. Riis, and Wilkinson M., editors, *Quantum Dynamics of Simple Systems*, volume 44 of *Proceedings of the Forty Fourth Scottish Universities Summer School in Physics*, page 360, London, 1996. NATO Advanced Study Institute, Institute of Physics Publishing.

[98] J.R. Klauder. The design of radar signals having both high range resolution and high velocity resolution. *Bell System Technical Journal*, 39:809–820, 1960.

[99] J.R. Klauder and B.S. Skagerstam. *Coherent states: Applications in physics and mathematical physics.* World Scientific, Singapore, 1985.

[100] J.R. Klauder and E. Sudarshan. *Fundamentals of Quantum Optics.* Benjamin, New York, 1968.

[101] P.L. Knight and B.M. Garraway. Quantum superpositions in dissipative environments: decoherence and deconstruction. In G.-L. Oppo, S.M. Barnett, E. Riis, and Wilkinson M., editors, *Quantum Dynamics of Simple Systems*, volume 44 of *Proceedings of the Forty Fourth Scottish Universities Summer School in Physics*, pages 199–238, London, 1996. NATO Advanced Study Institute, Institute of Physics Publishing.

[102] M.J. Leaseburg and L.R. Mead. Error bounds in maximum entropy approximations. *Journal of Mathematical Physics*, 34:6009–6015, 1993.

[103] X. Li and T. Chen. Efficient synthesis of parameterized gaussian-like filters by approximation. *Signal Processing*, 41:119–134, 1995.

[104] R. Lieu. Maximum entropy data analysis: another derivation of $S - \chi^2$. *Journal of Physics A*, 21:L63–L65, 1988.

[105] R. Lieu, R.B. Hicks, and C.J. Bland. Maximum entropy in data analysis with error-carrying constraints. *Journal of Physics A*, 20:2379–2388, 1987.

[106] A.K. Livesey and J. Skilling. Maximum entropy theory. *Acta Crystallographica*, 41:113–122, 1985.

[107] R. Loudon. *The Quantum Theory of Light.* Oxford University Press, Oxford, 1983.

[108] R. Loudon and P.L. Knight. Squeezed light. *Journal of Modern Optics*, 34:709–759, 1987.

[109] W.H. Louisell. *Radiation and Noise in Quantum Electronics.* Krieger, New York, 1977.

[110] S. Mallat. A theory for multiresolution signal decomposition: The wavelet representation. *IEEE Transactions on Pattern Analysis and Machine Intelligence*, 11:674–93, 1989.

[111] L. Mandel and E. Wolf. *Optical Coherence and Quantum Optics.* Cambridge University Press, New York, 1995.

[112] W. Martin and P. Flandrin. Detection of changes of signal structure by using the Wigner-Ville spectrum. *Signal Processing*, 8:215–233, 1985.

[113] W. Martin and P. Flandrin. Wigner-Ville spectral analysis of nonstationary processes. *IEEE Transactions on Acoustics, Speech, and Signal Processing*, 33:1461–1470, 1985.

[114] S. Marčelja. Mathematical description of the responses of simple cortical cells. *Journal of the Optical Society of America*, 70:1297–1300, 1980.

[115] L.R. Mead. Approximate solution of fredholm integral equations by the maximum-entropy method. *Journal of Mathematical Physics*, 27:2903–2907, 1986.

[116] L.R. Mead and N. Papanicolaou. Maximum entropy in the problem of moments. *Journal of Mathematical Physics*, 25:2404–2417, 1984.

[117] Y. Meyer. *Wavelets and Operators.* Cambridge University Press, Cambridge, 1992.

[118] L.K. Montgomery and I.S. Reed. A generalization of the Gabor-Helstrom transform. *IEEE Transactions on Information Theory*, 13:344–345, 1967.

[119] J. von Neumann. *Mathematical Foundations of Quantum Mechanics.* Princeton University, Princeton, 1955.

[120] C.H. Page. Instantaneous power spectra. *Journal of Applied Physics*, 23:103–106, 1952.

[121] A. Papoulis. *Signal Analysis.* McGraw-Hill, New York, 1977.

[122] A. Papoulis. *Probability, Random Variables and Stochastic Processes.* McGraw-Hill, New York, 3rd edition, 1991.

[123] S.F. Pereira, M. Xiao, H.J. Kimble, and J.L. Hall. Generation of squeezed light by intracavity frequency doubling. *Physical Review A*, 38:4931–4934, 1988.

[124] A.M. Perelomov. Coherent states for arbitrary Lie group. *Communications in Mathematical Physics*, 26:222–236, 1972.

[125] A.M. Perelomov. *Generalised coherent states and their applications.* Springer, Berlin, 1986.

[126] E.S. Polzik, J. Carri, and H.J Kimble. Atomic spectroscopy with squeezed light for sensitivity beyond the vacuum state limit. *Applied Physics B*, 55:279–290, 1992.

[127] M. Porat and Y.Y. Zeevi. The generalized Gabor scheme of image representation in biological and machine vision. *IEEE Transactions on Pattern Analysis and Machine Intelligence*, 10:452–468, 1988.

[128] M. Porat and Y.Y. Zeevi. Localised texture processing in vision: Analysis in Gaborian space. *IEEE Transactions on Biomedical Engineering*, 36:115–129, 1989.

[129] L. Qiu and A.C. Tsoi. The relationship between a time-varying model of non-stationary signals and its Wigner distribution. *Signal Processing*, 32:305–314, 1993.

[130] T. Reed and H. Wechsler. Spatial/spatial-frequency representations for image segmentation and grouping. *Image Vision and Computing*, 9:175–193, 1991.

[131] W. Rihaczek. Signal energy distribution in time and frequency. *IEEE Transactions on Information Theory*, 14:369–374, 1968.

[132] W. Rihaczek. *Principles of High-Resolution Radar.* McGraw-Hill, New York, 1969.

[133] J.S. Rowlinson. Probability, information, and entropy. *Nature*, 225:1196–1198, 1970.

[134] P.C. Russell, I. Khandaker, E. Glavas, D. Alston, R.V. Smith, and G.R. Jones. Chromatic monitoring for the processing of materials with plasmas. *IEE Proc.Sci.Meas.Technol.*, 141:99–104, 1994.

[135] P.C. Russell, D. Tomtsis, J. Cosgrave, L.K. Stergioulas, A. Vourdas, and G.R. Jones. Extraction of information from acoustic vibration signals using Gabor devices. preprint, University of Liverpool, 1997.

[136] B. Saleh. *Photoelectron Statistics.* Springer-Verlag, Berlin, 1978.

[137] B.E.A. Saleh and N.S. Subotic. Time-variant filtering of signals in the mixed time-frequency domain. *IEEE Transactions on Acoustics, Speech, and Signal Processing*, 33:1479–1485, 1985.

[138] W.P. Schleich, M. Pernigo, and Fam Le Kien. Nonclassical state from two pseudoclassical states. *Physical Review A*, 44:2172, 1991.

[139] E. Schrödinger. *Statistical Thermodynamics.* Cambridge University Press, Cambridge, 1948.

[140] B.L. Schumaker. Quantum mechanical pure states with Gaussian wave functions. *Physical Reports*, 135:317, 1986.

[141] C.E. Shannon. A mathematical theory of communication. *Bell System Tech. J.*, 27:379–423, 623–659, 1948.

[142] C.E. Shannon. Communication in the presence of noise. *Proceedings of the IRE*, 37:10–21, 1949.

[143] C.E. Shannon. *The Mathematical Theory of Communication.* University of Illinois Press, Urbana, 1949.

[144] J.H. Shapiro, H.P. Yuen, and J.A. Machado Mata. Optical communication with two-photon coherent states - Part I: Photoemissive detection and structured receiver performance. *IEEE Transactions on Information Theory*, 25:179, 1979.

[145] R.M. Shelby, Levenson M.D., S.H. Perlmutter, R.G. DeVoe, and D.F. Walls. Broad-band parametric deamplification of quantum noise in an optical fiber. *Physical Review Letters*, 57:691–694, 1986.

[146] J.E. Shore and R.W Johnson. Axiomatic derivation of the principle of maximum entropy and the principle of minimum cross-entropy. *IEEE Transactions on Information Theory*, 26:26–37, 1980.

[147] J. Skilling. The maximum entropy method. *Nature*, 309:748–749, 1984.

[148] J. Skilling. The axioms of maximum entropy. In G.H. Erikson and C.R. Smith, editors, *Maximum Entropy and Bayesian Methods in Science and Engineering*, Fundamental Theories of Physics, page 1. Kluwer Academic Publishers, Dordrecht, The Netherlands, 1988.

[149] J. Skilling. Classic maximum entropy. In J. Skilling, editor, *Maximum Entropy and Bayesian Methods*, Fundamental Theories of Physics. Kluwer Academic Publishers, Dordrecht, The Netherlands, 1989.

[150] J. Skilling and S.F. Gull. Algorithms and applications. In C. Ray Smith and Jr. W.T. Grandy, editors, *Maximum-Entropy and Bayesian Methods in Inverse Problems*, Fundamental Theories of Physics, pages 83–132, Dordrecht, The Netherlands, 1985. D. Reidel Publishing Company.

[151] M.I. Skolnik. *Introduction to Radar Systems.* McGraw-Hill, New York, 1980.

[152] R.E. Slusher, B. Yurke, P. Grangier, A. LaPorta, D.F. Walls, and M. Reid. Squeezed-light generation by four-wave mixing near an atomic resonance. *Journal of the Optical Society of America B*, 4:1453–1464, 1987.

[153] R. Smith, S. Ahmed, A. Vourdas, J.W. Spencer, P.C. Russell, and G.R. Jones. Chromatic modulation for optical fibre sensing - electromagnetic and speckle noise analysis. *Journal of Modern Optics*, 39:2301–2314, 1992.

[154] A.I. Solomon. Group theory of superfluidity. *Journal of Mathematical Physics*, 12:390–394, 1971.

[155] Special issue on speckle noise. *Journal of the Optical Society of America*, 1976. Vol. 66.

[156] L.K. Stergioulas and A. Vourdas. Quantum state engineering in terms of a few coherent states. University of Liverpool, (in preparation), 1997.

[157] L.K. Stergioulas and A. Vourdas. Robust quantum state engineering using coherent states on a truncated von-Neumann lattice. Preprint, University of Liverpool, 1997.

[158] L.K. Stergioulas, A. Vourdas, and Jones G.R. Optical fibre sensing using the maximum entropy method. In G.-L. Oppo, S.M. Barnett, E. Riis, and Wilkinson M., editors, *Quantum Dynamics of Simple Systems*, volume 44 of *Proceedings of the Forty Fourth Scottish Universities Summer School in Physics*, page 360, London, 1996. NATO Advanced Study Institute, Institute of Physics Publishing. (Abstract).

[159] L.K. Stergioulas, A. Vourdas, and G.R. Jones. Gabor representation of a signal using a truncated von-Neumann lattice and its practical implementation. University of Liverpool, (submitted to Signal Processing), 1996.

[160] L.K. Stergioulas, A. Vourdas, and G.R. Jones. Noise analysis in optical fibre sensing: A study using the maximum entropy method. In J. Skilling and S. Sibisi, editors, *Maximum Entropy and Bayesian Methods*, Fundamental Theories of Physics, pages 109–116. Kluwer Academic Publishers, Dordrecht, The Netherlands, 1996.

[161] D.L. Stewart, L.C. Potter, and S.C. Ahalt. Computationally attractive real Gabor transforms. *IEEE Transactions on Signal Processing*, 43:77–84, 1995.

[162] S. Szabo, P. Adam, J. Janszky, and P. Domokos. Construction of quantum states of the radiation field by discrete coherent-state superpositions. *Physical Review A*, 53:2698, 1996.

[163] A. Tagliani. On the application of maximum entropy to the moments problem. *Journal of Mathematical Physics*, 34:326–337, 1993.

[164] M.C. Teich and B.E.A. Saleh. Squeezed states of light. *Quantum Optics*, 1:153–191, 1989.

[165] M.C. Teich and B.E.A. Saleh. Squeezed and antibunched light. *Physics Today*, 43:26–34, June 1990.

[166] M. Tribus. Information theory as the basis for thermostatics and thermodynamics. *Journal of Applied Mechanics*, 28:106, 1961.

[167] M. Tribus. *Thermostatics and Thermodynamics: An Introduction to Energy, Information and States of Matter, With Engineering Applications*. D. Van Nostrand Company, Princeton, New Jersey, 1961.

[168] M. Tribus. The meaning of the word "probability". In J. Skilling and S. Sibisi, editors, *Maximum Entropy and Bayesian Methods*, Fundamental Theories of Physics, pages 143–155. Kluwer Academic Publishers, Dordrecht, The Netherlands, 1996.

[169] M. Tribus, P.T. Shannon, and R.S. Evans. Why thermodynamics is a logical consequence of information theory. *Journal of the American Institute of Chemical Engineers*, 12:244–248, 1966.

[170] M. Unser. Fast gabor-like windowed fourier and continuous wavelet transforms. *IEEE Signal Processing Letters*, 1:76–79, 1994.

[171] H. Urkowitz. *Signal Theory and Random Processes*. Artech House, Norwood, 1983.

[172] H. Urkowitz, C.A. Hauer, and J.F. Koval. Generalized resolution in radar systems. *Proceedings of the IRE*, pages 2093–2105, October 1962.

[173] J. Ville. Théorie et applications de la notion de signal analytique. *Câbles et Transmission*, 2:61–74, 1948.

[174] K. Vogel, V.M. Akulin, and W.P. Schleich. Quantum state engineering of the radiation field. *Physical Review Letters*, 71:1816, 1993.

[175] A. Vourdas. Gaussian bases for radar signal analysis. *Signal Processing*, 20:163–169, 1990.

[176] A. Vourdas. SU(2) and SU(1,1) phase states. *Physical Review A*, 41:1653–1661, 1990.

[177] A. Vourdas. Analytic representations in the unit disk and applications to phase states and squeezing. *Physical Review A*, 45:1943–1950, 1992.

[178] A. Vourdas. Superpositions of macroscopically distinguishable states in the presence of thermal noise. *Optics Communications*, 91:236, 1992.

[179] A. Vourdas. Coherent states on the m-sheeted covering group of SU(1,1). *Journal of Mathematical Physics*, 34:1223–1235, 1993.

[180] A. Vourdas. Resolution of the identity in terms of SU(2) coherent states and their use for quantum state engineering. *Physical Review A*, 54:4544, 1996.

[181] A. Vourdas and R.F. Bishop. Phase-admixed states: Coherence and incoherence. *Physical Review A*, 39:214, 1989.

[182] A. Vourdas and R.F. Bishop. Thermal coherent states in the Bargmann representation. *Physical Review A*, 50:3331–3339, 1994.

[183] A. Vourdas and R.H. Wiener. Photon counting distribution in squeezed states. *Physical Review A*, 36:5866, 1987.

[184] D.F. Walls. Squeezed states of light. *Nature*, 306:141, 1983.

[185] D.F. Walls and G.J. Milburn. *Quantum Optics*. Springer-Verlag, Berlin, 1994.

[186] J.W.T. Walsh. *Photometry.* Dover, New York, 1958.

[187] L. Wang, Chen C., and Lin W. An efficient algorithm to compute the complete set of discrete Gabor coefficients. *IEEE Transactions on Image Processing*, 3:87–92, 1994.

[188] E.P. Wigner. On the quantum correction for thermodynamic equilibrium. *Physical Review*, 40:749–59, 1932.

[189] P.M. Woodward. *Probability and Information Theory with Applications to Radar.* Pergamon Press, London, 1953.

[190] L.-A. Wu, H.J. Kimble, J.L. Hall, and H. Wu. Generation of squeezed states by parametric down conversion. *Physical Review Letters*, 57:2520, 1986.

[191] A.M Yaglom and I.M Yaglom. *Probability and Information.* Reidel, Dordrecht, 1983.

[192] J. Yao. Complete Gabor transformation for signal representation. *IEEE Transactions on Image Processing*, 2:152–159, 1993.

[193] N. Yen. Time and frequency representation of acoustic signals by means of the Wigner distribution function: Implementation and interpretation. *Journal of the Acoustical Society of America*, 81:1841–1850, 1987.

[194] H.P. Yuen. Two-photon coherent states of the radiation field. *Physical Review A*, 13:2226, 1976.

[195] H.P. Yuen and J.H. Shapiro. Optical communication with 2-photon coherent states. *IEEE Transactions on Information Theory*, 26:78, 1980.

[196] B. Yurke, S.L. McCall, and J.R. Klauder. SU(2) and SU(1,1) interferometers. *Physical Review A*, 33:4033–4054, 1986.

[197] B. Yurke and D. Stoler. Generating quantum mechanical superpositions of macroscopically distinguishable states via amplitude dispersion. *Physical Review Letters*, 57:13, 1986.

[198] B. Yurke and E.A. Whittaker. Squeezed-state-enhanced frequency-modulation spectroscopy. *Optics Letters*, 12:236–238, 1987.

[199] W.M. Zhang, D.H. Feng, and R. Gilmore. Coherent states: Theory and some applications. *Reviews of Modern Physics*, 62:867–927, 1990.

[200] Y. Zhao, L.E. Atlas, and R.J. Marks. The use of cone-shaped kernels for generalized time-frequency representation of nonstationary signals. *IEEE Transactions on Acoustics, Speech, and Signal Processing*, 38:1084–1091, 1990.

[201] Y.M. Zhu, R. Goutte, and M. Amiel. On the use of a two-dimensional Wigner-Ville distribution for texture segmentation. *Signal Processing*, 30:329–353, 1993.

[202] Y.M. Zhu, F. Peyrin, and R. Goutte. Equivalence between two-dimensional analytic and real signal Wigner distributions. *IEEE Transactions on Acoustics, Speech and Signal Processing*, 37:1631–1634, 1989.

[203] Y.M. Zhu, F. Peyrin, and R. Goutte. The use of a two-dimensional Hilbert transform for Wigner analysis of two-dimensional signals. *Signal Processing*, 19:205–220, 1990.

[204] M. Zibulski and Y. Zeevi. Oversampling in the Gabor scheme. *IEEE Transactions on Signal Processing*, 41:2679–2687, 1993.